Improved Heavy Oil Recovery by Non-Thermal Processes

ンゲレ，オドゥ，ピエール，ロナルド

https://doi.org/10.15017/1866290

出版情報：九州大学，2017，博士（工学），課程博士
バージョン：
権利関係：

IMPROVED HEAVY OIL RECOVERY BY NON-THERMAL PROCESSES

Nguele Odou Pierre Ronald

KYUSHU UNIVERSITY

九州大学
KYUSHU UNIVERSITY

IMPROVED HEAVY OIL RECOVERY BY NON-THERMAL PROCESSES

A Doctoral Dissertation

Submitted to the Department of Earth Resources Engineering,
Graduate School of Engineering, Kyushu University, Japan
In Partial Fulfillment of the Requirements for the Degree of Doctor of Philosophy

In

Earth Resources Engineering

By

Nguele Odou Pierre Ronald

September, 2017

ABSTRACT

Heavy oil is defined as liquid petroleum of 20 to 10 °API gravity at reservoir conditions, and the crude of which API is less than 10°API is termed as extra heavy. Heavy and extra-heavy oil reserves consist approximately of 21 and 32% of total oil reserves respectively, while those of light to medium are estimated at 47 %. This means there is a substantial volume of heavy oil, which sits within the reach of existing oilfields. Most of these oils are trapped within the pore throats of shallow, small and thin matrices including low permeable siltstones, sandstone and carbonate reservoirs. In theory, the increment in oil, from these mature reservoirs, is obtained by implementing a technique referred as improved oil recovery (IOR). The IOR has been classified mainly into two groups that are thermal and non-thermal methods. The former, in which the heat is supplied to the reservoir in form of steam, has been preferred for heavy and extra heavy oils, because steam injection is strongly expected to decrease the mobility of the oil and augments thereby the production. To date, the production scheme is slowly disfavored primarily because of the cost of stem generation. On the other hand, a typical non-thermal method consists of injecting a fluid (slug) that reduces either the interfacial tension (IFT) or the viscosity of the residual oil. However, a poor propagation of the slug lowers the efficiency of these methods. The implementation of either of these techniques, in a candidate mature heavy oil reservoir, is inherent to its petro-physical properties and the characteristics of the residual oil.

The scope of this research considered two candidate heavy oil formations. The initial IOR screening highlights the possibility of gas-miscible (CO_2) and chemical-IOR respectively to petro-physics of the candidate formations and the properties of the residual oil. The motivation was not only to evaluate their potential, but also to highlight the technical challenges. Ultimately, it was sought to propose a recovery scheme that increases the heavy oil production, while reducing associated energy cost. Both were investigated experimentally in this research.

This dissertation consists of six chapters.

Chapter 1 introduces the fundamentals of IOR, discusses on the various approaches in heavy oil recovery. Therein is also detailed the mechanisms inherent to heavy oil production and the screening criteria of IOR. The candidate formations, the properties of its untapped oils are presented.

Chapter 2 investigates the potential of CO_2 for the candidate formations, which was selected in respect of the petro-physical properties of the reservoir. The production was mimicked by injecting CO_2 both at its sub-critical and super-critical state (sCO_2) in candidate heavy oils (API 11.5 and 16.6). Conducted in a PVT analyzing cell, the results showed that sCO_2 has a better solvating potential than CO_2. The swelling of the candidate heavy oils increased in a linear fashion with the concentration of sCO_2 and was altered by the presence of reservoir water. It was further shown that sCO_2 promoted a stripping process of light fractions from the native oil during the development of the miscibility front, which was followed by the deposition of an appreciable amount of asphaltenes. This latter phenomenon was highlighted as major drawback for this IOR method. Further investigations in this regard revealed that not only the petro-physical properties of the candidate formation would dictate the concentration of aggregated asphaltene, but also the chemical composition of the crude oil and even the injecting conditions of sCO_2. If implemented in the candidate formation, it is shown that the injecting gas (sCO_2) would behave either as flocculent or coagulant. Subsequently, these properties would either control or enhance the amount of deposited asphaltene. It was concluded that sCO_2 was potentially viable for a heavy oilfield provided that proper injection conditions were maintained. However, given the initial concentration in asphaltene in the candidate heavy oils, sCO_2-IOR cannot be recommended.

In Chapter 3, the heavy oil production, in respect of the physico-chemical properties of the candidate heavy oils, is investigated. Therein is introduced a new class of surfactants (Gemini surfactants). Two lyophilized cationic Gemini surfactants i.e. *12-3-12* and *16-3-16* were used to formulate the aqueous micellar slugs. Their inherent physico-chemical properties were subsequently investigated. These included the critical micelle concentration (CMC), the adsorption and the surface tension. Their potential for surfactant flooding were shown as they were able to achieve (*i*) an ultra-IFT (order of 10^{-3} mN/m), (*ii*) high water and oil solubilization and (*iii*) a relative low adsorption on sandstone and dolomite. More interestingly, those properties were found pronounced when the micellar slug, prepared from a Gemini surfactant with a longer hydrophobic alkyl chain (n=16), was used. Additionally, the micellar slugs showed an interesting potential as corrosion inhibitor by neutralizing the acidic materials generated as by-product during sCO_2-IOR.

Chapter 4 introduces the concept of cationic microemulsions and their relevance to oil recovery. The ultra-low IFT, achieved in the microemulsions, was altered by (*i*) the length of

the alkyl chain of the primary surfactant, and the nature of the respective cosurfactant, (*ii*) the presence in divalent ions in the brine solution and (*iii*) the acidity of the residual oil. The rheology of the microemulsions revealed a pseudo-plastic behavior, which was altered by the formation salinity. Therein is also addressed the characterization of the cationic microemulsions.

Chapter 5 introduces a hybrid recovery-flooding scheme using microemulsions. The heavy production was performed by a series of core-flooding experiments, performed in Berea sandstone, representative of the formation rock. The production scheme consisted of the injection of microemulsion-gel type formulated exsitu, in water-flooded sandstone, at the trail of which low-saline water was injected. Conducted in the homogeneous Berea sandstones, up to 31% of the initial oil-in-place (IOIP) was recovered from the homogeneous water-flooded sandstone when the heaviest microemulsion formulation was injected. The oil recovery was lowered to 20.3% when the microemulsion was formulated from the micellar slugs prepared from the Gemini surfactants with the shorter alkyl chain. The microemulsion formulations prompted a series of chemical reactions with the native minerals and the residual petroleum fluids, which caused the formation of sludge in the effluent fraction. The sludge is believed to be the challenge in this recovery scheme. However, it was shown that altering the composition of the preflush water could mitigate the deposition.

Chapter 6 concludes this research by highlighting the feasibility of two methods. A comparative analysis and proposed solution in respect the inherent challenges are presented. Further suggestions in regard of microemulsion-flooding and asphaltene deposition are discussed.

ACKNOWLEDGEMENT

This work is dedicated to the memory of my late mother (Rose Nguele) and to my dad (Nguele Henri).

This research would have not been possible without guidance and the support of several individual who, in a way or another, have extended their valuable assistance.

My deepest gratitude goes to my supervisor Professor Kyuro Sasaki who has always been keen on sharing his experience, mentoring me and suggesting ever more fascinating and challenging ideas and concepts to work on.

I would like to acknowledge Professor Hiroshi Tashima for his critical comments.

I would like to thank Associate Professor Yuichi Sugai for his valuable help throughout my research. His assistance in supplying the materials and equipment during this work is greatly appreciated.

I would also like to acknowledge Professor Hikmat Said Al-Salim whom has been more than an academic advisor throughout my studies.

The financial support from the Ministry of Education, Culture, Sports, Science and Technology of Japan (MEXT) is acknowledged. My special gratitude goes to Japan Petroleum Exploration (JAPEX) and Lion LTD for kindly supplying the heavy oils and the cationic Gemini surfactants used in this research respectively.

I would also like to thank Brian Omondi, doctoral student at Kyushu University, for the collaboration and its valuable inputs and efforts for this work to be completed.

I am indebted to many of my family, friends and colleagues from REPS who through their sincere suggestions and fruitful discussions shaped this dissertation in so many ways.
In particular I would like to thank my sisters, Christiane, Florence and Marie-Paul whose moral support has been crucial in the final stretch of the dissertation. A special wink to my brothers Olivier and Yannick. This work would have not be complete without mentioning my fellows Guillaume Doudou, Abu B. Jalloh, Ibrahim and many others whom I did not cite explicitly.

TABLE OF CONTENTS

LIST OF FIGURES

LIST OF TABLES

Chapter 1.
INTRODUCTION

1.1 Oil Production and Fundamentals of Improved Oil Recovery

Crude oil refers to a mixture of hydrocarbons, yellow to black in color, of which density and viscosity are variable. The former is defined quantitatively by a parameter known as API (i.e. American Petroleum Institute). The latter (i.e. viscosity) is a key parameter as far as the production of an oilfield is concerned. In general, the crude oil is classified either by its oiliness (i.e. API) or the chemical composition. Thus, an API that ranges from 32° to 40° denotes a light crude oil. Medium crude oil has an API, which ranges from 27° to 32°. On the other hand, an API, from 8 to 14, characterized heavy oil. For any value of API below 8°, the crude oil is an extra-heavy oil (Simanzhenkov and Idem, 2003). In 1997, Rogner (1997) reported approximately 3,396 billion of barrels of heavy oils and 5,505 billion of barrels (bbl) of extra-heavy oils trapped within the reach of existing oilfields. Over two decades, these values have been decreasing to half showing thereby the interest in these fossil resources (Fig. 1.1). Conventionally, the life of a producing oil field is staged in three major stages including a primary, a secondary and a tertiary stage (Fig. 1.2). During the early stage of an oilfield, the natural resources are brought to the surface through the reservoir natural drive.

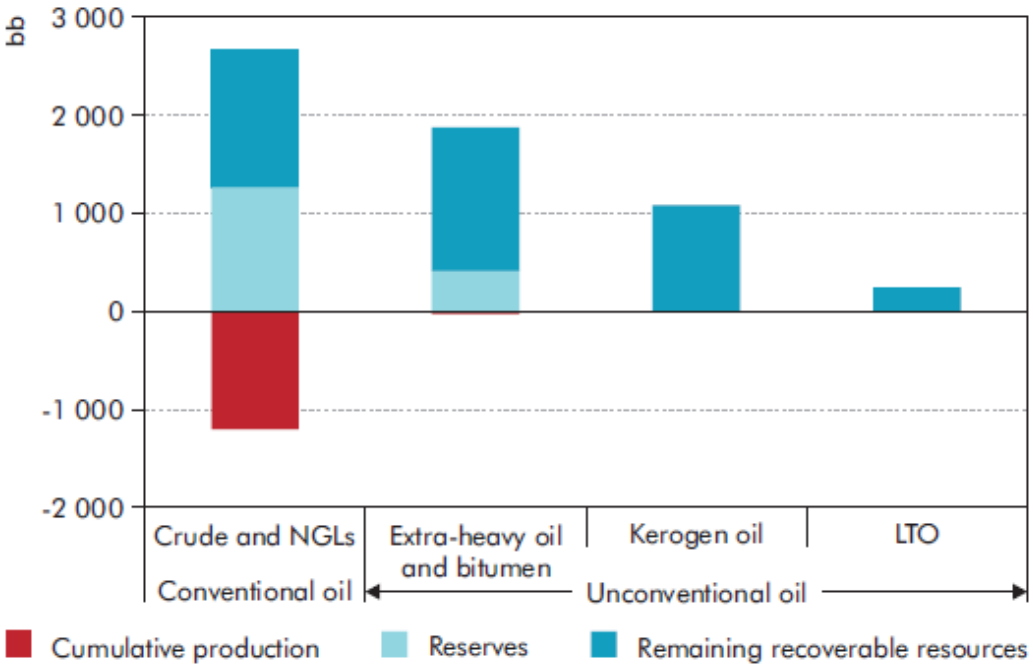

Fig. 1.1 Estimation of technically recoverable heavy oils and natural bitumen; from (IEA, 2013)

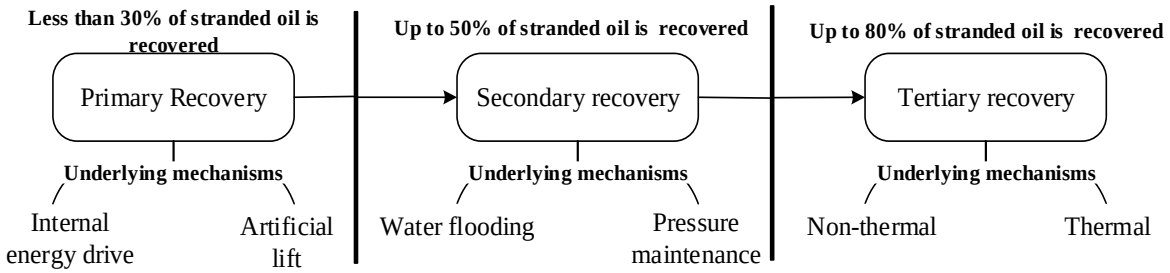

Fig. 1.2 Different stages of an oilfield life; modified from Kokal and Al-Kaabi (2010)

Five crucial parameters should be highlighted here in order to understand the underlying mechanisms of the oil production. These include (1) solution-gas drive, (2) gas-cap drive, (3) water-drive, (4) gravity drainage and (5) the mixed drive (Donaldson et al., 1989; Green and Willhite, 1998). A solution-gas drive is predominant if the drive energy is supplied by the expansion of the dissolved gases in the oil and water, which is reportedly the case for most of the oil reservoirs. If the reservoir is under-saturated, i.e. no free gas (es) dissolved within the oil, the driving force is provided only by the bulk expansion of the formation rock and liquids. It is worth mentioning that most of the heavy oil reservoirs are under-saturated, thus subject to this mechanism at the early life of the production. A gas-cap drive dominates the production in a primary recovery process when the gas-cap (that is the segregated gas overlying the oil deposit) expands. The trapped gas pushes the gas-oil contact downwards. As the production continues, it reaches the producing wells. As a consequence, the gas-oil ratio (GOR) increases substantially and more oil is produced.

Alagorni (2015) reviewed that the primary recovery by gas-cap drive mechanism could reach up to 40 % of the Initial Oil-in-Place (IOIP). If, however, the candidate oilfield has an aquifer, the governing mechanism is likely to be a water-drive. In this mechanism, the oil is produced as a result of the expansion of water into the formation, forcing the oil to move upwards. In this case, the production will decline at the water breakthrough. The fourth mechanism is the gravity drainage mechanism in which the density difference between the petroleum fluids (oil, gas and water) results in their natural segregation in the reservoir that forces further the oil to move upwards. This mechanism is commonly encountered in light crude oil formation. Unfortunately, the gravity drainage mechanism yields usually a low oil recovery and tends to be used in combination with other drive mechanisms (Donaldson et al., 1989). The last drive is a combination of aforementioned techniques, which tends to be encountered when none of aforementioned mechanisms, discussed above, prevails.

Regardless the mechanisms(s) that dictate(s) the early life of an oilfield, the recovery is generally low. Most of the oilfields reported a recovery as high as to 30% of IOIP during the primary recovery process, which means that there is a substantial amount of oil trapped underground. In order to boost the production, it is routinely accepted to inject a fluid (usually water) that maintains the pressure within the formation and increases subsequently the oil production. This technique is referred as secondary production. In this approach, water is usually preferred. Few notable heavy oilfields, specially located in the United Kingdom, have successfully implemented water-flooding (Jayasekera and Goodyear, 2000). The problem with water flooding lies mainly on the tendency of the water to channel and to override the residual oil primarily because of its low viscosity. These phenomena, often concomitant, rend the implementation of water flooding less effective or even not applicable to heavy oil and extra-heavy oil reservoirs. Nevertheless, where applicable, a classical water flooding could displace up to 50 % of IOIP (Mai et al., 2009). Furthermore, in a heavy oil reservoir in which the primary recovery is governed by gas cap drive, the secondary recovery technique considers rather the injection of a gas. Technica, the gases, produced at the first stage, are routinely injected back in the candidate formation. This method is known as gas flooding. It could be conjectured therefore that the choice of the secondary recovery method depends to a certain extent on the driving force during the early life of the reservoir.

The last stage of the production life of an oilfield is the tertiary recovery. This stage is implemented when the primary and the secondary recovery processes have become inefficient and economically not beneficial. The stage is termed as improved oil recovery (IOR) or enhanced oil recovery (EOR). Although, both terms are used interchangeably, they imply the increment in amount of oil. To be more accurate, IOR is the general term to designate any means implemented after secondary process that increases considerably the amount of oil recovered. The terminology EOR is more specific. It defines a technique (or a combination of techniques) implemented to decrease the residual oil saturation and increases subsequently the amount of produced oil (Thomas, 2008).

1.2 Tertiary Oil Recovery for Heavy Oil Reservoirs

Over the past decades, the extraction and the production of heavy and extra-heavy oils have relied on cold production despites the wide range of existing EOR methods. Fig. 1.3is an overview of EOR methods for heavy and extra-heavy oils.

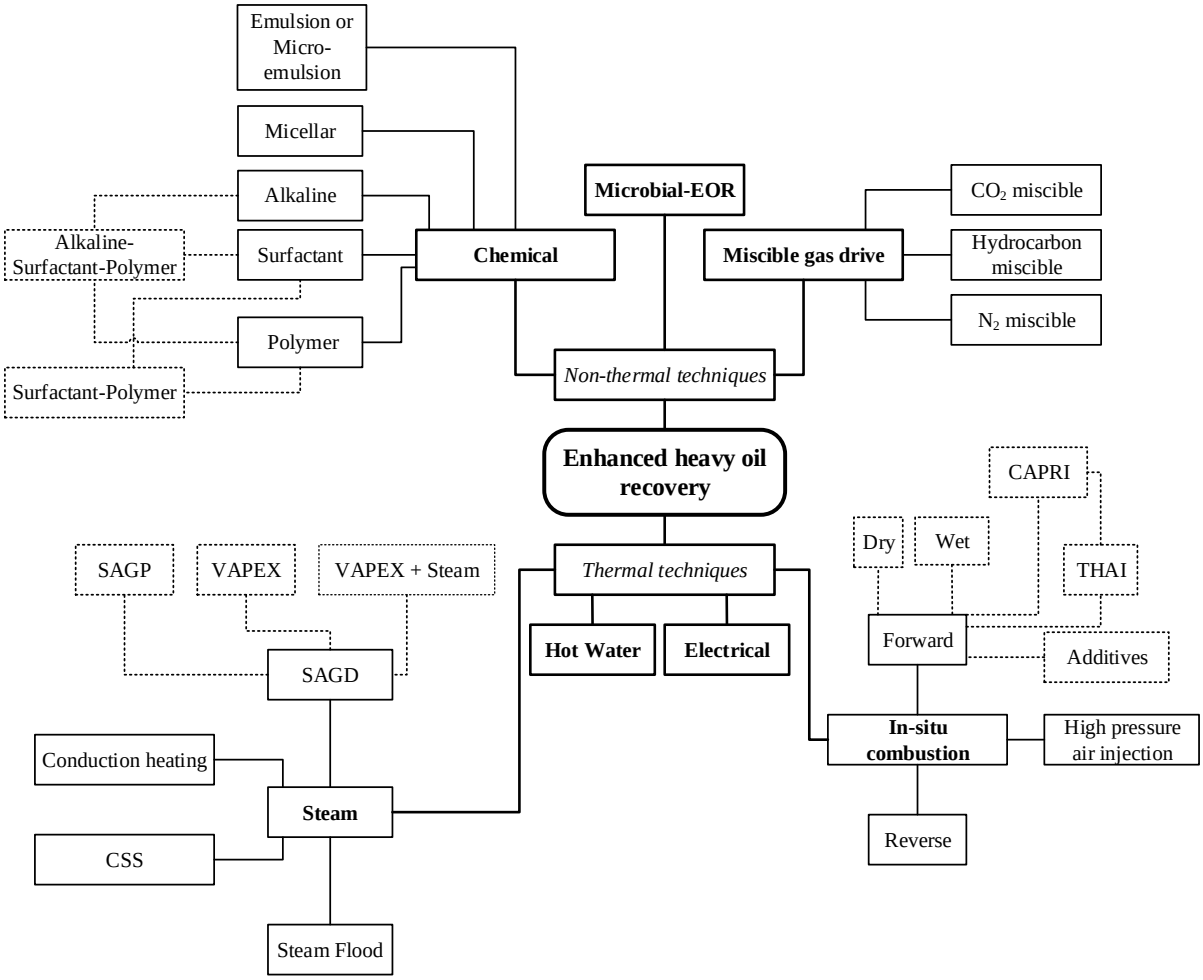

Fig. 1.3 An overview of enhanced oil recovery method; adapted from Thomas (2008)

1.2.1 Thermal methods

Thermal methods are the most advanced techniques among EOR methods, as long as the field experience and technology are concerned. They are best suited for heavy oils and tar sands. In these methods, the heat is supplied to the reservoir and tends to favor the vaporization of some of the oil. The supplied heat could be in form of vaporized water (steam), which is injected continuously into the oil layer (Fig. 1.4a).

However, steam-EOR is sensitive to the geometry and the petro-physical properties of the candidate formation. The steam creates, within the oil layer, a steam zone that not only lowers the viscosity of the heavy oil, but also increases the driving pressure for the oil to move (Shah et al., 2010). Some heavy oilfields have reported that when the heat (therein steam) was supplied in a cyclic manner Fig. 1.4b), the production increased quickly. The injection of high-pressure steam, followed by a soaking stage yielded a rapid payout with a recovery ranging from 10 to 40 % of IOIP. Steam assisted gravity drainage (SAGD) is another thermal method that has gained prominence within heavy oil operations.

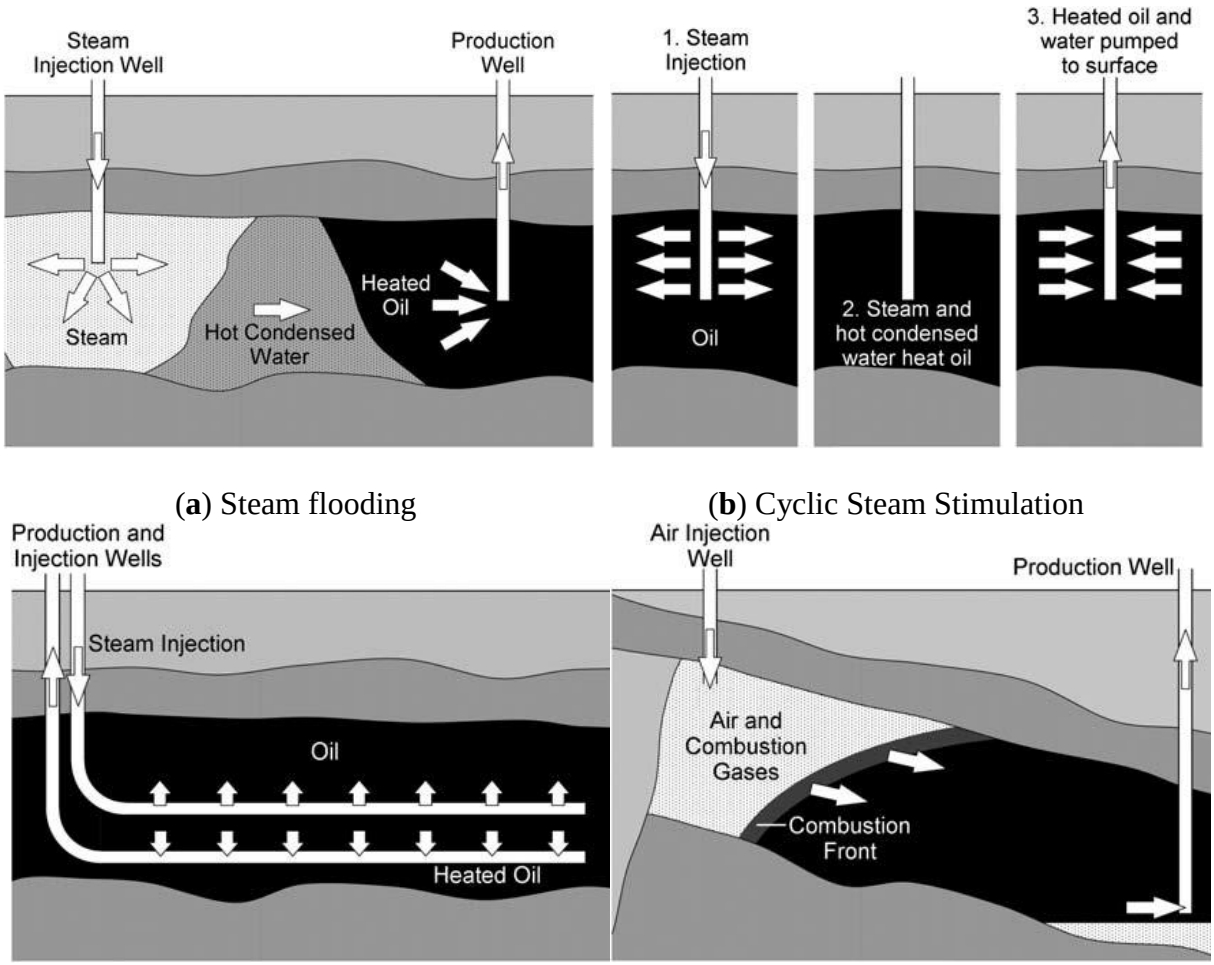

(**a**) Steam flooding (**b**) Cyclic Steam Stimulation

(**c**) Steam Assisted Gravity Drainage (**d**) In-situ combustion

Fig. 1.4 Schematic representation of heavy oil recovery by thermal methods; adapted from Shah et al (2010)

Its working principle, schematized in Fig. 1.4c, is quite similar to that of steam flooding at the difference of the steam chamber (Sasaki et al., 1999). This technique works best when the oil mobility is low, as steam channels are less likely to form. Unfortunately, this EOR method suffers also from its sensitivity to formation parameters including the thickness and the heterogeneity. In order to overcome these issues, modified forms of SAGD have been investigated including VAPEX that uses rather a solvent gas (or a mixture of solvents) to create a vapor chamber (Cuthiell et al., 2006). The vapor plays the same role as the steam chamber. Other variants include Steam and Gas Push (SAGP).

Also, it is possible to generate the heat in-situ, i.e. within the oil-bearing matrix (Fig. 1.4d). In this case, the EOR is referred as in-situ combustion, which consists of the injection of a hot air (or oxidizing gas) is injected on the oil bearing matrix (Selby et al., 1989). The contact between the two fluids sparks a combustion that further supplies the thermal energy, which prompts further the oil viscosity reduction. However, the low viscosity of the gas that overrides

the oil is reported to be a major drawback for this method. The density difference between the oxidizing gas and the oil is eliminated tentatively by an improved method known as Toe-to-heel air injection (THAI).

1.2.2 Non-thermal methods

Non-thermal methods encompass techniques that reduce primarily both the IFT and subsequently the mobility ratio. They are subdivided into miscible gas and chemical flooding. In the miscible displacement process, a foreign fluid (also called slug) is injected in the oil bank zone where the slug contacts the oil. The slug dissolves in the oil after a first (or multiple) contact(s). If the slug is a gas, the EOR is termed as gas-EOR, which works best in shallow deposits. Several gases have been tried with mitigated results. Routinely, gases considered in miscible gas-EOR include compressed air, acid sour gas, nitrogen (N_2), flue gas, hydrocarbon gases, and carbon dioxide (CO_2). The choice, however, is function of the formation, gas availability and costs (Taber et al., 1997a).

The use of CO_2, as slug for miscible gas-EOR, has been preferred over the other gases not only because it offers the possibility to sequester a greenhouse gas, but also because of its to ability to achieve a low minimum miscible pressure (MMP) for a wide range of crude oils. Moreover, it was highlighted that CO_2 at its supercritical state (thus termed as supercritical CO_2 or sCO_2) presents attractive properties for EOR (Table 1.1). The singular properties of CO_2 are effective in a formation deeper than 600 m. During the development of the miscibility front, CO_2 dissolves in the oil, resulting the oil swelling and viscosity reduction. The swollen oil tends to have a viscosity lower than that of the native oil. These concurrent mechanisms are even enhanced for light crude oils.

Table 1.1 Advantages and drawbacks of sCO_2; adapted from Hitchen et al. (1993)

Enhanced properties	Advantages	Disadvantages
Solvent Power	✓ Cannot be oxidized ✓ Miscible with gases in all proportion above its critical temperature ✓ Miscible with organic material	× High critical pressure and vapor pressure; × Low dielectric constant; × Lewis acid; × May induce low pH
Transport	✓Dense as liquid but mobile as gas ✓Low viscosity (1/10 < water) ✓High diffusion abilities in porous media	× May require handling high pressure equipment
Environment	✓ Low toxicity ✓ Good biocide towards fungi, bacteria and viruses.	×Could counterbalance EOR using microbial agents.

In the case of low pressure reservoirs (such as heavy oil formations), CO_2 will form an immiscible fluid, or will mix partially with the oil (Danesh, 1998). This will result of some oil to swell, which favors the viscosity reduction of the residual oil. Strictly speaking, CO_2 extracts the lighter fractions of the oil and promotes the deposition of heavier fractions. Often, this mechanism leads to asphaltene deposition, which is one of the major challenges of miscible CO_2-EOR (Speight, 2004). Furthermore, the low viscosity of CO_2 leaves usually a poor mobility control and sweeping efficiency. The latter case is, somewhat, overcome by injecting alternatively a small amount of CO_2 and large volumes of water. This technique is best known as Water-Alternating-Gas (WAG).

Chemical flooding encompasses a technique (or combination of techniques) that requires the injection of a chemical, which is either a polymer or a surfactant. The slug targets primarily the reduction of the IFT. Surfactant and/or polymer processes are the most prominent as far as EOR for heavy oil is concerned (Sheng, 2011). In both methods, the slug is a surfactant (usually a petroleum sulfonate) or polymer blended with a low-molecular alcohol (termed as cosolvent or cosurfactant) or even a micellar solution. At the leading edge of the slug, a preflush is routinely injected. The composition of the preflush is tailored to remove and/or neutralize the ionic elements that may reduce the efficiency of the slug. At the trail of the slug, a mobility buffer (usually a viscous water) is injected for the mobility control. One of the problems of surfactant-EOR is the loss of chemical. Phase partitioning and trapping, and the slug bypassing because of fingering, are equally reviewed as issues arising when a typical surfactant-EOR is implemented.

Microbial-EOR, also classified as non-thermal method, has been investigated since 1960 (Gray et al., 2008). This approach uses the potential of microbes to generate a surfactant in-situ, which is termed as bio-surfactant (Thomas, 2008). In fact, the microorganisms react with the residual oil to yield either bio-surfactant, slimes (polymers), biomass and/or gases such as CH_4, CO_2, N_2 and H_2 as well as solvents and certain organic acids. Oil recovery mechanisms in microbial EOR are similar to those of the classic chemical methods, which include IFT reduction, emulsification, wettability alteration, improved mobility ratio, selective plugging, viscosity reduction, oil swelling and increased reservoir pressure due to the formation of gases. Increase in permeability can result from the acids formed (Thomas, 2008).

1.3 Emerging IOR Technologies

1.3.1 In-situ conversion with electrical heating

This method, patented by Shell in 1980, uses the sub-surface heating to convert kerogen into cleaner transportation fuels and gas (Speight and Loyalka, 2007) ; kerogen is the primary form of inorganic and insoluble hydrocarbons that occurs in the source rock. This method, defined as upgrading, is reported to contribute to pollution of aquifers.

1.3.2 Microemulsion flooding

This method has been gaining prominence in the petroleum industry especially for the extraction of residual light oils but is still under investigation for heavy oils. Microemulsions, more stable than emulsions, are injected in the reservoir and prompt displacement of trapped oil. This approach is thought to be commercially viable primarily because of (1) their lower energy requirement, (2) their potential to develop an ultra-low IFT and (3) their high interfacial area (Bera and Mandal, 2015; Nguele et al., 2016c; Santanna et al., 2009).

1.3.3 Nanofluid flooding

Even more recently, the potential of nanoparticles (NP) and nanofluids have been explored for EOR (Devendiran and Amirtham, 2016). Although the studies are still at the embryonic stage, it has been reported that nanofluids formulated from alumina (Al_2O_3) or iron oxide (Fe_2O_3) have the ability to reduce greatly the viscosity of the residual oil. Likewise, silica (SiO_2) NP has shown a potential in altering the IFT.

1.4 IOR Screening Criteria

Several tertiary methods have been investigated over the past decades with mitigated results. This is so because the choice, the implementation and the success of an IOR technique is affected by the geometry of the candidate reservoir, the properties of the residual oil.

Traditionally, surface mining and thermal methods (steam methods) have been preferred for the production of viscous oils. Unfortunately, they are not only there are so sensitive to the geometry of the reservoir that their applicability is narrowed to specific oilfields, but also, they tend to have a high energy requirements. On the other hand, the sequestration of CO_2, a greenhouse gas, has proven potential as displacing agent for stranded viscous oils. Although successful for light crude oils, this tertiary recovery technique is less attractive for heavy oils primarily because of the flow assurance issues arisen during the gas injection. These issues include asphaltene, wax and resins deposition (Zhang et al., 2007).

Table 1.2 Screening criteria in respect of petro-physical properties of formation and candidate oil characteristics[a]

EOR PROCESS			Reservoir Characteristics					Crude oil Characteristics		
			S_o (%)	*Requirements*	K (mD)	D (m)	T (°C)	API (°)	μ (cP)	*Chemical composition*
Thermal		Steam EOR	≥ 40	High φ and K Sandstone	≥ 200	≤ 1,500	Not critical	8 - 25	≤ 100,000	Not critical
		In-situ combustion			≥ 50	≤ 3,833	≥ 60	10 -27	≤ 5,000	Asphaltic components to help coke deposition
Non-thermal	Miscible displace-ments	Miscible CO_2	≥ 20	Carbonates Sandstones	Not critical if sufficient injection rate can be maintained.	Appropriate to allow injection pressure greater than MMP*	-	≥ 22	≤ 10	High percentage of intermediate HC
		N_2 or flue gas	≥ 40	Carbonates with few fractures. Sandstones	Not critical if uniform	≥ 2,000	Not critical	≥ 35	0.4	High percentage of light fractions
		Hydrocarbon	≥ 30	Carbonates with minimum fractures Sandstones		≥ 1,333	Can have significant effect on MMP*	≥ 23	≤ 3	
	Chemical methods	Chemical	≥ 50	Sandstone preferred. Can also be used for carbonates	≥ 10	≤ 3,000	≤ 90	Not critical		Organic acids needed to achieve lower IFT with alkaline methods
		Alkali	≥ 35					> 20	< 35	
		Polymer						>15	< 150	Not critical

[a] S_o: oil saturation; K: average formation permeability; D: formation depth; T: average formation temperature, *API*: American Petroleum Institute; μ: Oil viscosity; φ:porosityEmerging EOR Technologies

Clearly there is no single EOR method that would be applicable to all formations. Hence, a screening process must take into account not only the crude oil characteristic, but also the petro-physical properties of the candidate formation (Table 1.2). In fact, the signs (≤ or ≥), written in Table 1.2, should not be used. According to Taber et al. (1997a, 1997b), the limiting values have come from the process-mechanisms and successful field projects. This is to say that the chosen parameter to select an EOR, be it a petro-physical property of the reservoir or the crude oil property, is not absolute. Therefore, one should see Table 1.2 as a guideline. For example, if the candidate formation is shallow (i.e. $D \leq 3{,}000$ m), Table 1.2 suggests that steam-EOR and/or chemical flooding is feasible.

For a tertiary oil recovery to be effective, the method should efficiently mobilize the droplets to create an oil bank that could be propagated to the production wells. This is to say that an EOR should target primarily the reduction in the oil saturation (S_o) below residual oil saturation (S_{or}), which is feasible only by altering either the capillary number (Ca) and/or the mobility ratio (M). The former parameter defines the ratio of viscous forces that keep the residual oil stranded within the pore throats of the formation to the interfacial tension (IFT) acting across the interface oil/water and it is defined by,

$$Ca = \frac{v\mu}{\sigma} \tag{1.1}$$

where v is the velocity of the displacing fluid or slug (in m/sec), μ is viscosity of the residual oil (in Pa.s) and σ is the IFT across the interface oil/water (in N/m).

A water-flooded formation leaves behind a poorly swept region with *Ca* in the order of 10^{-7}. Practically, this means only the decrease in IFT could reduce the residual oil saturation further. Thomas (2008) reviewed that a decrease of 50% of S_o required an increase in *Ca* of about three magnitudes. The mobility ratio acts at both the microscopic level and macroscopic levels,

$$M = \frac{k_{r_1}}{\mu_1} \times \frac{\mu_2}{k_{r_2}} \tag{1.2}$$

where k_{r1} and k_{r2} are the relative permeability of injected fluid or slug and the displaced oil respectively (in mD) and μ_1 and μ_2 are the respective viscosities of slug and oil (in cP).

It is admitted conventionally that for a value of *M* greater than 1, the displacement of the residual oil by the slug is unfavorable. In fact, it indicates that the slug flows more readily than the oil, which is known as oil channeling. The channeling is the primary reason why a large area of the oil-bearing matrix is left unsweep after a classic water flooding. On the other hand, a mobility ratio lower than 1, the viscosity of the slug is large enough to favor the displacement of the residual oil.

1.5 Problem Statement and Research Objectives

1.5.1 Problem statement

In this research, the two heavy oil fields were considered. They are located in the northern Japan. The petro-physical properties of the fields and the respective physico-chemical of the residual oils are shown in Table 1.3. It was conjectured in the earlier sections that increasing the heavy oil recovery from mature oilfields using thermal-EOR techniques for viscous oils require large volumes of water (steam- EOR for instance) and a high-energy consumption. Therefore, based on Table 1.2, neither of thermal-EOR could be implemented. However, the petro-physical data from the candidate fields as well as those of the residual oils show that both gas-miscible and chemical methods could be suitable.

Table 1.3 Presentation of the candidate heavy oilfields [a]

	Petro-physical properties				*Physico-chemical properties of residual oil*				
	D, (m)	*OIP*, (m^3)	Rock type	Code	API, (^{o})	*Sp. gr*, (-)	μ, (cP)	*MW*, (kg/kmol)	AN, (mg KOH/g)
Field-1	1738	220	Sandstone	Oil-J1	11.6	0.988	874	338.5	0.72
Field-2	1958			Oil-J2	16.6	0.955	50	266.6	0.56

[a] *D*: formation depth; *OIP*: Oil-in-Place, *API*: American Petroleum Institute; *Sp. Gr.* : specific gravity measured at 15^{o}C; μ: viscosity measured at 30^o; *MW*: molecular weight; *AN:* acid number

In this regard, three (03) main objectives were set for this project:

(1). Evaluate the technical applicability of gas-miscible and chemical methods for the candidate heavy oil fields.

(2). Highlight their technical challenges.

(3). Propose new recovery scheme, which eliminates (or at least reduces) the energy consumption.

1.6 Thesis Outline

This dissertation is organized in six chapters with this chapter serving as chapter 1 (Introduction).

Chapter 2 investigates the potential of CO_2 for the candidate formations, which was selected in respect of the petro-physical properties of the reservoir. The conclusions are drawn from the experimental results of CO_2 injected at its supercritical state. Also, therein is addressed systematically the issues of oil foaminess and asphaltene deposition. The latter is the crux of the chapter. Two thermodynamic models are presented, based on which the effects of the petro-physical properties of the candidate formations and the physico-chemical parameters of both the candidate residual oils and the gas.

In Chapter 3, a new class of surfactant (Gemini surfactants) is presented. The formulations of the respective micellar slugs are addressed. Therein is investigated the physico-chemical properties of the micellar slugs including the critical micelle concentration (CMC), the static adsorption and the surface tension. Aforementioned parameters were selected in respect of their usefulness for oil recovery. Also, it is highlighted the potential of micellar slug as corrosion inhibitor.

Chapter 4 introduces the concept of cationic microemulsions and their relevance to oil recovery. The ultra-low IFT, achieved in the microemulsions, was altered by (*i*) the length of the alkyl chain of the primary surfactant, and the nature of the respective cosurfactant, (*ii*) the

presence in divalent ions in the brine solution and (*iii*) the acidity of the residual oil. The rheology of the microemulsions revealed a pseudo-plastic behavior, which was altered by the formation salinity. Therein is also addressed the characterization of the cationic microemulsions.

In Chapter 5, core-flooding experiments are carried out to evaluate the potential of microemusions to displace residual oils. The core flood tests are performed in sandstone plugs, representative of the formation rock. The oil-bearing matrices are altered to fracture or highly porous medium to investigate the mechanistic displacements of the microemulsion formulations. Not only the effect of the composition of the preflush is studied, but also the interactions crude oil-microemulsion-reservoir brine are discussed. The technical challenges inherent to microemulsion flooding conclude the chapter.

Chapter 6 concludes this research by highlight the feasibility of the two methods. A comparative analysis and proposed solution in respect of the inherent challenge are presented. Further suggestions in regard of microemulsion-flooding and asphaltene deposition are discussed.

Chapter 2.
HEAVY OIL PRODUCTION BY SUPERCRITICAL CO_2

2.1 Fundamentals of Gas-Miscible Recovery

Miscible gas flooding including carbon dioxide flooding (CO_2-EOR) is reported to be the second largest recovery technique applied in a heavy oilfield after thermal methods (Kokal and Al-Kaabi 2010). CO_2-EOR operates in a simple manner. Given the right injection conditions, CO_2 mixes with the resident petroleum fluids behaving like a thinning agent. The oil, of which viscosity has been reduced, is flushed out from the reservoir by water (Donaldson et al., 1989). The slug (CO_2) comes in contact with reservoir fluids and distributes the resident fluids prior at immiscible state into distinct thermodynamic phases that include gas-rich, hydrocarbon-rich (or oil-rich) and water-rich phases during the development of the miscibility front.

Miscibility is reached within the reservoir through a phase composition change subsequent to a multiple-contact and mass transfer between candidate oil, the formation brine and the slug. This is to say that the displacement is theoretically efficient when the thermodynamic properties of the slug and those of the resident fluids become similar. In which case, the system is said to be at its pseudo-equilibrium state. However, the complex nature of the crude oil renders the phase distribution computation extensive and laborious. Thus, in order to account the concentration of the dissolved gas within the residual oil, it is acceptable to have to model the candidate oil as a single component (or pseudo-component). In this research, this was performed by modeling the heavy oils from their respective assays (Nguele et al., 2016d). It is worth highlighting that the implementation of miscible CO_2-EOR is challenged by the deposition of heavy organic fractions (i.e. asphaltene deposition). The heavy hydrocarbon fractions are stripped out from the native crude oil during CO_2 flooding (Zhang et al. 2007). Asphaltene is reported to cause well plugging, pipeline fouling as well as desaphalting original crude (Wilt et al. 1998).

Considering the choice of CO_2-EOR for the candidate oilfield, the study focused on the mechanisms of CO_2 and sCO_2 dissolution and asphaltene deposition in the candidate heavy oils in respect to the pseudo-equilibrium state developed during the miscibility front. The motivation, here, lied on the evaluation of their significance during the consideration of miscible sCO_2-EOR. These objectives were tackled by considering two thermodynamic algorithms that compute in a more realistic manner (1) the amount of dissolved gas within the

oil phase and (2) the concentration in aggregated asphaltene. Both models were derived from experimental investigations.

2.2 Improved Oil Recovery and Reservoir Thermodynamics

2.2.1 Three-phase equilibrium calculations

We conjectured that oil production, by miscible CO_2-EOR, is accompanied by the change in fluid composition, pressure and temperature. The challenge here is to determine accurately the equilibrium conditions at which the dissolution (and thus the displacement) is optimal. In this context, it is important to apply thermodynamic concepts. The detailed development of the thermodynamic model of mole fraction of CO_2 slug is presented by Nguele et al. (2016b).

2.2.2 Thermodynamics of asphaltene deposition

The mechanisms inherent to asphaltene deposition are still subject to debate. However, it is accepted that the asphaltene deposition is subsequent to a mass transfer between the gas (CO_2) and the residual oil. In other words, asphaltene aggregation and its deposition depend on the physico-chemical changes occurring within the reservoir during the development of the miscibility front between CO_2 and the residual oil. Also, the existing thermodynamic models, proposed for the understanding, the modeling and the prediction of the phase behavior of asphaltene deposition, are for most, developed based on how asphaltene fraction is defined in the crude oil. In this regard, several models have been proposed. However, they are conventionally grouped into two categories including:

(1) *The solubility model*, which postulates that asphaltene and its solvent phases are in liquid state in the oil. Their thermodynamic properties are generally derived from the Flory–Huggins-type solution theory, using an energy interaction parameter estimated from Hildebrand's solubility parameter (Mannistu et al., 1997).

(2) *The solid model* treats the oil as a multicomponent mixture in which the heaviest component is split into two pseudo-components including a non-precipitating and a precipitating component. The former is believed to remain soluble in the oil throughout the production while the latter forms the aggregated asphaltene (Nghiem et al., 1993). From this model, two other approaches were derived including the colloidal and the micellization models. Both consider asphaltenic materials as macromolecules whose size and nonpolar van der Waals interactions dominate the asphaltene-phase behavior. Inherent thermodynamic

properties are calculated from a modified version of statistical association fluid theory (SAFT) EoS (David Ting et al., 2003).

Our proposed approach has thermodynamic inclination, however was derived from the simplified solubility model presented by Chung and Jones (1991). The suggested model postulated that the fraction of asphaltene that aggregates, flocculates and/or precipitates, occurred within the asphaltene phase, which is implicit to soluble asphaltene. This is to say that the maximum soluble asphaltene, derived from the model, estimated the concentration in aggregated asphaltene. The computation procedure of soluble asphaltene and that of the corresponding concentration in aggregated asphaltene is presented in Nguele et al. (2016a, 2016d).

2.3 Experimental Section

2.3.1 CO_2 and sCO_2 injection

CO_2 (99.99% pure) was selected as primary slug. The gas injection was performed in PVT equipment. Its working principle and the schematic are presented in Nguele et al. (2015). Table 2.1 summarizes the gas injection conditions as performed in this study.

The injection scheme was designed to replicate the production of under-saturated oil of which the recovery mechanism is liable to bubble-point pressure. For each injection, CO_2 (or sCO_2) was allowed to contact the candidate heavy oil (Oil-J1/2) or the mixture (Oil-J1/2 - brine) for a minimum of 72 hours. The pressure within the PVT analyzing cell was increased step-wise after each pseudo-equilibrium state was reached during the test. At the end of the gas injection, the cell was slowly depressurized. The vapors were routed towards a gas-trapping cell, which was designed to trap the lighter (or vaporized) fractions of the oils.

Table 2.1 Experimental conditions for CO_2 injection

Binary system			
Investigated system	Injecting pressure (MPa)	Operating temperature (^oC)	Gas state
CO_2 - Oil-J1	2.85	45	Sub-critical
CO_2 - Oil-J1	7.63	36	Supercritical
CO_2 - Oil-J2	7.00		
Ternary system			
CO_2 - Oil-J1 – 2% NaCl	3.12	45	Sub-critical

2.3.2 Quantification of asphaltene in the candidate heavy oils

To extract organic materials, the residual oil titration was performed. It aimed at estimating the initial concentration in asphaltenic materials within the samples. The experimental procedure was modified from ASTM D3279. The experimental procedure is described below:

(1) Dissolve 5g of Oil-J1 (or Oil-J2) in 10 mL of toluene at 90°C to ensure a complete dissolution.
(2) Centrifuge the mixture for 30 mins at a constant speed of 5000 rpm.
(3) Separate the supernatant fluid from the precipitated organic matters by gravimetric filtration.
(4) Allow the supernatant fluid to equilibrate overnight to allow a phase separation at a constant temperature of 25°C.
(5) Mix the supernatant with heptane. The solution should be in the the ratio of 1:5 (v:v).
(6) Weigh the filter paper.
(7) Separate by vacuum filtration the deposited organic materials from the supernatant fluid.
(8) Remove the resin and the wax by hot pentane.
(9) Repeat Step # 6 until the effluent becomes clear in color.
(10) Weigh the filter paper at the end of the vacuum-filtration.
(11) Estimate the concentration in asphaltene by differencing the weight of the filter paper from step #9 to Step #5.

2.4 Phase Equilibria Results

2.4.1 CO_2 solubility at sub- and supercritical conditions

In a typical miscible CO_2-EOR, the interest is to quantity the amount of CO_2 that dissolves in the oil-rich phase. From the thermodynamic model presented by Nguele et al. (2016b), we computed the mole fraction of the gas (x_{CO2}). Upon which, CO_2 (or sCO_2) solubility (R_s) was derived,

$$R_s = \frac{x_{CO_2} \big/ (1 - x_{CO_2})}{W_{in}} n^l_{CO_2} \tag{2.1}$$

where x_{CO2} defines the mole fraction of CO_2 (or sCO_2) in the oil-rich phase calculated from the Vapor-Liquid model (dimensionless); n^l_{CO2} is the number of moles of CO_2 (or sCO_2) in the liquid phase (in mol) and W_{in} the weight of Oil-J1 (or Oil-J2) within the cell (in g).

The results, presented in Fig. 2.1, highlight the dependence of the solubility on the nature of the crude and/or the injecting gas. We observed, for example, that for the same type of crude oil (i.e. Oil-J1), CO_2 solubility was 58% higher than that of sCO_2 taken as slug. Also, we noticed that sCO_2 dissolved evenly in both candidate heavy oils. Regardless the thermodynamic state of the slug, the solubility of both gases increased steadily with the equilibrium pressure until a deflection (i.e. curvature or flattening) was reached.

Above which the solubility of either gas was fairly constant at least at the supercritical conditions (Fig. 2.1a). Injected at the sub-critical pressure, the solubility curve flattened and then increased suddenly. Thus, we defined the pressure at which the curve changed in shape as the bubble-point pressure (p_b).

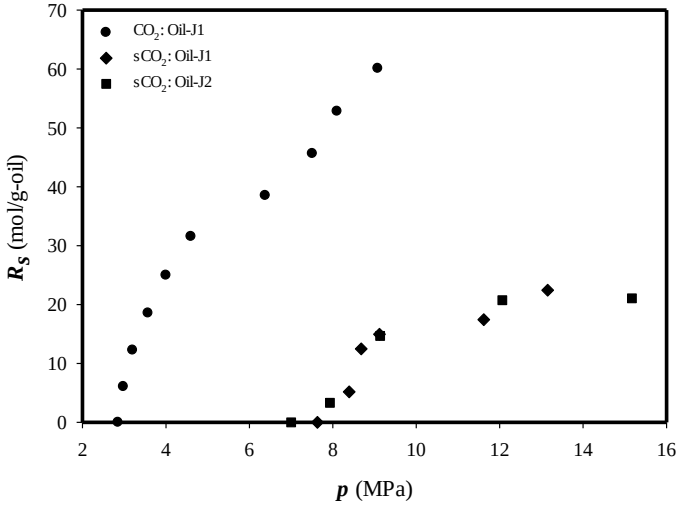

(**a**) Solubility of CO_2 in heavy crude oils at sub- and supercritical conditions

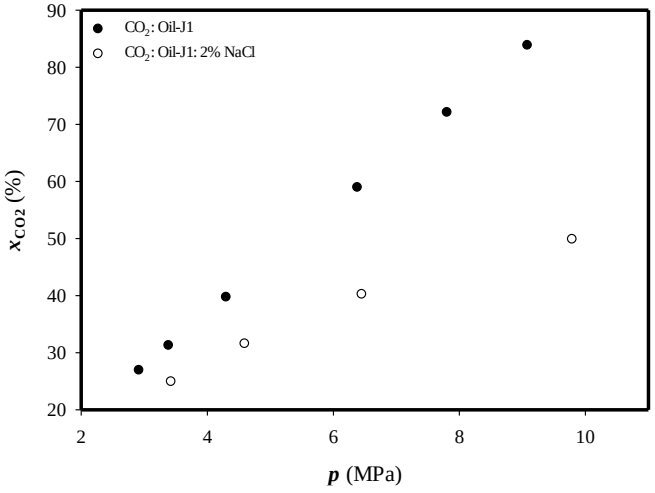

(**b**) Effect of reservoir water

Fig. 2.1 Solubility of CO_2 in heavy crude oils at sub- and supercritical conditions and effect of reservoir water

The analysis of Fig. 2.1, in respect of the experimental bubble-point pressure, showed that a larger gas solubility does not necessarily imply a higher bubble-point pressure. Rather, the solubility was found subsequent to the thermodynamic state at which the gas is injected. To understand the ability of sCO_2 to develop a better miscibility compared to sub-CO_2 and thus the bubble-point pressure, an insight could be drawn its polarity of sCO_2 vis-à-vis of that of residual crude oil. Crude oil polarity relies upon its constituents, in particular the hetero-compounds found in the heaviest fractions of oil, which are primarily resins and asphaltenes. Also, CO_2 is normally non-polar but at its the supercritical state, it becomes more polar (Raveendran et al., 2005).

Because the slug and the candidate oil are polar fluids, they could mix easily. This means thermodynamically that sCO_2 perturbs the stability of the three intermolecular forces that govern the miscibility front. These forces are hydrogen bonding, dipole-dipole and Van Der Waals forces. Thus, the results, conveyed by Fig. 2.1a, suggested that the difference in sCO_2 solubility in the samples could be justified primarily by the solvation strength of the slug, which itself is influenced by the kinetic and/or stability of the equilibrium of intermolecular forces and the chemical composition of the oil.

In general, the residual oil coexists with the formation water, also called formation brine. In this research, we considered synthetic formation brine primarily composed of sodium chloride (NaCl). The effect of divalent ions was neglected at this stage. While computing the mole fraction of slug that dissolves into the oil-rich phase (Fig. 2.1b), we found a decrease of about 35% on the average. This is explained by the fact that CO_2, upon contacting the mixture (oil+ brine), partitioned into three phases including oil-rich, brine-rich and gas-rich phases. These results suggested that the brine develops a kinetic barrier towards free mixing of slug i.e. decreases its solvating power.

2.4.2 Oil foaminess

Producing heavy oils by CO_2-EOR implies the formation of foamy oil, which is subsequent to its swelling. The foamy oil has a lower viscosity than the native oil, which was observed experimentally during CO_2 injection carried in this research (Fig. 2.2a). If one considers that oil swelling, and thus its foaminess, is a strict consequence of gas dissolution in the oil phase, then we can define a swelling factor (S_f) as,

$$S_f = \left(\frac{V_{foam}}{V_{oil,in}} - 1 \right) \tag{2.2}$$

where S_f is the swelling factor (dimensionless); V_{foam} is the volume of foamy oil (in cm^3) and $V_{oil,\,in}$ is the volume of crude oil prior to the gas injection (in cm^3).

We found that the swelling increased with gas solubility following a linear regression (Fig. 2.2b). At sub-critical conditions and for the system (Oil-J1: CO_2) the linear fitting curves was given by equation (2.3):

$$R_s = 156.6S_f + 10.5, \text{ with } R^2 = 0.9\,64 \tag{2.3}$$

On the other hand, at the supercritical conditions, equations (2.4) – (2.5) expressed the linear relation between the oil swelling and the gas solubility. Thus, for Oil-J1:

$$R_s = 38.1S_f + 17.4, \text{ with } R^2 = 0.999 \tag{2.4}$$

Likewise for Oil-J2:

$$R_s = 83.1S_f + 37.9, \text{ with } R^2 = 0.987 \tag{2.5}$$

Having shown above that the solubility was higher when CO_2 was used, one might have expected that the amount in foamy oil would increase with the dissolved CO_2 concentration.

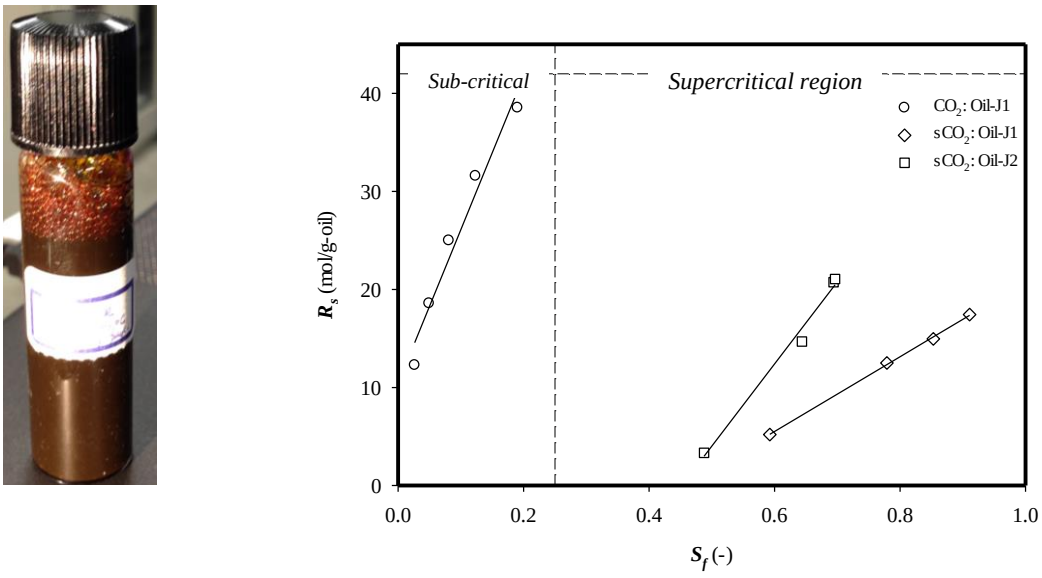

(**a**) Swollen Oil-J1 (**b**) Oil swelling

Fig. 2.2 Heavy oil swelling during sub- and supercritical CO_2 injection

The results, conveyed herein, stated otherwise. The swelling was rather found higher in sCO_2. For instance, for the same type of oil (Oil-J1), the swelling factor increases for about 8 times when sCO_2 was used comparatively to CO_2. Based on equations (2.3) – (2.5), one may postulate that gas swelling (and thus the foaminess) is linear function of the solubility, in which two thermo-physical parameters including *proportional coefficient of gas solubility* (dimensionless) and the *correction factor* could be defined. Aforementioned factors were crucial in explaining the behavior of the advancing gas during the oil swelling.

A higher value of *proportional coefficient of gas solubility* implied that the slug was highly soluble in the considered oil. Taking in account the thermodynamic considerations, we believed that the *proportional coefficient of gas solubility* highlights on how fast the miscibility is developed. Thus, a high coefficient would imply plausibly a rapid dissolution with a low bubble-point pressure while a reverse trend might state otherwise. Also, the non-uniformity in *correction factors* could be justified by how the miscibility front is developed within the cell. Care should be taken if afore-presented coefficients were to be used. From the results above discussed, we were lead to think that further investigations on sCO_2-EOR should be conducted. We were particularly interested to look into its influence on the mechanisms of asphaltene deposition.

2.5 Asphaltene Aggregation and Deposition

Fig. 2.3a shows the maximum volume of soluble asphaltene and aggregated asphaltene as function of the saturation pressure both computed from thermodynamic model. Below the bubble-point region, p_b, the maximum volume of the asphaltene soluble with the pseudo-equilibrium pressure increased steadily with the pressure and thus sCO_2 (Fig. 2.3a). This observation was contrasted in the maximum aggregated asphaltene (Fig. 2.3b). In fact, both maximum soluble and aggregated asphaltene mirror each other. In other words, the more asphaltene is soluble, the less it aggregates.

The two mechanisms were concurrent and inherent to sCO_2 solubility. However, the pattern changed at/near the experimental bubble-point pressure at which the solubility and the aggregation were less altered. In estimating the amount of deposited asphaltene (Table 2.2), the results were found to corroborate with the literature, which states that the deposition in asphaltene is higher at the bubble-point pressure.

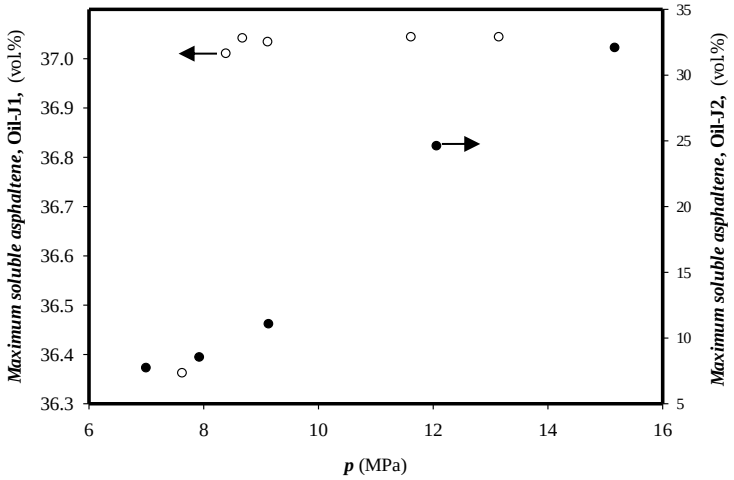

(**a**) Oil-J1

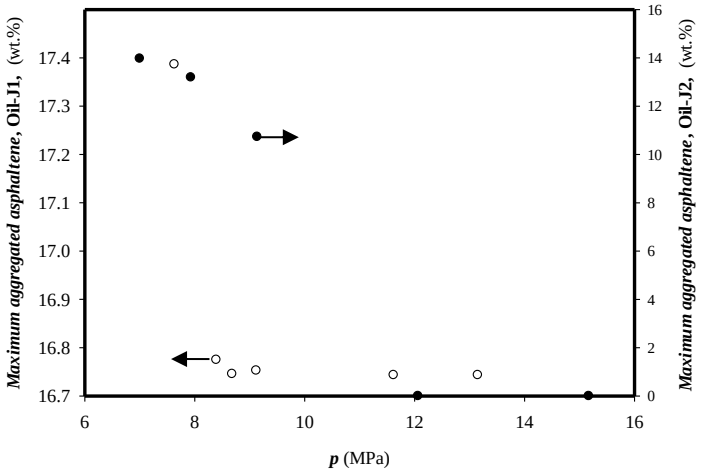

(**b**) Oil-J2

Fig. 2.3 Estimated maximum soluble and aggregated asphaltene

With the belief that asphaltene is in suspension in the crude oil and its stability is controlled by the concentration in sCO_2 within the oil-rich phase, then the solubility parameter of asphaltene phase could support our results. Porte et al. (2003) suggested that the dispersion forces between the slug and oil act upon the polarizability of either sCO2 and/or oil. To which, one should account the oiliness of the oil (i.e. *C/H* ratio).

Table 2.2 Results of aggregated asphaltene during sCO_2 injection[a]

	Deposited asphaltene ($\times 10^2$ wt. %)			
	At the bubble-point pressure [a]	At the end of gas injection [b]	Flue gas [b]	Relative deposition[c], (%)
Oil-J1	16.7	6.6	-	11.9
Oil-J2	4.90	2.0	0.04	3.51

[a] Estimated from the thermodynamic model (Nguele et al., 2016a, 2016d);
[b] Determined by oil titration; [c] Relative deposition (%) = 100× deposited asphaltene at bubble-point pressure / estimated asphaltene in the feed oil (Hu et al., 2004).

Therefore, the attraction between the asphaltene molecules and the polar CO2, due to the weak Van Der Waals forces, favor the aggregation of asphaltene molecules. This results invariably to an increase in its concentration within the oil-phase. Furthermore, these results showed to a certain degree, the potential of sCO_2 as aggregating (or flocculating) agent, which could be beneficial to oil industry were the dissolution of waxy materials are required.

2.5.1 Effect of the slug composition

To study the effect of slug composition on asphaltene solubility, we considered not only the injection of pure sCO_2 (performed experimentally), but also that of an impure sCO_2 that was modeled. An impure gas was defined as sCO_2 diluted with a lean gas. In this assumption, we simulated the results for two impure gases including sCO_2 enriched with methane (CH_4) and sCO_2 enriched with a mixture of ethane (C_2) and propane (C_3). The two gases were mixed at a ratio of 1:1 (v:v). The results are presented in Fig. 2.4.

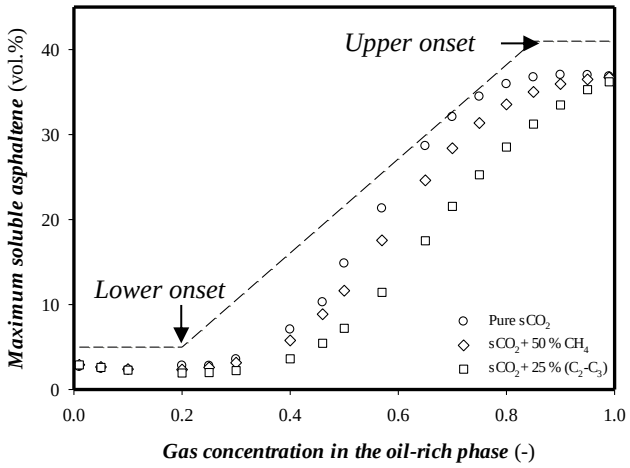

(**a**) Oil-J1

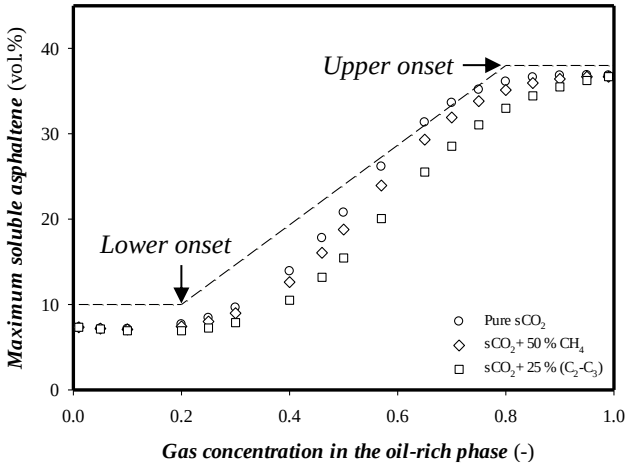

(**b**) Oil-J2

Fig. 2.4 Sensitivity analysis of slug purity on asphaltene solubility

Our analysis revealed that the gas composition plays a key role in the alteration of the solubility of asphaltene in the oils. The solubility of asphaltene increased with the concentration of slug within the oil. Regardless the oiliness of the crude oil; asphaltene was found less soluble in the candidate oil when an impure gas was used. Fig. 2.4 conveyed interesting insights on the behavior of the gas when it contacts the candidate oils:

The solubility of asphaltene follows an *S*-shape for both candidate oils regardless the purity of the slug. The shape described somewhat the behavior of the gas. At this point, it seems that the oiliness of the oil, rather than its chemical composition, governed the shape of asphaltene solubility and to a further extent the degree of solubility of the asphaltene molecules. Fig. 2.4 revealed further that at the bubble-point pressure, if the slug concentration is low enough, then an aggregation of heavy fractions might be promoted. However, rather to deposit, the aggregates re-dissolve presumably because of the weak thermodynamic equilibrium. We defined the concentration at which the aggregates started to re-dissolve (or to disaggregate) and later to flow as suspended particles within the oil as *lower onset concentration.* It was further seen that the disaggregation continued until a concentration in gas at which asphaltene was found totally miscible within the oil. The concentration was termed as *upper onset concentration*. Both lower and upper concentrations were chosen by analogy to lower/upper onset pressure (Tarek, 2007). These results suggested also that the composition of the candidate oil would enhance the flocculating potential of sCO_2.

At a fixed concentration of the slug, we found an average decrease in asphaltene solubility of 24 and 12% in Oil-J1 and Oil-J2 respectively (Fig 2.5). These results were observed when the minimum miscible pressure (MMP) of sCO_2 increases only of about 2% (that was the computed MMP of sCO_2+CH_4). Similarly, aforementioned values were 7% lower when the MMP decreased of only 0.13%. In practice, it is convenient to inject a gas of which MMP is low. Therefore, we estimated the theoretical MMPs of the gas investigated using Yuang's correlation for pure sCO_2 and Sebatian's correlation for impure gases (Sebastian et al., 1985; Yuan and Johns, 2005). The estimated MMPs were plotted then against the experimental onset concentrations. The results, Fig. 2.5, showed that if the sCO_2-EOR should be implemented in respect of the mitigation of asphaltene deposition, the preferential order should seemingly followed sCO_2 > sCO_2+Lean gas > sCO_2+CH_4. However, it should be highlighted that both *lowe*r and *upper onset concentrations* were fairly altered by the impurity of gas.

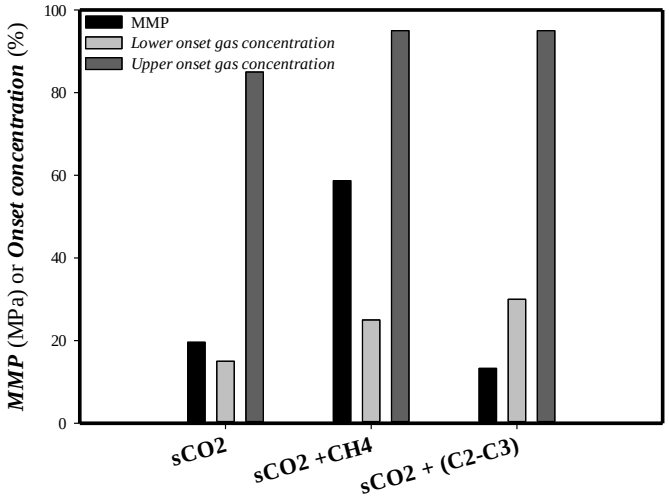

(**a**) Oil-J1

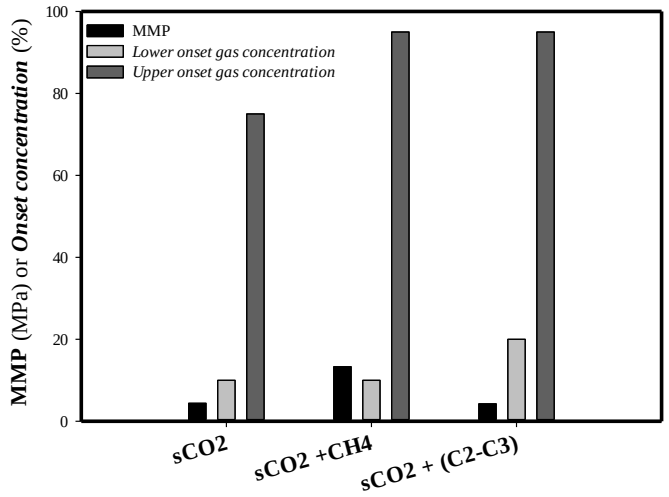

(**b**) Oil-J2

Fig. 2.5 Onset concentrations as function of MMP

2.5.2 Pseudo-equilibrium temperature

Temperature is a parameter believed to have a lesser impact to asphaltene aggregation compared to reservoir pressure and oil composition. However, if asphaltene is considered in suspension in oil, thus its thermodynamic stability (i.e. aggregation and/or dissolution) should be a function of the temperature (Holmberg et al., 2002). This means that upon injecting sCO_2, the pseudo-thermodynamic equilibrium, which is reached within the oil-bearing matrix, will influence the concentration in asphaltene. Taking in account these considerations, three temperatures (40, 55 and 70^{o}C) were selected. It is worth highlighting that 55^{o}C was assumed to be the temperature of the candidate formation. The results are illustrated in Fig. 2.6.

Therefrom, it is suggested that given a same slug, the higher temperature, the lower the asphaltene solubility and inversely the higher the amount of aggregated asphaltenes. Both

lower and *upper concentrations* for all investigated samples were less altered by the change in temperature. Furthermore, the onset concentrations were found dependent of the nature on the oil. We observed that the solvating power of sCO_2 increased with the temperature. Considering the fact sCO_2 solubility was higher in lighter crude, these observations probably explain the results in Fig 2.6. Not only the dipole-dipole forces between sCO_2 and the asphaltene molecules were weakened, but also the solvating power of the asphaltene-phase (represented herein by solubility parameter) decreases with the temperature. Therefore, it is rational to expect that the behavior of the slug change between the two onsets concentrations prompting the re-dissolution of asphaltenes (Fig. 2.4). However, it should be noted that the mechanisms discussed above, are inherent to the initial concentration of the residual oil in asphaltene.

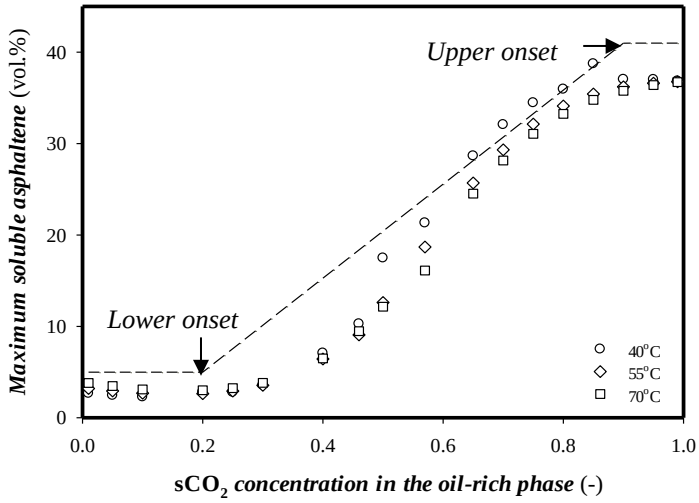

(**a**) Oil-J1

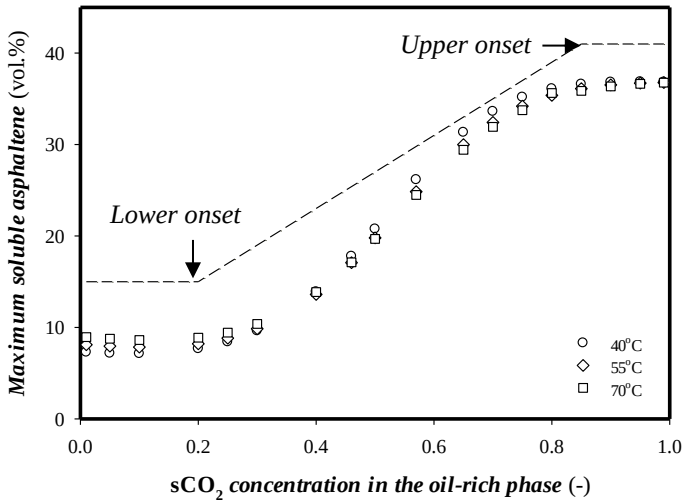

(**b**) Oil-J2

Fig. 2.6 Effect of reservoir temperature on asphaltene aggregation

This primary analysis has highlighted the technical feasibility of sCO_2-EOR. However, special care is required notably during the gas injection. Unfortunately, the initial concentration in asphaltene in the candidate heavy oils and the geometry of the formations are not suited for sCO_2-EOR.

2.6 Summary

A preliminary study for the potential of miscible sCO_2-EOR for the candidate heavy oils was performed in respect of gas solubility and asphaltene deposition was discussed in this chapter. Their pertaining mechanisms were tentatively explained. Using the candidate heavy oils, a pure CO_2 was injected at both sub-critical and supercritical conditions. Two thermodynamic algorithms, developed from the crude oil assays, were used to account the concentration in CO_2 in the oil-rich phase and the volume of aggregated asphaltene. The key findings are listed below:

(1). The solubility of CO_2 and sCO_2 were strongly influenced by the oiliness of the candidate oil and the injecting conditions. The mechanism of dissolution of CO_2 (or sCO_2) was inherent to the kinetics and the stability of the equilibrium of intermolecular forces developed between slug and candidate heavy oil during the development of the miscibility front. This mechanism is enhanced when CO_2 was at its supercritical state, which yields invariably to a higher bubble-point pressure.

(2). Heavy oil swelling, and thus the foaminess of the oil, prompted by dissolved gas, increased linearly with the slug solubility. Two thermo-physical parameters including *proportional coefficient of gas solubility* and *correction factor* were defined. The former gave an insight of the rate at which swelling occurs while the latter suggested how the miscibility front is developed within the cell.

(3). The solubility parameters of asphaltene-phase decreased with the increase in saturation pressure, which itself enhanced the solvating strength of sCO_2. Both phenomena, occurring concurrently, caused invariably a more soluble asphaltene.

(4). The concentration and purity of sCO_2 force asphaltene solubility to increase following an *S*-shape. Near the bubble-point pressure, and depending on oil composition, sCO_2 developed a potential as either a flocculent or a coagulant.

(5). Pseudo-equilibrium temperature altered the solubility parameter of asphaltene and that of sCO_2, which prompted the re-dissolution of candidate heavy oils.

(6). SCO_2-EOR has a potential for the candidate oils in respect of the properties, however constringent injection considerations are required.

Chapter 3.
HEAVY OIL PRODUCTION BY CHEMICAL METHODS

3.1 Chemical Recovery: Background

A chemical method, among the existing EOR techniques, involves the injection of a chemical, which supplements the natural reservoir energy by interacting with the rock-oil-brine system. This creates favorable conditions for maximum oil recovery (Green and Willhite, 1998). These interactions EOR involve generally the lowering of the interfacial tension (IFT), the rock wettability alteration and a favorable phase behavior. The sequential steps in a classical chemical-EOR are schematized in Fig. 3.1.

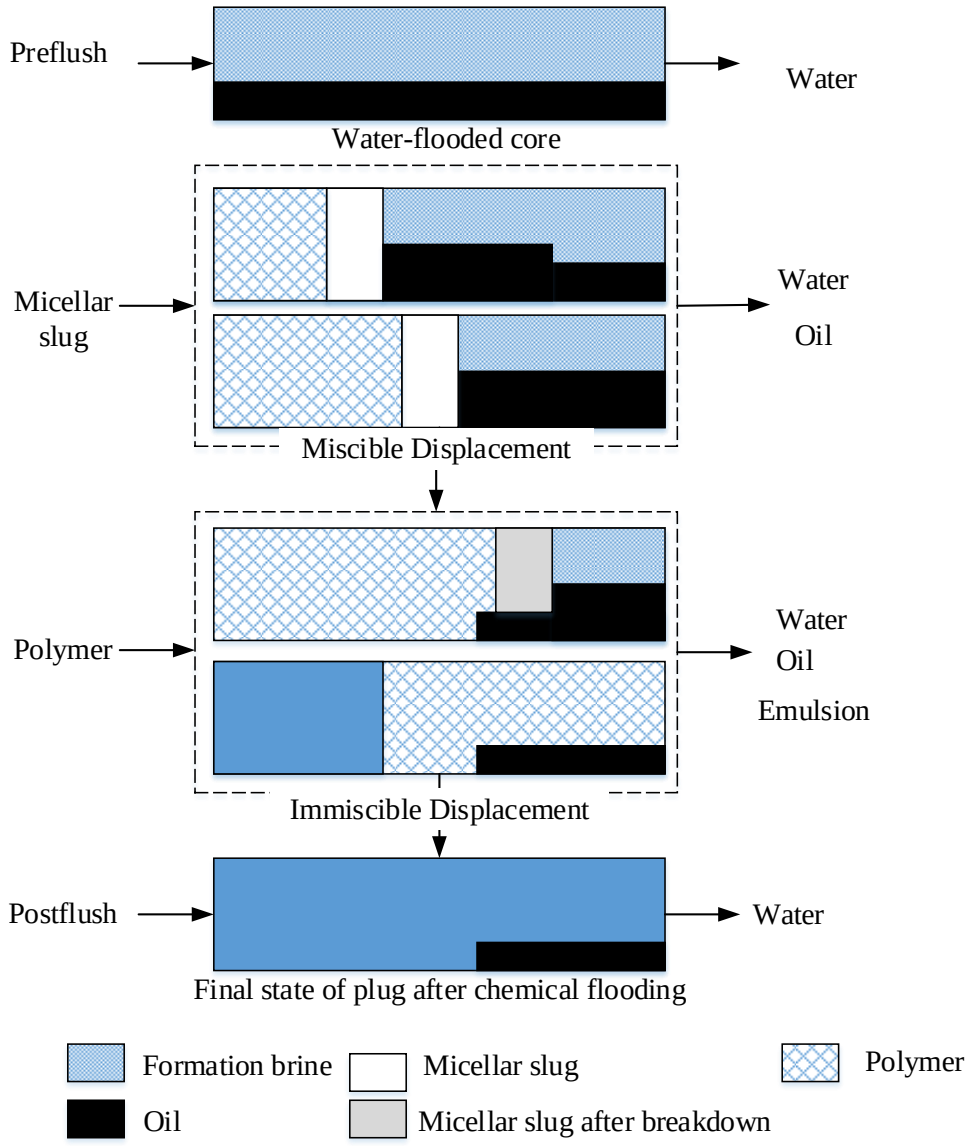

Fig. 3.1 A schematic representation of a typical chemical-EOR; adapted from Green and Willhite (1998)

The reservoir is pre-flushed usually with a low-saline water (also called buffer solution) of which purpose is to neutralize the divalent ions that reduce the efficient of the slug. The slug could be a surfactant, an alkali, a polymer or a combination of them. In principle, the surfactants are used primarily to lower the oil-water IFT and to modify the wettability of the reservoir rock. They can be either water-based or gas-based. If the slug is primarily made up from an alkali, the underlying mechanism is the in-situ generation of soap and the increase of pH. In the former approach, they are blended with the preflush to give a method referred as enhanced water flooding. In the latter case, however, the chemical-EOR is referred as the foam-EOR.

It is worth mentioning that either of these chemicals can be combined to complement each other in various forms of recovery methods. At the trail of slug, a viscous water (also refers as postflush or chase water) is injected. The main purpose is to keep the mobility control. Adding a gentle amount of polymers thickens the viscosity of the water. Despite the high potential of chemical-EOR in increasing recovery, it only accounts for less as far as the recovery of heavy crudes is involved. With the development of surface chemistry, it has been shown that a certain class of surfactants could even lower the IFT, to what is defined, as ultra-low IFT i.e. lower than 10^{-3} mN/m. These surfactants are referred as Gemini surfactants (GS). The laboratory trials reported that GS reduces better the oil viscosity compared to monomeric surfactants having the same alkyl chain.

3.2 Gemini Surfactants: A New Class of Surfactants for Heavy Oil Recovery

A GS is defined as a surfactant made up of two amphiphilic moieties connected at the level of, or close to, the head groups by a spacer group (Sekhon, 2004). GS was first reported in 1971 when Bunton et al (1971) synthesized bis-quarternary ammonium halides. These surfactants were referred then as bipolar surfactant or bis-quarternary ammoniums. It was found later that GS have a better bactericidal activities compared to their monomeric counterparts (Devinsky et al., 1985).

A typical GS consists of three main parts including a hydrophobic tail, a hydrophilic head and spacer (Fig. 3.2). This chemical structure justifies the code *m*-*s*-m commonly used for GS, in which *m* is the number of carbon in the tail and *s* the spacer. The position of the spacer plays an important role in the surface activity of the GS.

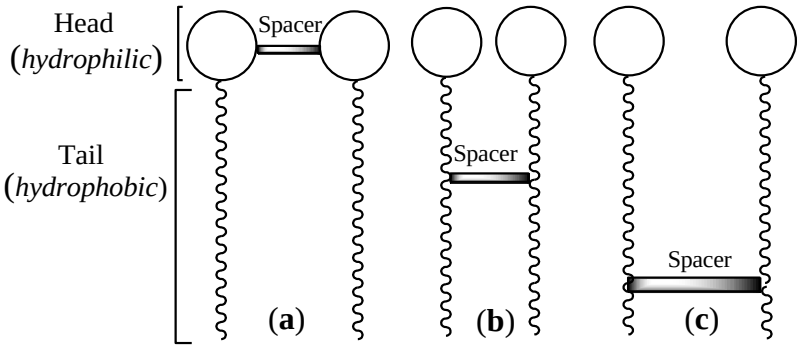

Fig. 3.2 Chemical arrangement of dimeric Gemini surfactant showing the position of spacer

The link between the two monomers could be located either between the two active heads (Fig. 3.2a), or in between the hydrophobic chain (Fig. 3.2b) or even towards the end of the tail (Fig. 3.2c). In the latter case, GS is said to be in its bola-form surfactants with a branched alkyl chain, and they do not show many interesting properties (Gao, 2012). GS can be synthesized in such a way that its hydrophobic tail has a variable length. Moreover, the polar group of a conventional GS is anionic (Fig. 3.3a), cationic (Fig. 3.3b) or nonionic also referred as zwitterionic (Fig. 3.3c).

The interesting features developed by GS have attracted much attention as potential agents in various industrial applications. The recent development reported the synthesis of trimeric-type (*m-s-m-s-m*) to multi-armed, poly-ionic, or even oligo-meric Geminis (Diamant and Andelman, 2003; Gao and Sharma, 2013; Yoshimura et al., 2004; Zana, 2002). Menger et al.(2000) reviewed that cationic Gemini surfactants can be readily synthesized by heating a mixture of the reagents in dry ethanol under reflux for two or three days and purifying the product by recrystallization.

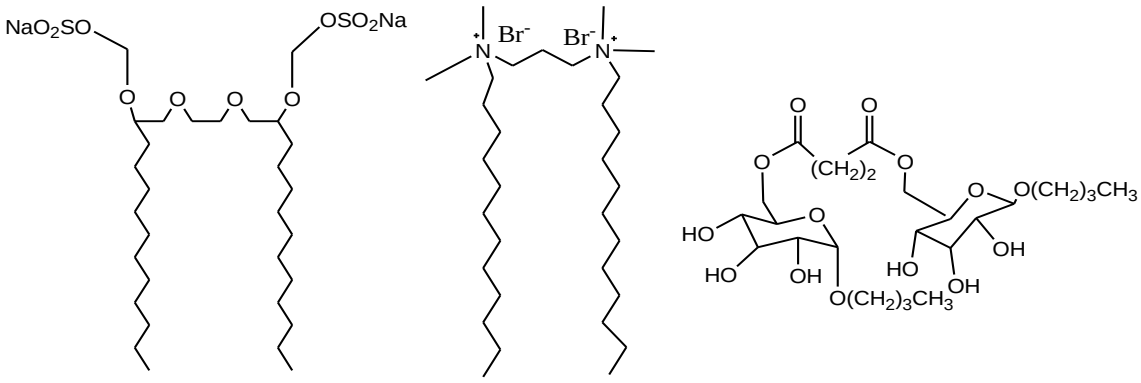

(**a**) Sulfate Gemini surfactant using propylene sulfonate (Gao and Sharma, 2013)

(**b**) Ammonium Gemini surfactant using dibromo compound (Nguele et al., 2015a)

(**c**) Ester-linked Gemini surfactants from butyl glucopyranosides (Castro et al., 2002)

Fig. 3.3 A sample representation of different types of Gemini surfactant representation

On the other hand, anionic surfactants are synthesized primarily from sulfonates materials. For EOR applications, anionic surfactants show consistently low adsorption at neutral to high pH on both sandstones and carbonates and are generally preferred over cationic surfactants. This explains why cationic surfactants are generally used as cosurfactants in surfactant flooding. They could be used as chemical agents to promote wettability alteration from oil-wet to water-wet in a carbonate formation (Sheng, 2011). Cationic surfactants are unfortunately disfavored because of their strong adsorption in sandstone rocks. This latter reason limits their application in most oil sandstone reservoirs.

3.3 Specific Properties of Cationic Gemini Surfactants in Respect of Improved Oil Recovery

The unique properties of cationic GS included a low micelle formation, a high oil and water solubilization and greater emulsifying properties compared to their monomeric counterparts. These singular features are beneficial to oil industry and would be elaborated in the following sections.

3.3.1 Critical micelle concentration

Critical micelle concentration (CMC) defines the exact concentration at which micelles (or aggregates) are formed. This parameter has a great importance when surfactant is to be considered for chemical-EOR. It is reported that the CMC of Gemini are much lower than their monomeric counterparts with the same length in alkyl chain. CMC is reported not only to be dependent on the chemical structure of the surfactant, but more interestingly to the spacer group (Table 3.1).

Zana et al.(1991) hypothesized that the nature and length of the spacer group influence the type and the shape of micelles. Both features define the CMC. It is important to notice that the lower the CMC, the higher the surface tension. During a typical chemical flooding, the slug targets the reduction IFT to a value low enough to decrease the mobility ratio.

Table 3.1 Basic properties of some bis-quaternary alkylammonium chlorides[a]

Length of the alkyl chain	*CMC* (*10^{-3} mol)	σ_{CMC} (mN/m)	$Foam_{@0min}$ (mL)
10	3.2	36.5	40
12	0.78	37.0	280
14	0.14	39.0	270
16	0.02	42.2	100

[a] CMC: critical micelle concentration; σ_{CMC}: surface tension at the CMC. The data taken from Kim et al.(1996)

The lowest IFT is referred as ultra-low IFT and is within the range of 10^{-3} mN/m. Also, the laboratory investigations have revealed that the ultra-low IFT is usually reached at the CMC above which the residual oil is either solubilized or emulsified (Sheng, 2010). This is so because the GS has the tendency to pack closely at the interface oil/water compared to the monomer counterpart. This property promotes a monolayer adsorption of the surfactant molecules at the said interface in a manner to achieve an ultra-low IFT (Gao, 2012).

3.3.2 Solubilizing and emulsifying potential

A micellar slug injected, above its CMC, promotes usually induces either a solubilization or emulsification of the residual oil. It is not rare that both phenomena occur concurrently. The slug prompts the formation of emulsions, which are either be very stable if a high viscous polymer is used as slug or the residual oil has a high content in acid materials or unstable (Sheng, 2011). These mechanisms are crucial in mobilizing the untapped crude oil especially if the residual oil has a naphthenic-based nature (heavy oil for example).

In this regard, Dam et al. (1996) showed that cationic GS are better solubilizing agents than conventional surfactants, which is so because of the shape of the micelles yielded during the micellization process. For instance, the literature reports that when the micelles take a tubular shape, the tendency for oil solubilization is tremendously enhanced. Using toluene and hexane as synthetic oil, Dam et al. (1996) concluded that oil solubilization is significantly higher when a GS is used than conventional surfactants. Additionally, the emulsifying strength of GS have been highlighted by Yoshimura et al. (2013) who reported the formation of stable emulsions from amino-based GS. Using squalane oil ($C_{30}H_{62}$), they found that GS has a better emulsifying propensity.

3.3.3 Corrosion inhibitor

During the production life of an oilfield, the water cut of oil well ascends quickly and the corrosion of oil well arises a serious threat to the production. Routinely, a corrosion inhibitor is usually injected in the reservoir. The problem here lies on the cost and the efficiency of the corrosion inhibitor. In order to provide an alternative, Achouri et al. (2001) investigated the potential of cationic GS as corrosion inhibitor. The study was conducted in a strong acidic environment (HCl, 1 M). Their results showed that cationic GS acts mainly as cathodic inhibitor by adsorbing on the electrode surface and forming a protective layer.

3.4 Experimental Section

3.4.1 Materials

3.4.1.1 Synthetic oil

We assessed the solubilizing (or emulsifying) potential of the micellar slug using a synthetic crude oil, which was prepared from hexadecane, decane and ethylbenzene at a fixed ratio of 60/30/10 (% volume).

3.4.1.2 Surfactants

The cationic slugs were formulated from two lyophilized cationic Gemini surfactants. The surfactants had a white color and were coded as *12-3-13* and *16-3-16* in respect of the length of the hydrophobic tail and the spacer. Fig. 3.4 illustrates the chemical structures with their respective IPUAC names (Favre and Powell, 2013). *12-3-13* and *16-3-16* were synthesized, and supplied by Lion Corporation (Tokyo, Japan).

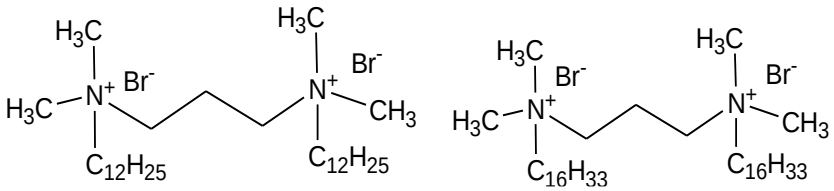

(**a**) *12-3-13* or Trimethylene-1, 3-bis (dodecyl dimethyl ammonium bromide)

(**b**) *16-3-16* or Trimethylene-1,3-bis(hexadecyl dimethyl ammonium bromide)

Fig. 3.4 Chemical structure of investigated cationic Gemini surfactants

The properties are shown in Table 3.2. The surfactants were 99.9% pure and were used as received.

Table 3.2 Physical properties of investigated cationic Gemini surfactants [a]

Surfactant	*Type*	Purity (%)	Free NH_3 (%)	*MW* (g/mol)
12-3-12	Cationic	97.1	0.2	630.1
16-3-16		96.8		740.6

[a] *MW*: molecular weight

3.4.1.3 Brine solutions

The composition and properties of brine solutions are summarized in Table 3.3.

Twelve brine solutions were prepared, in-house primarily at 25°C, from sodium chloride (NaCl, 99.99% pure), calcium chloride ($CaCl_2$, 99.99% pure), magnesium chloride hexahydrated ($MgCl_2$,$7H_2O$, 99.99% pure), sodium hydrogenocarbonate ($NaHCO_3$, 99.99% pure), potassium chloride (KCl, 99.99% pure) and magnesium sulfate ($MgSO_4$, 99.99% pure).

Table 3.3 Chemical composition and properties of brine solutions [a]

B1	B2	B3
Na^+: 983; Cl^-: 1517; TDS: 2,500; *MW*= 18.10 g.mol^{-1}.	Na^+: 1,967; Cl^-: 3,033; TDS: 5,000; *MW*= 18.20 g.mol^{-1}.	Na^+: 2,950 Cl^-: 4,550; TDS: 7,500; *MW*= 18.30 g.mol^{-1}.
B4	B5	B6
Na^+: 3,934; Cl^-: 6,066; TDS: 10,000; *MW*=18.41 g.mol^{-1}	Na^+: 5,901; Cl^-: 9,099; TDS: 15,000; *MW*=19.22 g.mol^{-1}	Na^+: 7,868; Cl^-: 12,132; TDS: 20,000; *MW*=18.81 g.mol^{-1}
B7	B8	B9
Na^+: 11,802; Cl^-: 1 8,198; TDS: 30,000; *MW*=19.22 g.mol^{-1}	Na^+: 17,703; Cl^-: 27,297; TDS: 45,000; *MW*=19.82 g.mol^{-1}	Na^+: 23,604; Ca^{2+}: 79; Cl^-: 36,431; TDS: 60,115; *MW*= 20.21 g.mol^{-1}
B10	B11	B12
Na^+: 1,472; Ca^{2+}: 123; Mg^{2+}: 79; Cl^-: 48,558; TDS: 80,231; *MW*= 21.04 g.mol^{-1}	Na^+: 47,207; K^+: 42; Ca^{2+}: 159; Mg^{2+}: 120; Cl^-: 72,918; TDS: 120,443; *MW*= 22.38 g.mol^{-1}	Na^+: 59,011; K^+: 58; Ca^{2+}: 202; Mg^{2+}: 160 Cl^-: 91,160; HCO_3^-: 44; TDS: 150,635; *MW*= 23.55 g.mol^{-1}

[a] Na^+: sodium ion; K^+: potassium ion; Ca^{2+}: calcium ion; Mg^{2+}: magnesium ion; Cl^-: chloride ion; HCO_3^-: hydrogenocarbonate ion; SO_4^{2-}: sulfate ion; TDS: total dissolved solids; all concentrations are given in ppm.

3.5 Methods

3.5.1 Preparation of aqueous slugs from cationic Gemini surfactants

Given the lyophilized form of the supplied surfactants, we aimed first at determining their solubility in aqueous phase. For this purpose, low saline water was considered as base fluid. For commercial considerations, we targeted to formulate the aqueous slugs of which concentrations were 0.25 and 0.15 wt. % for *12-3-12* and *16-3-16* respectively. The experimental sequence was as follows:

(1). Measure accurately 0.127g and 0.076 g of *12-3-12* and *16-3-16* respectively.

(2). Prepare a base fluid of which concentration is 2 wt. the base fluid was divalent ions-free.

(3). Dissolve *12-3-12* (or *16-3-16*) in the base fluid.

(4). Stir the mixture for a minimum of 2 hours until a complete dissolution is achieved (if any).

(5). Allow the solution to equilibrate overnight.

At this stage, we observed that neither *12-3-12* nor *16-3-16* could be dissolved fully in the base fluid (Fig. 3.6a). Thus, in order to increase the solubility of a surfactant, a third chemical must be added. The literature reports that the added chemical is usually a low-molecular weight alcohol, which is known as *cosolvent* or *cosurfactant*. Both terms, often used loosely, are distinguished actually by their functions in the base fluid.

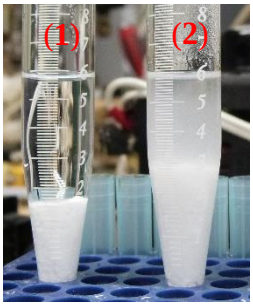

(**a**) Gemini surfactant in 2wt.% NaCl; (1) *12-3-12* and (2) *16-316*

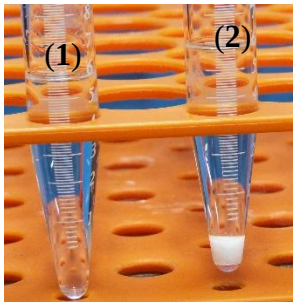

(**b**) Gemini surfactant in (2wt.% NaCl + TBA); (1) *12-3-12* and (2) *16-316*

Fig. 3.5 Solubility of *12-3-12* and *16-3-16* in different base fluids

In this chapter and throughout, the added chemical will be referred as *cosurfactant* as we aimed at enhancing the solubility of the GS. We investigated a wide array of chemicals including among which only four solvents were selected based on the dissolution of Gemini surfactants (Fig. 3.6b). These include a low molecular weight alcohol (methanol or MeOH), a branched alcohol (ter-butyl alcohol or TBA), a polysorbate (Tween 20) and an ionic solvent (NaOH). All the solvents had a purity of 99.9% and were used as received. The experimental sequence, using the selected solvents, was as described below:

(6). Prepare a new base fluid of which concentration of 1% using the former base fluid and either of the solvent

(7). Repeat the steps #1 ~ #5.

Eight different micellar slugs were prepared therefrom. Their physico-chemical properties are outlined in Table 3.4.

Table 3.4 Physico-chemical properties of micellar slugs[a]

Gemini surfactant		Cosurfactant		Slug								
C_0 (wt.%)		Type	C_1 (wt.%)	C_T (mM)	*MW* (g.mol^{-1})		*ρ* (g/cm^3)		*pH* (-)		Experimental Code	
0.25[b]	0.15[c]	MeOH	1.0	54.2	21.2[b]	20.8[c]	1.026[b]	1.025[c]	9.80[b]	7.30[c]	R$^{2\,b}$	H$^{2\,c}$
		Tween 20		53.9	34.5[b]	32.8[c]	1.076[b]	1.093[c]	4.10[b]	4.50[c]	R$^{3\,b}$	H$^{3\,c}$
		NaOH		54.4	21.4[b]	21.0[c]	1.018[b]	1.100[c]	12.3[b]	12.3[c]	R$^{4\,b}$	H$^{4\,c}$
		TBA		54.2	22.1[b]	21.7[c]	1.065[b]	1.012[c]	7.10[b]	7.80[c]	R$^{5\,b}$	H$^{5\,c}$

[a] C_0: concentration of Gemini surfactant; C_1: concentration of cosurfactant; C_T: concentration of the slug; *MW*= molecular weight of slug solution; *ρ*: its density; pH= its potential in hydrogen;
[b] R^x designed the formulations prepared from *12-3-12*;
[c] H^x labeled designed the formulations prepared from *16-3-16.*

3.5.1.1 Critical micelle concentration

Static surface tension and the critical micelle concentration (CMC) were determined using capillary rise method. Throughout the test, the tubes were immersed in a water bath, which temperature was kept constant at 25^{o}C. The rise of the liquid between the surface of the tube test and the meniscus formed by the liquid inside the capillary tube was read. For each measurement, the experiment was repeated until successive values agreed within a value of 0.01 cm. To avoid any form of contamination aforementioned, the capillary tube test was replaced to a new one after each measurement. The readings were used further to compute the surface tension,

$$\sigma = 1/2\,\rho g r h \tag{3.1}$$

where ρ is the density of the slug (in g/cm^3), r is the radius of the capillary tube (in cm^3), h is the rise of the liquid due to the capillary forces, (in cm^3) and g is gravity (in cm/s^2).

3.5.1.2 Solubilization potential

The experimental sequence is described below:

(1) Introduce 4 ml of synthetic oil and 4 ml brine (B1 – B12) solution in a graduated tube test.
(2) Add 1 ml of R^x (or H^x). H^5 was used for this trial test.
(3) Agitate the tube test at a constant speed for a minimum of 2 hours.
(4) Allow the mixture to equilibrate at 40^{o}C for a minimum of 2 weeks.

3.5.1.3 Static adsorption determination

We quantified the slug retention following the methodology presented by Goddard et al. (2004). Four types of adsorbents were selected including dolomite, Berea sandstone, kaolinite and montmorillonite. The experimental procedure is described below:

(1). Crush and weigh approximately 7 g adsorbent.
(2). Dry the sample overnight at 120^{o}C to remove any form of water.
(3). Immerse, at a weight ratio of 1:20 v/v, the adsorbent into either R^x or H^x.
(4). Shake the mixture for 14 hours at 25^{o}C.
(5). Leave the tube tests to equilibrate for a minimum of 25 days.
(6). Collect the supernatant liquid for spectral analysis every week for 6 weeks.

UV-Visible spectrophotometer (Model 2450, Shimadzu, Japan) was used to perform spectral analysis. The concentration of the supernatant fluid was monitored and converted to adsorption using equation 3.2,

$$A_s = \left(\frac{C_0 - C_i}{W_a S_a} \right) r V_{slug} \tag{3.2}$$

where A_s is the adsorption of the slug (in mg/g-rock), C_o is the initial concentration of the slug, C_i is the concentration of the slug at the sampling time, ρ is the density of the supernatant fluid (in g/cm^3), V_{slug} is the added volume of slug, W_a the weight of the adsorbent (in g) and Sa the surface area of the adsorbent (cm^2/g).

3.5.1.4 Corrosion and inhibiting activity of dimeric quaternary ammonium salts

To evaluate the inhibiting potential of the slug, we selected for this purpose H^5 and Oil-J1. The detailed experimental procedure is described below:

(1) Introduce 10 mL of Oil-J1 in a cell of the PVT.
(2) Inject sCO_2. In this experiment, sCO_2 was injected at 8 MPa and 55^{o}C.
(3) Allow the gas to contact the oil until the saturation pressure is reached.
(4) Depressurize the cell and collect the foamy oil to perform infrared analysis.
(5) Mix Oil-J1 +H^5 at volume ratio 1:20.
(6) Repeat step #1 to #3 and allow the contact for a minimum of 14 days
(7) Repeat step #4.

The spectra analysis was conducted in on attenuated total reflectance Fourier Transform Infrared Spectroscopy (ATR-FT IR model 620, Jasco, Japan). The values obtained were based on transmittance with a wavelength scan ranging from 400–4000 cm^{-1}. The equipment was set at 16 scans with a generated spectrum having a resolution of 0.4 cm^{-1} for 3028 cm^{-1} in the band for methane.

3.6 Physico-Chemical Analysis of Aqueous Micellar Slugs

3.6.1 Surface tension and critical micelle concentration

The results of the surface tension measurements are shown in Fig. 3.6. Therefrom, it could be seen that the surface tension decreased sharply with the concentration. This pattern was observed for all the investigated slugs. The decrease was steady until the pattern changed abruptly (Fig. 3.6a) or remained fairly constant (Fig. 3.6b).

The summary of the experimental CMC, for all the prepared slugs, is outlined in Table 3.5.While comparing our CMC results presented herein with those published in the literature (Zana et al., 1991), the CMC of slugs blended with cosurfactant were 8 times lower in the average. Likewise, the CMC of the slug formulated with surfactant of different alkyl chain but with the same type of cosurfactant was 11% lower for the slugs prepared from *12-3-12*. The results suggested that the nature of the cosurfactant, the concentration in salt in the aqueous phase and the length of hydrophobic tail of the surfactant influence both the CMC and the static surface tension.

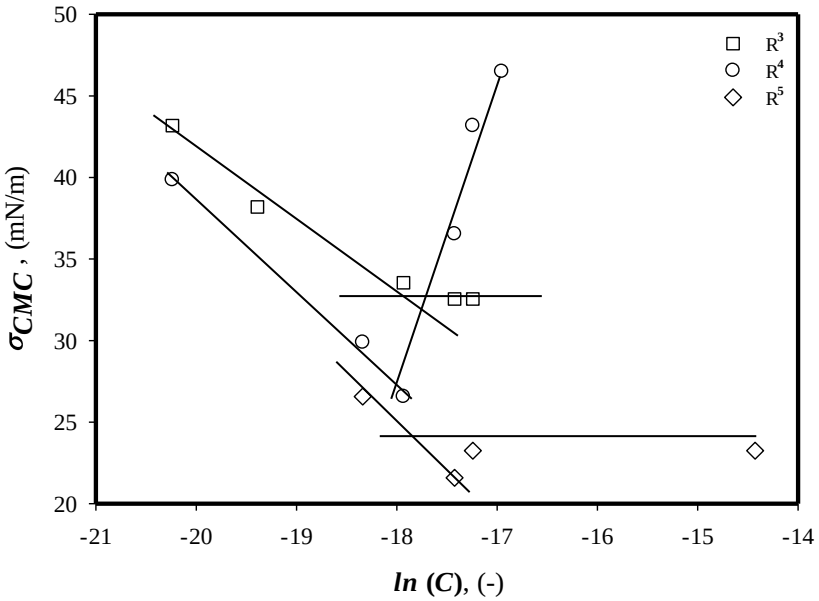

(**a**) R^x formulations

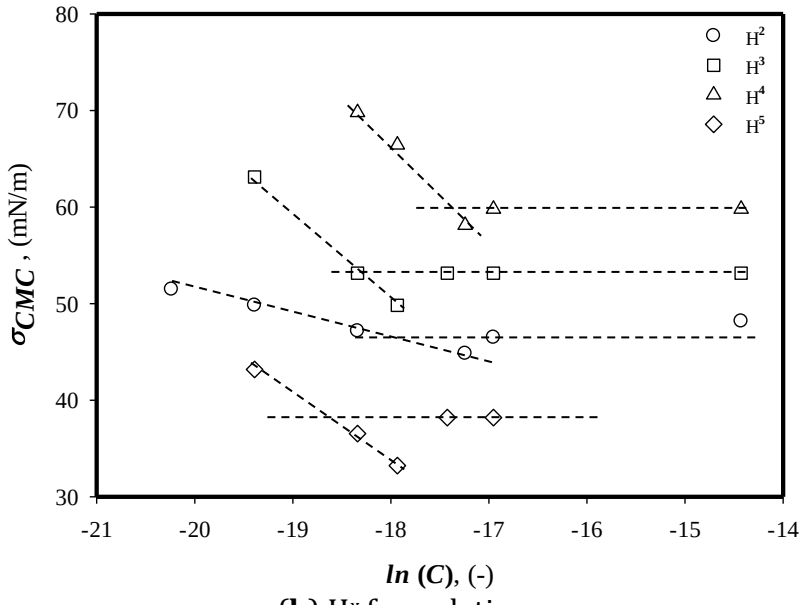

(**b**) H^x formulations

Fig. 3.6 Experimental determination of CMC of cationic slugs

Table 3.5 CMC and surface tension of investigated slugs in low saline water[a]

Slug	MW (g.mol^{-1})	CMC (*10^{-5} mol/dm^3)	σ_{CMC} (mN/m)
R^2	21.2	0.21	30.2
R^3	34.5	2.27	33.0
R^4	21.4	1.11	26.6
R^5	22.1	1.13	23.3
Zana et al (1991)[a]	-	11	40.0
H^2	20.8	2.16	46.0
H^3	32.8	0.84	52.0
H^4	21.0	1.68	60.0
H^5	21.7	0.62	37.5

[a] *12-2-12*

3.6.1.1 Effect of cosurfactant

From Table 3.5, it appeared clearly that the CMC is altered by the nature of the solvent used to enhance its solubility. In order to quantify the effect of the cosurfactant, we used the dielectric constant, which accounts its solvating strength. Two different patterns were observed therefrom (Fig. 3.7).

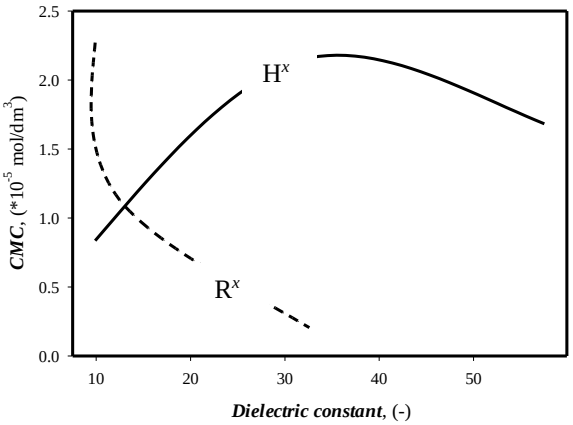

(a) CMC at 25° C in 0.5 wt.% NaCl

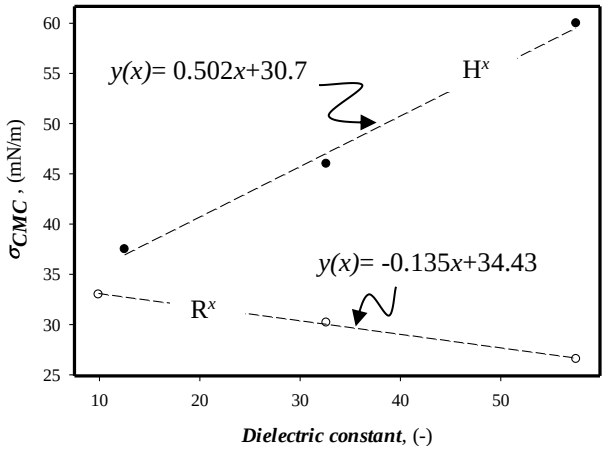

(b) Surface tension at the CMC at 25° C in 0.5 wt.% NaCl

Fig. 3.7 CMC and surface tension alteration as function of the dielectric constant of micellar slugs

3.6.1.2 Effect of salinity

In order to investigate the effect of the salt concentration, we selected four slugs including R^2, R^3, H^2 and H^3. We spanned the salinity from B2 to B12. The results are presented in Fig 3.9. The surface tension decreased steadily with the concentration in salt. It was interesting to see with the appearance in bivalent ions (M^{2+}) within the saline water, the surface tension of R/H^x decreased abruptly (Fig. 3.8a). Therefore, it could be inferred that the presence of M^{2+} acts upon the micellization process. In fact, we think that M^{2+} redistributes the ionic forces. Both mechanisms occur concurrently.

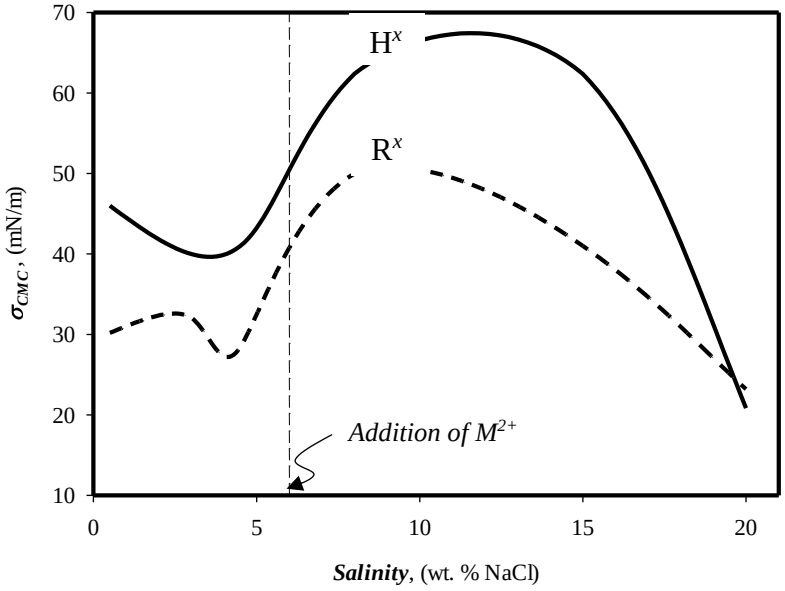

(a) R^x and H^x

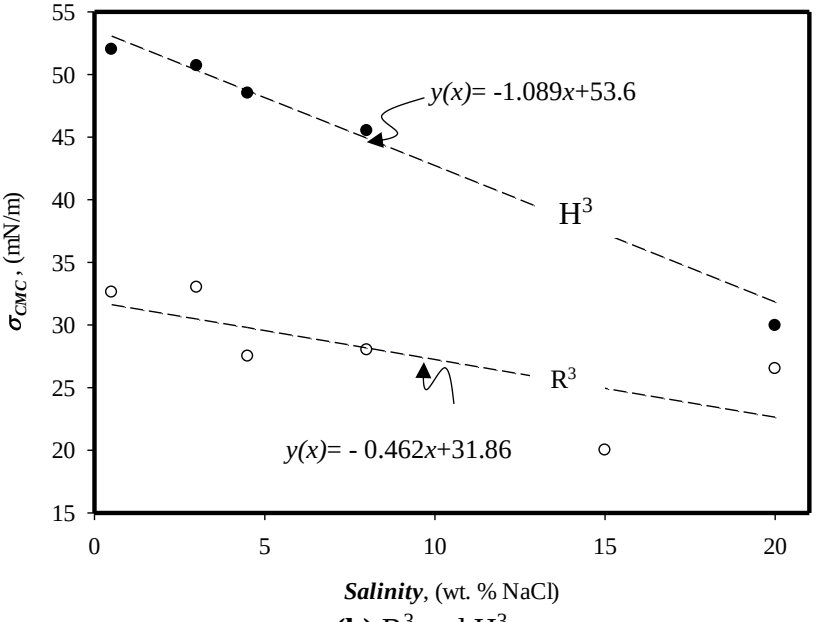

(b) R^3 and H^3

Fig. 3.8 Effect of salt concentration and divalent ions on CMC and surface tension

The observations discussed above, were contrasted when Tween 20 was used as cosurfactant (Fig. 3.8b). Rather, we found that the surface tension decreased monotonically with the increase in salt concentration and that in M^{2+} in the aqueous phase. The results conveyed here, showed that the micellar slugs formulated blended with Tween 20, are likely to withstand the reservoir brine composition if they were injected as slugs. From a thermodynamic point of view, the energy of micellization (ΔG^o_M) that is the energy requires for the micelles to form, gives deeper understanding of the differences.

The free energy of micellization is defined as,

$$\Delta G_M^O = (2-\alpha)RT\ln(CMC) \tag{3.3}$$

where ΔG^o_M is the free energy of micellization per mole of Gemini surfactant containing two alkyl chains (kJ.mol^{-1}), α is a constant based on the alkyl chain (α =0.21 for R^x and α =0.11 for H^x , (Gao, 2012); R is the gas constant (R= 8.314 J·mol^{-1}·K^{-1}); T is the temperature of the experiment (in K) and CMC is the critical micelle concentration of the slug (mol/m^3).

Fig. 3.9 shows that the energy, required for the micelles to form (also called the energy of micellization), is dependent of the alkyl chain and the spacer group (s) (Hua and Rosen, 1991; Nguele et al., 2015a). Depending of the length of the hydrophobic tail and the nature of the spacer, the polarity across the slug is redistributed. This means the more apolar is the spacer, the lower the static surface tension (Fig. 3.8b).

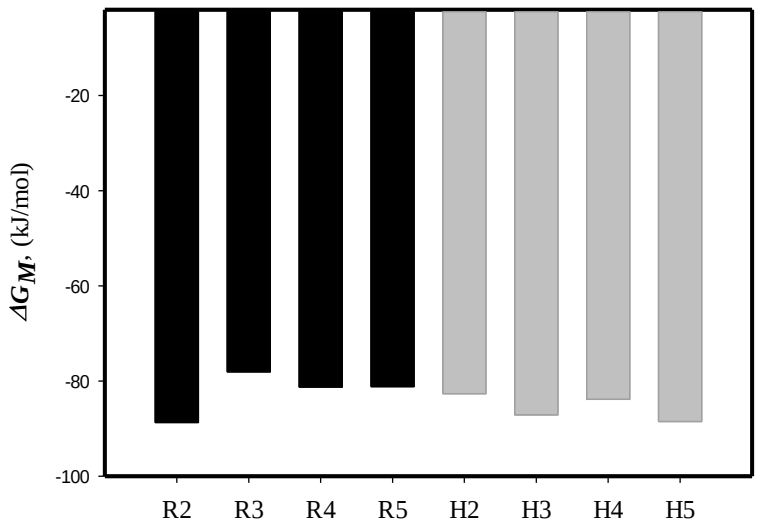

Fig. 3.9 Energy of micellization of slugs at 0.5 wt. NaCl%

Therefore, we can hypothesize that the increase in surface tension for H^x slug (Fig. 3. a) is plausibly due to its polarizability inherent to the length of its hydrophobic tail. The former phenomenon is concurrent with the micellization energy.

3.6.2 Evaluation of solubilization potential of cationic Gemini surfactants

Oil solubilization is an emulsion (or colloidal dispersion) distinguished by the size of the molecule. Prior evaluating the solubilizing potential of the slugs in the actual crudes, we performed a trial test on a synthetic crude oil; the results from this trial test are depicted in Fig. 3.10. The solubilization ratio of oil (V_o/V_s) and that of the water (V_w/V_s) were defined as the fraction of the volume solubilized crude oil or brine respectively to the volume of surfactant in the microemulsion phase. Both parameters were obtained by measuring the volume of each different phase of the microemulsion. V_o/V_s decreases with the increase in salinity and a reverse trend was observed for V_w/V_s. These patterns are well-established in the literature (Sheng, 2011).

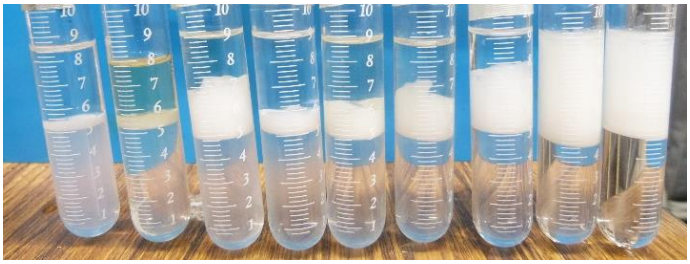

(**a**) Pictograph of solubilization trial test

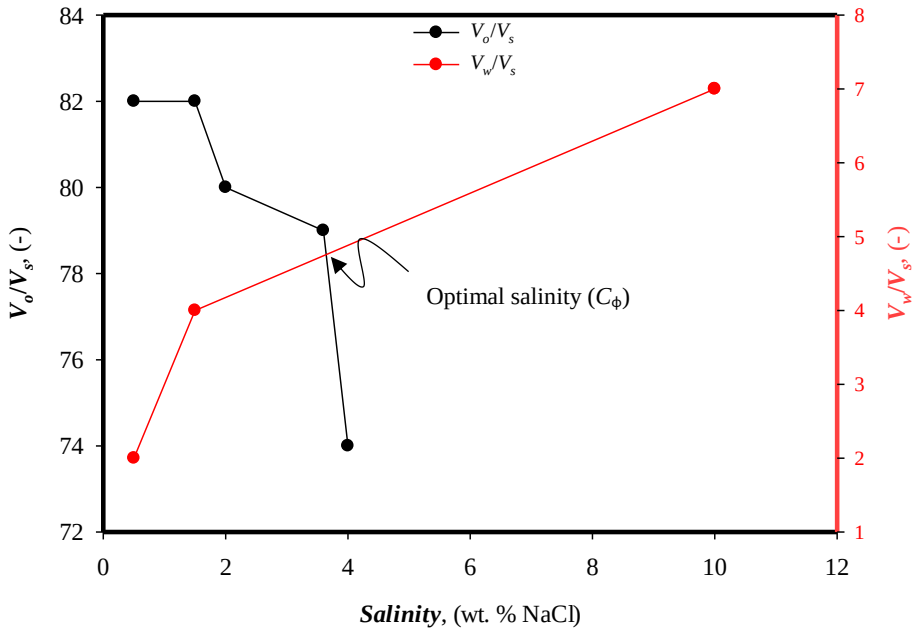

(**b**) Solubilization plot as a function of salinity

Fig. 3.10 Evaluation of solubilizing potential of H^5

The salinity, at which the two curves intercepted, is known to be the optimal salinity (C_ϕ). For this trial test, C_ϕ was found at 38,000 ppm. This point is of a great importance as far as the micellar flooding is concerned. It is reported that at the optimal salinity, the minimum achievable IFT is reached. Sheng (2011) reviewed that a value of V_o/V_s (or V_w/V_s) equal or greater than 10 is suitable to develop an ultra-IFT. From Fig. 3.10it could be seen that the investigated slug could withstand not a high salinity medium, but also it could develop a high solubilization potential. Based on these promising results, we spanned the investigations on the actual candidate oils.

3.6.3 Adsorption study at solid/slug interface

Surfactant retention or loss is one of the major drawbacks of chemical-EOR. The surfactant is adsorbed during its journey from the injector to the oil bank and it is enhanced by several factors including (*i*) the mineralogy of the adsorbent, (*ii*) the composition of the slug and (*iii*) the flow rate and the injecting conditions (Green and Willhite, 1998). Fig. 3.11 presents the results of static adsorption of R^4 in Berea sandstone as a function of time and the pH and the summary of the results is outlined in Table 3.6.

Based on the CMC results, both the adsorption amount of surfactant (Γ) and the minimum average area occupied by a molecule of surfactant (A) were computed using relations (3.4) and (3.5) respectively.

$$\Gamma_{cmc} = -\frac{1}{nRT}\left(\frac{\partial\sigma}{\partial \ln C}\right) \tag{3.4}$$

where Γ_{cmc} is the adsorption amount at the CMC (mol/m^2), $\left(\frac{\partial s}{\partial \ln C}\right)$ is the slope of the plot of surface tension vs. concentration, R is gas constant, (J/mol. K), T is the experiment temperature (K); n is a dimensionless value which depends on the number of species constituting the surfactant and the adsorbing (i.e. saline water). n=3 for dimeric-type surfactant (Davies and Rideal, 1961),

$$A_{CMC} = 10^{14} / \Gamma_{cmc} N \tag{3.5}$$

where Γ_{cmc} is the adsorption amount at the CMC, (mol/m^2), N is Avogadro's constant = 6.02 x10^{23} mol^{-1}.

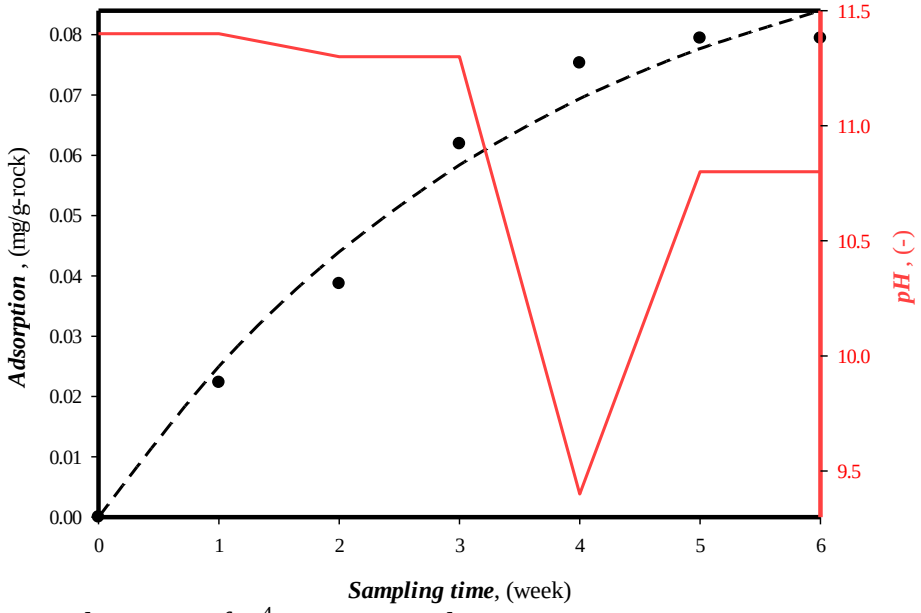

Fig. 3.11 Static adsorption of R^4 in Berea sandstone

The adsorption was found higher in kaolinite for all the investigated slugs while the lowest values were obtained in Berea sandstone. For example, an average adsorption of 0.419 mg/g-rock was observed when kaolinite was used as adsorbent. The value was lowered to 0.057 mg/g-rock when Berea sandstone was rather used (Table 3.6). The low content of clay in Berea sandstone, explains this large gap. A further analysis, in respect of the surface area occupied by the micelles and the micelle adsorption, shows that those parameters influenced the concentration of slug adsorbed. For example, an increase of about 63% in surface area (from R^4 to R^5) prompted the adsorption to increase of about 6% in Berea sandstone. Likewise, a surface area 28 times higher (from H^2 to H^5) yielded an adsorption in kaolinite of about 50%.

Table 3.6 Summary of static adsorption experiments[a]

Micellar slug properties			*Adsorption*	
Slug code	Γ_{cmc} ($\times 10^6$ mol/m^2)	A_{cmc} (Å^2. molecule^{-1})	Adsorbent	A_s (mg/g-rock)
R^2			Kaolinite	0.264
R^3	1.13	146.7	Dolomite	0.377
R^4			Kaolinite	0.419
	3.02	54.91	Berea sandstone	0.057
			Montmorillonite	0.151
R^5	8.08	20.55	Berea sandstone	0.060
			Dolomite	0.120
H^2	0.69	241.0	Kaolinite	0.291
H^3	3.02	54.91	Dolomite	0.367
H^4			Kaolinite	0.437
	19.4	8.565	Berea sandstone	0.024
			Montmorillonite	0.126
H^5	2.23	74.47	Berea sandstone	0.070
			Dolomite	0.080

[a] Γ_{CMC} slug adsorption at CMC; A_{CMC} minimum average area occupied the slug at the CMC

These results suggested that the larger micelles, the higher the adsorption, which could be enhanced by the surface area of the candidate adsorbent (e.g. kaolinite or montmorillonite) and/or the nature of the cosurfactant. Looking at the mineralogy of the adsorbent, dolomite, $CaMg(CO_3)_2$, in contact with reservoir water, dissolves to yield carbonate ions (CO_3^{2-}). Negatively charged, ions CO_3^{2-} attach preferentially to the hydrophilic head of the surfactant (-NH_4^+). Considering the mechanisms discussed earlier, the retention in dolomite, which decreased with the length in alkyl, is justified.

Moreover, it could be seen that the adsorption was 3% higher when R^3 was used instead of H3. Likewise, the adsorption was 2 times higher when R^5 was used instead of H^5. These increments were concomitant with minimum area occupied by the micelles. If one anlayzes Table 3.5 and Table 3.6 concurrently; it becomes obvious that the slug with the highest CMC adsorbed more on the dolomite.

3.6.4 Inhibiting potential of cationic Gemini surfactants

Fig. 3.12 shows the spectra obtained from infrared analyses. Three major regions of absorption were clearly noticeable at 3000 - 4000 cm^{-1} (strong), (1400-1700 cm^{-1} (strong) and 500-1000cm^{-1} (fair). The first band is characteristic of vibration of –OH. Pronounced after injecting sCO_2 injection comparatively to raw heavy crude, the peak hints at the occurrence of a chemistry that has invariably led to the build-up in hydroxylated materials. This point is supported by Okumura et al. (1990) who proved that peak is also characteristic of the vibration of solvated hydronium ions i.e. $H_3O^+ \cdot (H_2)_n$.

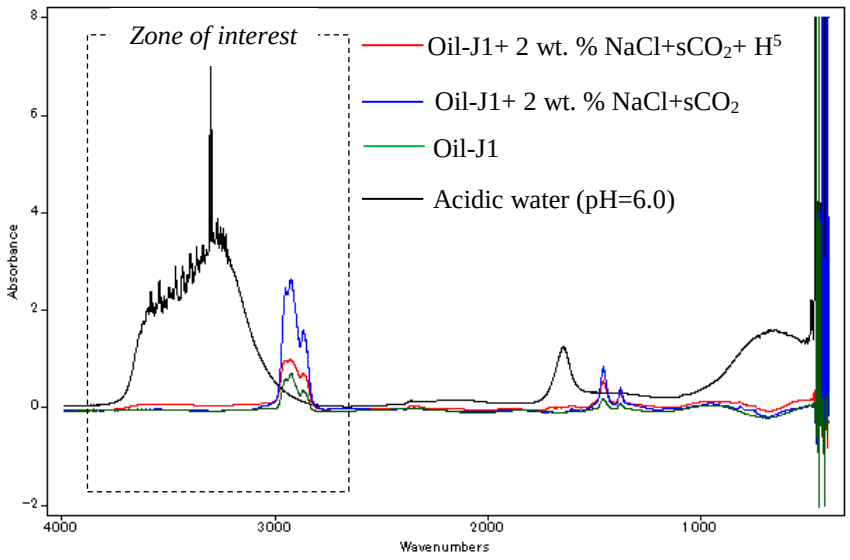

Fig. 3.12 Infrared absorption spectra of Oil-J1, (Oil-J1+2 wt.% NaCl+sCO_2) and (Oil-J1+sCO_2+H^5); adapted from (Nguele et al., 2016c)

Table 3.7 Results of acidity inhibiting factor

	Acidity factor, A_f, (-)	
	1400 – 1800 cm^{-1}	3000 – 4000 cm^{-1}
Acidic water	1.00	1.0
Oil-J1	0.33	0.67
(Oil-J1 + 2% NaCl)+sCO_2	0.56	0.99
(Oil-J1+ 2% NaCl+sCO_2) + H^5	0.85	0.92

This point is supported by Okumura et al. (1990) who proved that peak is also characteristic of the vibration of solvated hydronium ions i.e. $H_3O^+ \cdot (H_2)_n$. Thus, we sought of quantify the concentration of acidic materials. This was done by introducing a parameter termed as *acidity factor* (1-A_f) of which computation scheme is detailed in Nguele et al. (2016)**.** Table 3.7 shows an increase of about 48% in acidic materials after injecting sCO_2. However, when mixed with only 1% of micellar solution, the concentration in acidic materials decreased of about 8% in acidic materials. This suggested that micellar solution alleviated the acidity. However, the underlying mechanism was not well understood. Nevertheless, we hypothesized that the mixture (oil+ sCO_2+slug) undergoes a complexation process that leads invariably to the mitigation of the acidity.

3.7 Summary

This chapter has discussed about the physico-chemical properties of formulated slugs. The major findings are highlighted below:

(1) The formation salinity altered the achievable surface tension and the length of the alkyl chain.

(2) The addition of a non-ionic surfactant not only minimized the influence of the salinity, but also increased (or decreased) the surface tension at the CMC for the micellar slugs prepared from the longer and shorter alkyl chains respectively.

(3) The presence of divalent ions altered the CMC regardless the length of the alkyl chain, the cosurfactant and the concentration.

(4) An ultra-low interfacial tension (order of 10^{-3} mN/m) was achieved for all the micellar solutions prepared with a low-surfactant concentration.

(5) The cationic slugs adsorbed following a Langmuir adsorption type with a plateau value that follows the sequence kaolinite > montmorillonite > and dolomite > Berea sandstone. The large surface area of kaolinite adsorbent explained the highest retention.

(6) The slug mitigated the formation of acidic materials yielded as co-products during sCO_2-EOR.

Chapter 4.
PROPERTIES OF CATIONIC MICROEMULSIONS

4.1 Background

Schulman et al. (1959) reported the term microemulsion (ME), for the first time, to describe a multiphase system consisting of water, oil, surfactant, which forms a transparent solution. This definition was amended later by Danielsson and Lindman (1981). They proposed, what is referred as the most effective and complete definition of ME to date. ME was defined as a system consisting of water, oil and amphiphilic material, which is optically isotropic and thermodynamically stable. Over past decades, the potential of ME, as displacing agent for light to medium oils, has been investigated extensively. These investigations were pioneered by Holm (1971) who reported a high extraction efficiency at elevated temperatures using sodium sulfates. Further works have proved the technical feasibility of ME-EOR primarily because of (*i*) their lower energy requirements (Magdassi et al., 2003), (*ii*) their potential to develop an ultra-low interfacial tension (IFT) (Bera et al., 2012) and (*iii*) high interfacial area. From a thermodynamic point of view, MEs are relatively stable compared to emulsions.

Few works have tackled the use of cationic Gemini surfactants to develop MEs for a possible application in EOR, presumably because of the retention on the reservoir rocks. Nevertheless, Shah and Schechter(1977) reported that when the concentration in salt within a solution containing oil, water and a surfactant is increased, the solubilization of oil and water will decrease and increase respectively. In other words, the increase in salinity gradient promotes the formation of different types of ME that spans from a lower phase (*l*) at a low-saline medium, a middle phase (*m*) at an intermediate salinity to an upper phase (*u*) in a high saline environment (Bera et al. 2015). Another terminology uses Winsor type I (WI) to describe an *l*-phase and Winsor type II (WII) for an *u*-phase and Winsor type III (WIII) to refer a *m*-phase (Reed and Healy, 1977). In a typical type I system, the surfactant forms an oil-in-water (O/W) ME in the aqueous phase, while a water-in-oil (W/O) ME is predominant in the oleic phase in a type II. Both are unfavorable for an EOR application, as the ultra-low IFT desirable cannot be achieved. In a type III, however, a bi-continuous phase consisting of surfactant, water and dissolved hydrocarbons is promoted. The latter case is highly desirable for surfactant-EOR (Pillai et al., 1999).

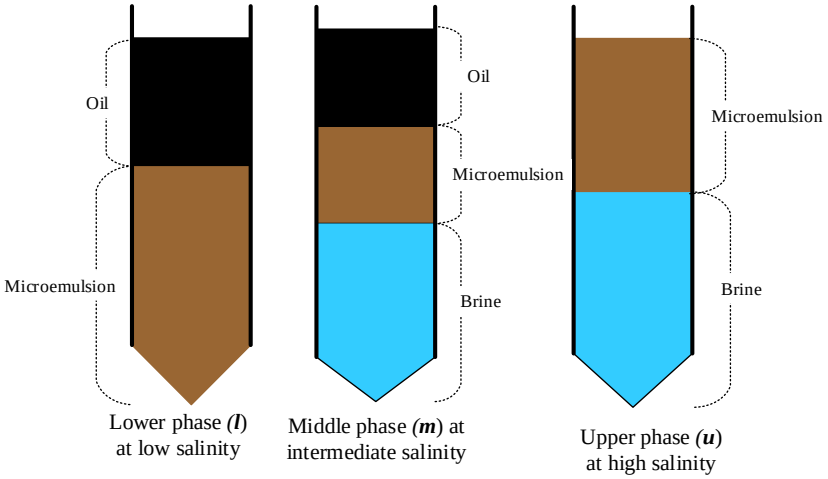

Fig. 4.1 Schematic representation of Winsor microemulsion

Not only salinity and surfactant concentrations are said to alter properties of MEs, but also various parameters such as the cosurfactant type, the molecular structure of Gemini structure, crude oil acidity and the reservoir (Cayias and Schechter, 1976; Healy et al., 1976; Novosad, 1982; Puerto and Reed, 1983). Considering afore-discussed points, the present chapter will screen the physico-chemical properties of cationic microemulsions formulated from aqueous micellar slugs. To do so, MEs will be prepared from the slugs and their alteration in respect of the candidate heavy oils properties and those of candidate formation properties investigated. A mechanistic study and characterization of MEs will be also conducted.

4.2 Experimental Section

4.2.1 Materials

4.2.1.1 Petroleum fluids

The two candidate heavy crude oils, Oil-J1 and Oil-J2 were used in this section. Prior performing any experiment, the crudes were centrifuged for 2 hours at 4,000 rpm to ensure a complete dewatering and the removal of any form of emulsified oil.

Twelve brine solutions of which the concentration spans from low to high, were selected to represent the connate water. The compositions are summarized in Table 3.3.

4.2.1.2 Aqueous micellar solutions

The slugs R^2 - R^5 and H^2 - H^5 were used as primary solubilizing agents. The preparations of the slugs and their respective properties are presented in Chapter 3.

4.2.2 Methods

4.2.2.1 Preparation of microemulsion from candidate heavy oils

The experimental sequence is described below:

(1) Introduce 4 ml of Oil-J1 (or Oil-J2) and 4 ml brine (B1 – B12) solution in a graduated test tube.

(2) Add 1 ml of R^x (or H^x).

(3) Agitate the test tube at a constant speed for a minimum of 2 hours.

(4) Allow the ME formed to equilibrate at 40°C for a 4 weeks.

4.2.2.2 Microemulsion rheology

At the end of the salinity scan test, the corresponding ME was collected from the tube and introduced in the measuring tube of Brookfield viscometer (Model LV DVI-Prime) priory heated at 55°C.

4.3 Phase Behavior of Micellar Slugs

Phase behavior tests, as primary screening investigation when a surfactant is considered, include the salinity scan; the aqueous stability and the oil scan tests. The two formers were conducted in this research and they targeted the determination the optimal salinity slug and the achievable IFT.

4.3.1 Salinity scan test

Fig. 4.2 is a sample photograph of the salinity scan test of Oil-J2 after a month of equilibration at 55°C. Therefrom, it could be seen that the oil solubilzation (V_o/V_s) decreased with the increase in salt concentration with the aqueous phase. A reverse trend was observed, however, for the water solubilization (i.e. V_w/V_s). The middle phase (WIII) was achieved at saline concentration of 8 wt. % NaCl. Moreover, the solubilization ratios were averaged at 210 and 63 for V_o/V_s and V_w/V_s respectively. However, we conducting the test for R/H^3 slugs, an atypical pattern of solubilized water was observed. In fact, both solubilization ratios were found to decrease concurrently with the increase in salt in the aqueous phase. The trend contrasted with the literature that states that the increase in salinity concentration promotes a concurrent decrease in oil and water solubilization ratios (Sheng, 2011). In sought of highlighting the underlying mechanisms, one should look at the interactions slug-brine, slug-oil at their respective interfaces.

In fact, when the slug contacts the brine solution, the charged head of the surfactant, dissolved within, develops an electrostatic attraction with dissolved salt. This effect (salting effect) increases with the concentration in inorganic cations including monovalent ions (Na^+ and/or K^+) and/or divalent ions ($Ca^{2+}$and/or Mg^{2+}).

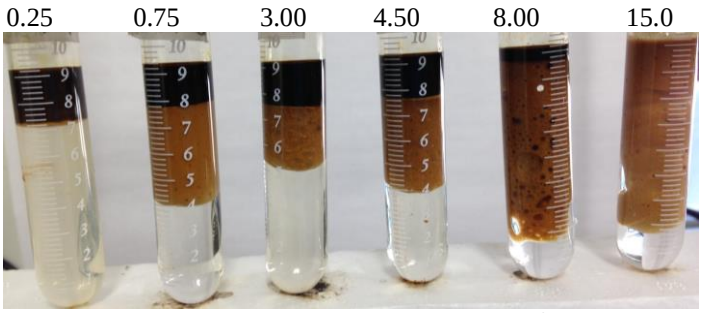

(**a**) Photograph of salinity scan test of (Oil-J2 + R^4+ *x* wt. % NaCl)

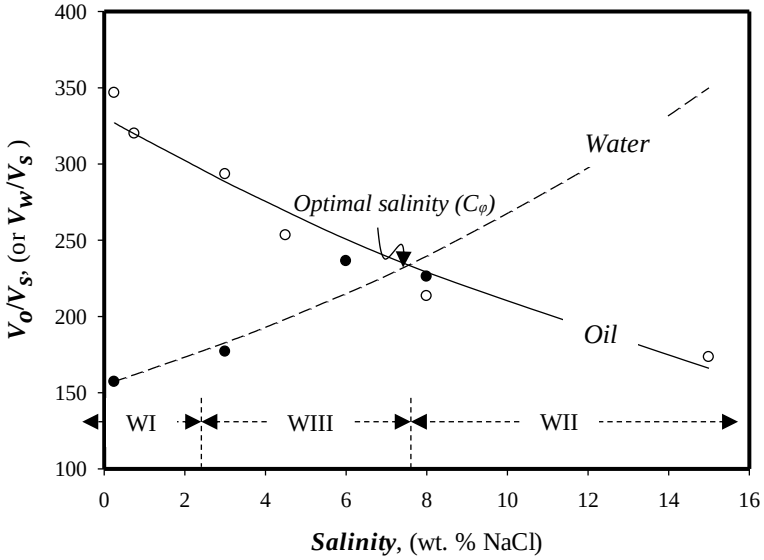

(**b**) Solubilization plots

Fig. 4.2 Solubilization plots as a function of salinity of Oil-J2

If a slug is prepared from a surfactant or a mixture (surfactant/cosurfactant) that has fewer interactions with the ionic solution such as Tween 20, then the salting effect is hindered or counterbalanced, which explained the atypical behavior of R^3 or H^3 slugs. In order to evaluate the achievable IFT at the optimal salinity from the solubilization ratios, several correlations are proposed in the literature (Huh, 1979; Nelson and Pope, 1978; Reed and Healy, 1977).In this research, we estimated the achievable IFT using Huh relation because of its simplicity and its accuracy (Huh, 1979),

$$\sigma_{mo} = \frac{C_{Ho}}{\left(V_o/V_s\right)^2} \tag{4.1}$$

$$\sigma_{mw} = \frac{C_{Hw}}{\left(V_w/V_s\right)^2} \tag{4.2}$$

where σ_{mo} and σ_{mw} represent the IFT at the equilibrium between ME, heavy crude oil and water respectively (in N/m), C_{Ho} and C_{Hw} are empirical dimensionless values ranging from 0.1 to 0.35. In general, C_{Ho} and C_{Hw} are determined experimentally.

Table 4.1 confirmed that the optimal salinity, and thus the achievable IFT, of cationic micellar slugs is sensitive to (1) the length of the alkyl chain of the primary surfactant used to prepare the slug and the nature of the cosurfactant, (2) the presence in divalent ions (M^{2+}) in the brine solution and (3) the acidity of the crude oil.

Table 4.1 Summary of optimal salinity from the salinity scan tests [a]

Slug		Oil-J1				Oil-J2			
		Before M^{2+}		After M^{2+}		Before M^{2+}		After M^{2+}	
		C_φ	σ_φ	C_φ	σ_φ	C_φ	σ_φ	C_φ	σ_φ
R^x	R^2	-	-	-	-				
	R^3	26.0	3.25E-04	-	-	-	-	-	-
	R^4	-	-	12.8	1.33E-5	4.70	6.89E-06	8.60	7.14E-6
	R^5	1.60	2.80E-02	-	-	-	-	-	-
H^x	H^2	4.02	2.59E-06	-	-	-	-	-	-
	H^3	5.40	5.67E-6	-	-		-	-	-
	H^4	4.50	3.00E-05	12.4	1.87E-06	2.5	2.93E-6	11.0	2.31E-6
	H^5	-	-	7.80	7.50E-6	3.84	1.20E-2	-	-

[a] C_φ: optimal salinity (in wt. % NaCl); σ_φ: achievable IFT at the optimal salinity (in mN/m); M^{2+}: divalent ions (i.e. Ca^{2+}, Mg^{2+} or both)

4.3.2 Presence of divalent ions

Divalent ions (M^{2+}) were introduced to model the aqua-ions resulting from the leaching process occurring in a water-flooded formation. They contribute to the hardening of brine, thus tend to promote an incompatibility of the slug with certain oil reservoirs. While conducting the salinity scan test (Table 4.1), we observed that none of the slugs could achieve an ultra-low IFT under hard conditions except those R^4 and H^4.

In fact, their salinity scans showed a change in solubilization curves with the appearance of M^{2+} (Fig. 4.3). For the same type of oil, the achievable IFT, at the optimal salinity, decreased of about 79.3% using R^4 when the test was shifted from a soft saline medium to hard saline water. The decrease was lowered to 53% when the slug H^4 was used instead. These observations suggested that the presence M^{2+} does not promote a slug incompatibility with the micellar slugs.

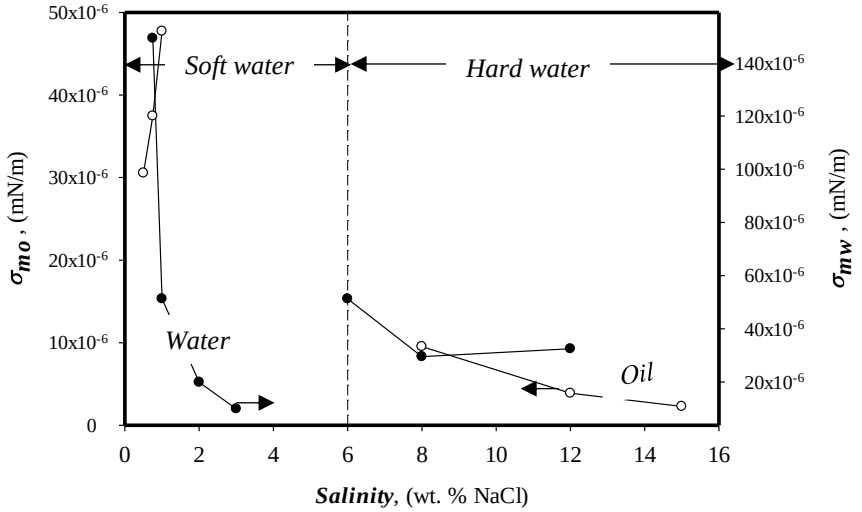

(**a**) Oil-J1+R^4+ *x* wt. % NaCl

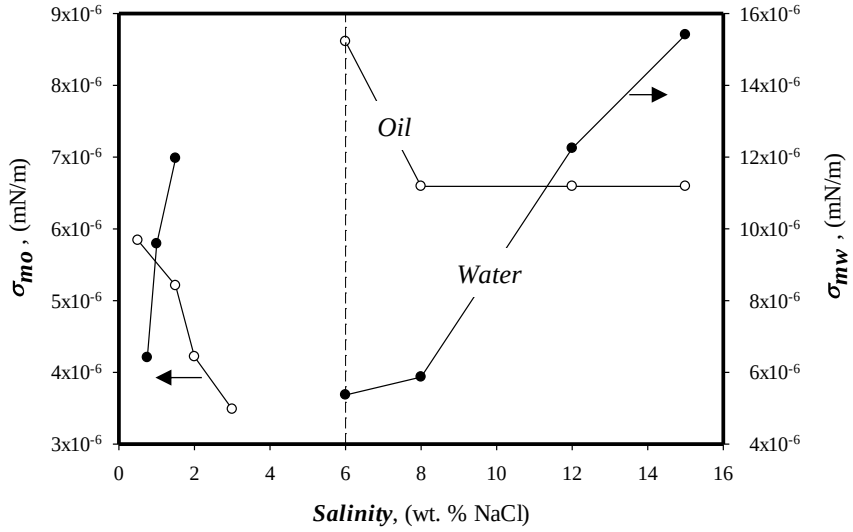

(**b**) Oil-J2+H^4+ *x* wt. % NaCl

Fig. 4.3 Solubility plots of Oil-J1 and Oi-J2 as function of salinity and formation hardness

Rather, they act upon the reduction of the IFT, which was thought inherent to (1) the electrostatic repulsion forces between the hydrophilic head and the M^{2+} (Yoshimura et al., 2004) and the hydrophobic interactions between alkyl chain of the Gemini surfactant (Sjoblom et al., 1996). Upon changing the crude oil (Fig. 3.14b), we observed an IFT reduction of about 67.3% when H^4 was used, but an increase of IFT of about 10% when R^4 was considered.

The increase observed for the system R^4/Oil-J2 highlighted an incompatibility of the slug with the resident aqueous phase. In this case, the slug pushes the equilibrium towards the upper phase of the microemulsion. The complex [M^{2+}- R^4] become oil-soluble (Green and Willhite, 1998). Plausibly, given the experimental conditions a complexation process may occur and further promotes an intra-molecular rearrangement within the micellar solution (Nguele et al.,

2015a). The “new slug” is thought to exhibit singular properties, different from the native slug, which participate at the alteration of the interface oil/brine. In fact, in a fairly alkaline medium, Pine (2011) showed that quaternary ammoniums are subjected to molecular rearrangements including Stevens and Sommelet-Hauser arrangements. Thus, during the pre-micellization process in hard and saline water, the slug may plausibly undergo through chemistry by equation (4.3)

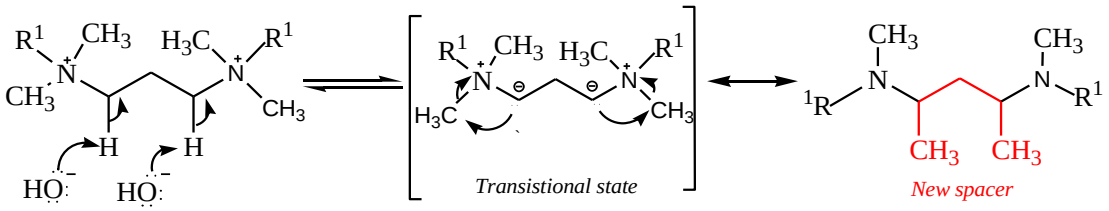

(4.3)

where is R^1 is alkyl radical i.e. dodecyl or hexadecyl.

4.3.3 Effect of crude oil acidity and cosurfactant

The crude oil composition is quantified by parameter, known as Equivalent Alkane Carbon Number (EACN), which defines a dimensionless number that expresses the hydrophobicity of oil (Cayias and Schechter, 1976). A good correlation is generally obtained for synthetic oils, but converges poorly when the model is extended to actual crude oils. This is so because of the complexity in chemical composition of the crude oil (Shah and Schechter, 1977).

We proposed a more simplistic approach, by introducing a parameter termed as Average Carbon Number (*ACN*), to represent rather the chemical composition of the candidate heavy crudes oils (Nguele et al., 2016c). Considering a crude oil of which assay shows *n* hydrocarbon compounds of x_i mole fraction each, *ACN* is expressed mathematically by,

$$ACN = \frac{1}{n}\sum_{i}\left(x_i C_i\right) \tag{4.4}$$

where C_i is the carbon number *i*.

Equation (4.4) did not aim to substitute EACN. Rather, it proposed an easier route to model crude oil if its assay is available. Also, it is worth noting that this concept cannot be blindly applicable to all the crudes as the ME is not solely dependent of the crude oil type.

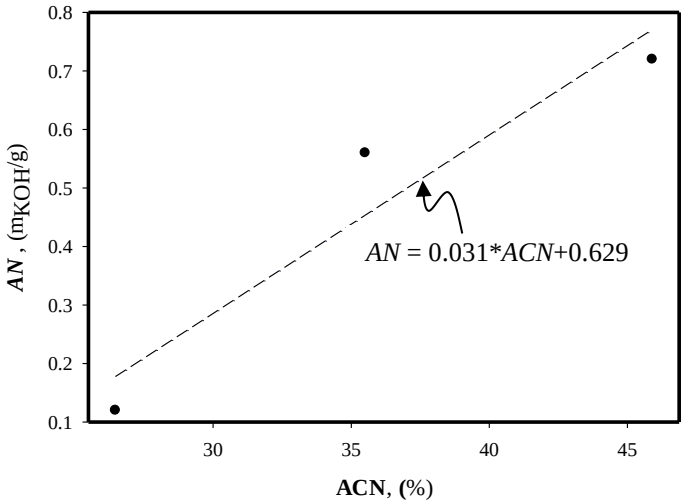

Fig. 4.4 Crude oil acidity as function of average carbon number

Fig. 4.4 correlated the computed *ACN* with the crude oil acidity herein expressed by the acid number. The crude acidity within the oil increased in a linear fashion with the *ACN*, with the highest value obtained for the heaviest crudes. With the knowledge that the acid number accesses the concentration in organic acids materials within the crude oil, thus solubilizable materials, we could correlate therefore the ACN with the alteration in optimal salinity (Fig. 4.5). On the average, in soft saline water, the optimal salinity was higher when the microemulsions were formulated from R^x. (Fig. 4.5a). A reverse observation was found when the microemulsion were prepared in hard water. (Fig. 4.5b). Moreover, the acidity of the crude oil increased the optimal salinity of about 20% if the slug was changed from R^4 to H^4. However, the optimal salinity of the microemulsions, derived from Oil-J2, was less altered in the presence of M^{2+} regardless the type of slugs used.

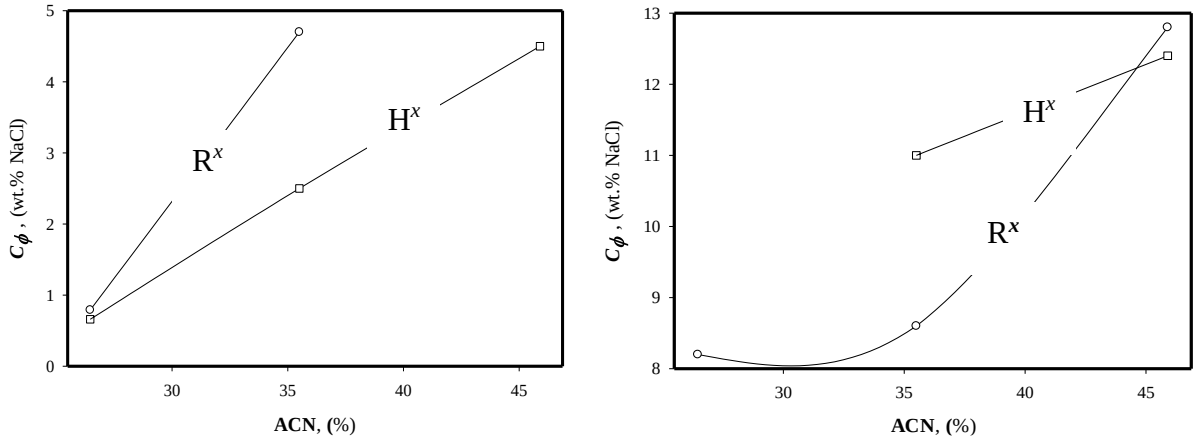

(**a**) Soft saline water (**b**) Hard saline water

Fig. 4.5 Alteration of optimal salinity by the crude oil acidity

4.3.4 Effect of reservoir temperature

The temperature dependence was investigated by the salinity scan test performed at 25, 40 and 55^{o}C using Oil-J1 and H^{5} as slug. The results are shown in Fig. 4.6. The tolerance to reservoir salinity was found to increase with the temperature. Zielilqski et al. (1989) postulated that for a monomeric alkylammonium, the energy of formation of micelles decreases monotonically with the temperature. In other words, CMC is temperature-dependent. If we recall that CMC defines the optimal salinity, and thus achievable IFT, then we may plausibly think that reservoir temperature yields positive standard entropy of micelle formation. Experimentally, this would be seen by an increase in hydrophobic effect (Schick, 1963). The kinetics of micelle formation in the equilibrated aqueous phase increased with the heat, thus the ME formed, shifts from lower to middle phase. From this mechanism will result an alteration of both the optimal salinity and the achievable IFT.

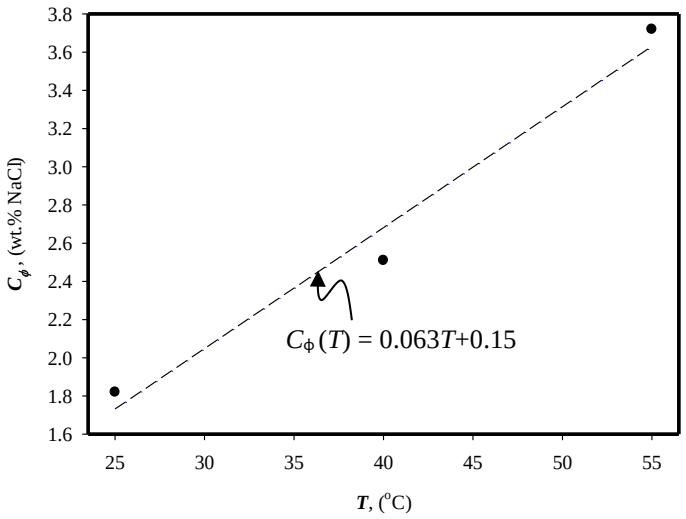

Fig. 4.6 Effect of reservoir temperature on the optimal salinity; 44.4% Oil-J1+11.2 % H^{5}+ 44.4% NaCl

4.4 Mechanistic Analysis and Characterization of Microemulsions

4.4.1 Rheology of microemulsions

In the previous chapters, it was conjectured that the viscosity of the slug is a key parameter when designing an EOR technique. This is so because of the fingering and channeling effects that are often encountered when a low viscous material is used as displacing agent. The viscosity of a specific fluid depends mainly on both microscopic and macroscopic internal structures and interactions.

Fig. 4.7 shows the results of the measurements of the microemulsions prepared from R^4/H^4, which were selected because of their consistency. Therefrom, the native oils and the cationic microemulsions regardless the slug, exhibited a pseudo-plastic behavior i.e. their respective viscosities decreased with the shear rate. This observation was consistent with the non-Newtonian behavior of microemulsion reported by Bennett et al. (1981). On the average, the apparent viscosity of microemulsion formulated from the longer alkyl chain (H^4) was 13 and 60% higher than that of those formulated from R^4 and the native oil respectively (Fig. 4.7a). These values increased to 77 and 94% when Oil-J2 was investigated (Fig. 4.7b). The difference lied primarily on the solubilizing potential of R/H^x slugs.

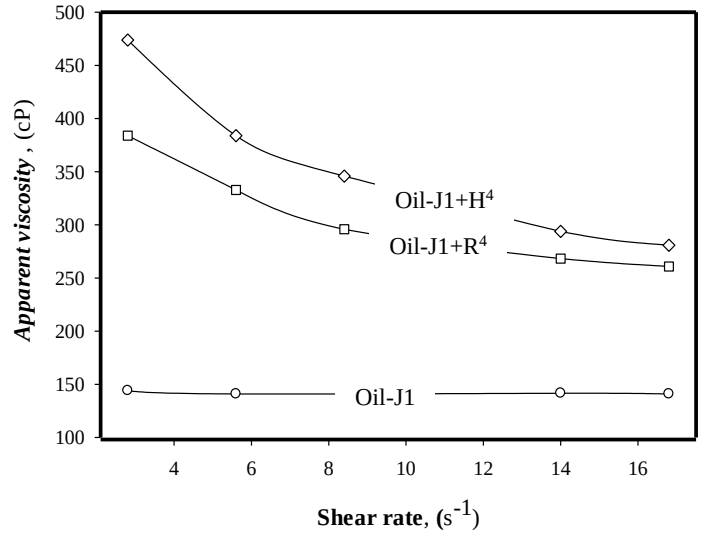

(**a**) Oil-J1

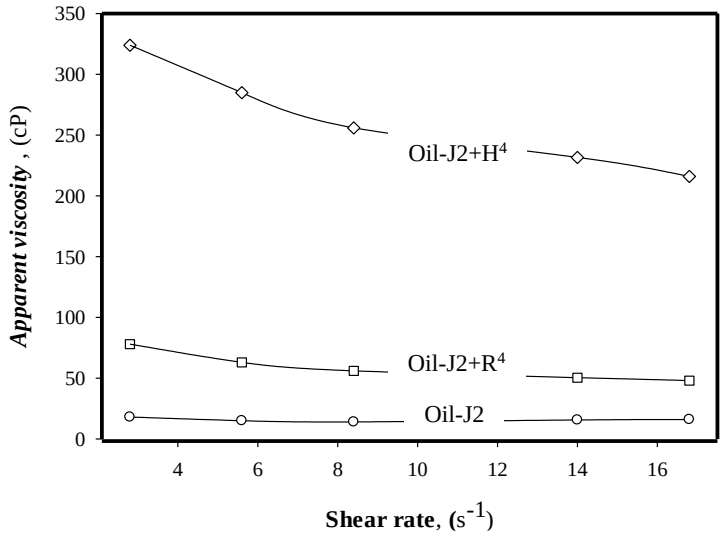

(**b**) Oil-J2

Fig. 4.7 Rheology of microemulsions at reservoir temperature

If the chemical structure of cationic GS is recalled, it appears that the micellar slugs prepared from longer molecular chains have higher solubilization/emulsification degree. We think that H^4 developed within the microemulsion a better (and stronger) droplet clustering and fusion. The latter effect is referred as microemulsion percolation. Both effects were more pronounced than their respective counterparts with prepared from the shorter alkyl chain. As a result, a modification of internal structure of the microemulsion is yielded, which is visualized experimentally by the increase in the apparent viscosity (Eicke and Christen, 1974). As the clustering is function of the alkyl chain, for the same type of oil, the longer the alkyl chain of the surfactant, the more viscous is the microemulsion.

We investigated the effect of the salinity on the microemulsions obtained when R^4 when selected as a slug. The results show that the viscosity of the microemulsions increased with the salinity. The heaviest microemulsions were observed at/around the optimal salinity (Fig. 4.8). It was interesting to see that the viscosity of the microemulsion followed the trend to the salinity scan test i.e. the formation of the ME. Our results are reported similarly in the literature (Dashti, 2014). According to Garcia-Rio et al. (1994), the viscosity and the water solubilization capacity of cationic microemulsions phase are altered by the salt content and the acidity/alkalinity. With the knowledge that H/R^4 were both enhanced by sodium hydroxide (NaOH), it is rational to think that this alteration was also inherent to the interaction cosurfactant-brine.

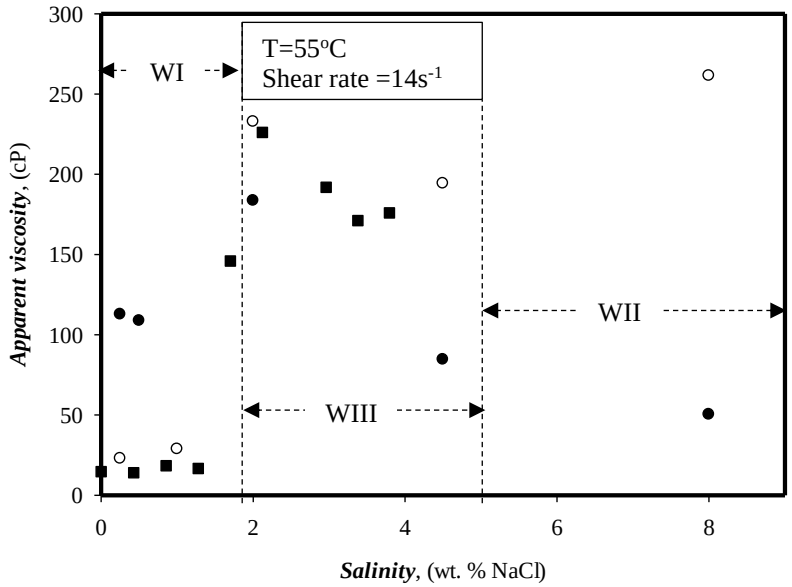

Fig. 4.8 Effect of salinity concentration on the rheology of microemulsions; (○) Oil-J1; (●) Oil-J2, (■) Literature from Dashi (2014); The microemulsion consisted of 44.4% Oil-J1 (orJ2) – 44.4% brine – 11.2% R^4

4.4.2 Particle size analysis

The microemulsion were further characterized as results of the atypical behavior and/or trend observed during the rheological tests. We sought of understanding the extent to which the salinity, the increase in M^{2+} concentration impacts the formation of microemulsions. For this purpose, we extracted the ME developed from R^4 at different salinities.

The particle sizes of the extracted ME were analyzed based on the microscopic photographs (Fig. 4.9). The particle sizes were found to increase not only with the salinity but also with the concentration in M^{2+} (Fig. 4.9). Water-in-oil (W/O) and oil-in-water (O/W) emulsions clustered upon increasing the concentration in M^{2+} (Fig. 4.9a and 4.9b). These results suggested the formation of reverse micelles that explains subsequently the high viscosity (Fig. 4.7 and 4.8). The ME behaves as if the M^{2+} develop an electrostatic/electrical field that promotes the clustering of water and oil molecules. Following this postulate, we thought of establishing a correlation between the concentration in M^{2+}, the salinity, the acidity and an eventual electrical field.

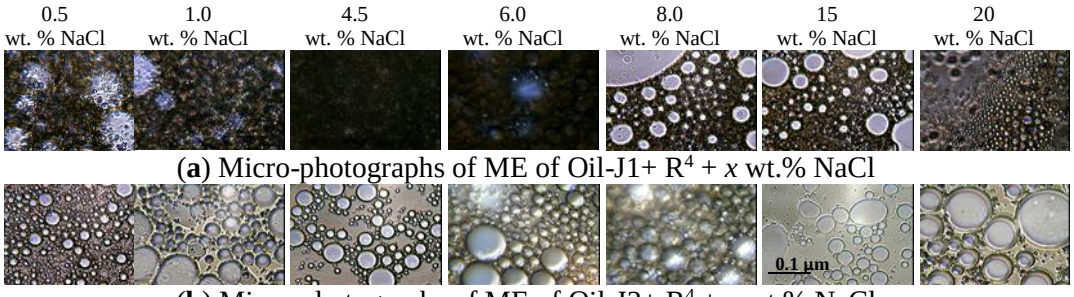

(**a**) Micro-photographs of ME of Oil-J1+ R^4 + *x* wt.% NaCl

(**b**) Micro-photographs of ME of Oil-J2+ R^4 + *x* wt.% NaCl

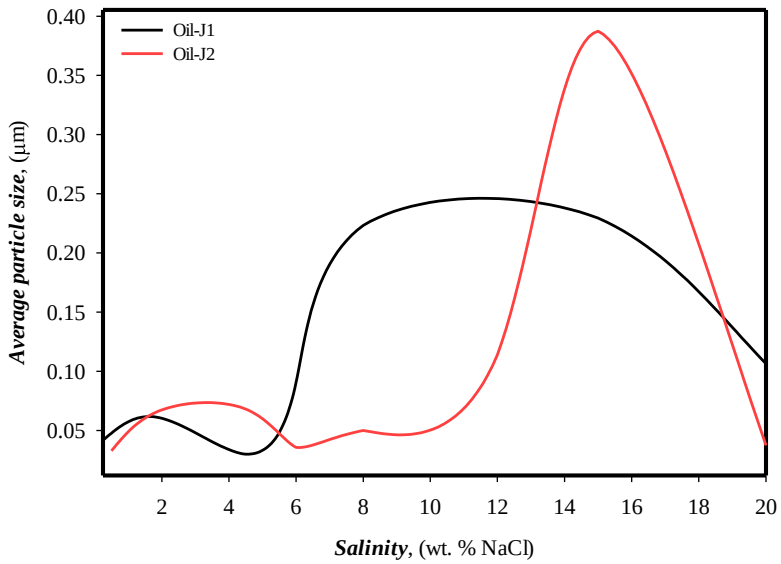

(**c**) Particle distribution

Fig. 4.9 Particle size distribution of microemulsions

Let consider a heavy oil (A) in which petroleum acids (AH) are dissolved. Upon contacting saline water, Ramakrishan and Wasan (1983) suggested that petroleum acids equilibrate in both aqueous (*w*) and oil phase (*o*),

$$HA_o \leftrightarrow HA_w \tag{4.5}$$

HA_w dissociates further to yield petroleum carboxylates (A^-),

$$HA_w \leftrightarrow H^+ + A^-;\ E_1 = E_1^0 + 0.059\log\left([H^+]\left([A^-]\right)\right) \tag{4.6}$$

Equation (4.6) suggests that two redox couples are involved in this reaction including (HA_w/H^+) and (A^-/HA_w). If the microemulsion is formed in hard saline water, Cannan et al.(1938) stated that a complex (AM^+) is formed following equation (4.7),

$$M^{2+} + A^- \leftrightarrow AM^+;\ E_2 = E_2^0 + 0.059\log\left([M^{2+}]\left([A^-]\right)\right) \tag{4.7}$$

This relation also shows that (AM^+/M^{2+}) and (A^-/AM^+) appeared as redox couples. Combining (4.6) and (4.7),

$$HA_w + M^{2+} \leftrightarrow AM^+ + H^+;\ \Delta E = 0.059\log\left(\frac{[M^{2+}]}{[MA^+][H^+]}\right) \tag{4.8}$$

From equation (4.8), it could be seen that hard formation water promoted the formation of complexes within the microemulsions that are sensitive to acidity/alkalinity. This equation validated the results afore-presented. M^{2+}, positively charged, may induce an electrical field, *E*, expressed by equation (4.9),

$$E = k_e \frac{q_{M^{2+}}}{D^2} \tag{4.9}$$

where *D* is the distance between M^{2+} and A^- (dimension of length). To a further extent, *D* could be attributed to the diameter of the cluster. Moreover, the electrical field (*E*) is related to its electric potential (ΔE) by equation (4.10),

$$\Delta E = DE \tag{4.10}$$

Combing equations (4.6) - (4.10) and solving them for *D*, the set of equations is obtained,

If $[M^{2+}] = 0$, $\quad 1/D = \beta\left(pH - \log\left(\sum Na^{+} - 10^{-pH}\right)\right)$ (4.11)

If $[M^{2+}] > 0$, $\quad 1/D = \beta\left(pH - p[M^{2+}] + \log\left([M^{2+}]_i - [M^{2+}]\right)\right)$

(4.12)

where $\beta = 0.059/\left(kq_{M^{2+}}\right)$ and $p[M^{2+}]$ = - log $[M^{2+}]$.

Equation (4.11) was taken as governing model of electrical distribution forces in a low-saline medium while equation (4.12) represented the model when the aqueous phase was saturated with M^{2+}. Based on which, the sensitivity of the reservoir acidity was evaluated (Fig. 4.10). The model highlighted clearly the dependence of the particle sizes of ME with the electrostatic forces, the acidity (Fig. 4.10a) and the salinity (Fig. 4.10b).

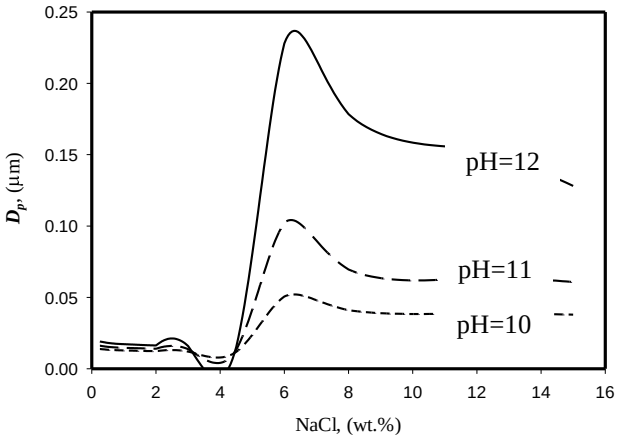

(a) At different pH

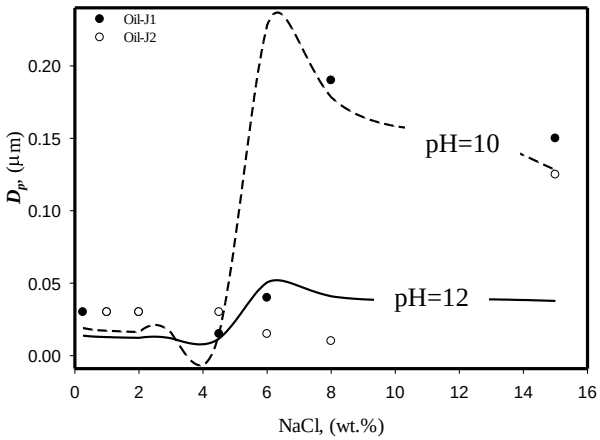

(**b**) Particle size distribution as function of salinity

Fig. 4.10 Sensitivity analysis of reservoir acidity on clustering and particle size distribution

At low concentration of M^{2+} (in a sandstone reservoir for instance), the electrical field, prompted by salinity, will force W/O and O/W to cluster. Also, the particle size diameter is expected to be low under these circumstances. With these findings, one may expect that the slug, in a heavy oil sandstone reservoir may be efficient. With the increase in M^{2+} concentration, the electrical field decreases as consequence of an increase of *D*. The complex MA^{+} acts as repelling agent forcing the molecules of water (or oil) to increase in size, thus its viscosity increases (Fig. 4.7). These observations were found true at pH $\geq$ 8 at which negative values in *D* were found. We were led to the conclusions that particle sizes of ME are altered sequentially by the formation salinity, its resident acidity and the concentration in M^{2+}.. At a pH equal or near to 10, the particles sizes of ME followed seemly the pattern and the magnitude of electrostatic model on average of $0.53D - 0.73D$ for Oil-J2 and Oil-J1 respectively. Hence, we believed that the particle sizes could be explained, and perhaps predicted, by an electrostatic model. To mitigate the effect of M^{2+}, i.e. injecting the slug in a carbonate reservoir, we should reduce the sharp increase observed in Fig. 4.10b.

4.5 Summary

This chapter has discussed about the physico-chemical properties of formulated slugs and those of their inherent microemulsions. The major findings are highlighted below:

(1) The achievable IFT increased linearly with the reservoir temperature, but remained within the ultra-low range i.e. magnitude of 10^{-3} mN/m.

(2) The micellar slugs, enhanced by an ionic cosurfactant, were not altered by the increase in divalent ions.

(3) The viscosity of the microemulsions showed a pseudo-plastic behavior, with the heaviest microemulsion yielded by the slug prepared from the cationic Gemini surfactant with the longer alkyl chain.

(4) The reservoir salinity increased the viscosity of the microemulsions in such a way that the highest value was recorded at/around the optimal salinity.

(5) The particle sizes of emulsions increased with the formation salinity and the concentration in M^{2+} as result of a clustering of water and oil molecules.

Chapter 5.
EXPERIMENTAL EVALUATION OF HEAVY OIL PRODUCTION BY MICROEMULSION FLOODING

5.1 Theoretical Approach

In theory, the chemical-EOR requires the injection of a slug, which solubilizes (or emulsifies) the acidic parts of the residual oil following the steps shown in Fig. 5.1a. The oil solubilization (or emulsification) mechanism occurs in-situ i.e. within the interstices of the reservoir rock in which the oil ganglia are trapped. In other words, the slug acts upon capillary forces that hold oil stranded. To be more explicit, the ratio of viscous forces to interstitial forces (capillary number) is so high (order of 10^{-7}) at the end of primary recovery that the only route to produce more oil is to lower the interfacial tension.

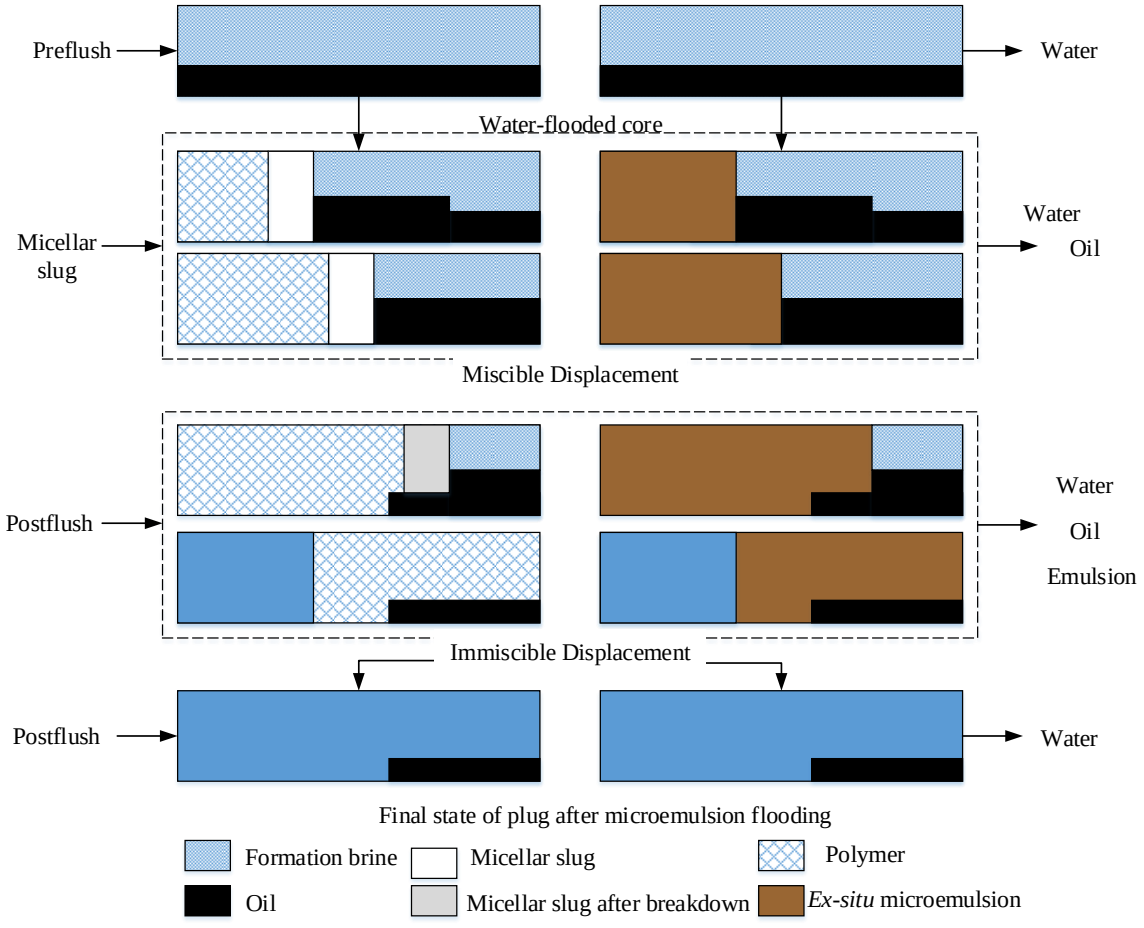

(a) Classical chemical-EOR **(b)** Microemulsion gel-type

Fig. 5.1 Schematic representation of oil mobilization by microemulsion flooding

However, for the slug to be efficient, it is recommended to use large volumes of preflush of which the composition is tailored to neutralize the divalent and sulfate ions. It is worth noting that lowering the IFT of the residual oil is not sufficient as a typical chemical-EOR suffers principally of poor propagation, surfactant retention and injectivity loss. Therefore, injecting viscous water at the trailing edge of micellar slug mitigates the former issue. The polymer keeps the viscosity drive as the slug propagates in the reservoir. To have additional oil, low-saline water (referred as chase water or postflush) is injected at the rear of the polymer.

An alternative production scheme could consider the injection of a fully solubilized oil (that is the microemulsion) following the scheme illustrated in Fig. 5.1b. In this production scheme, a microemulsion is formulated ex-situ and injected in the oil-bearing matrix. The microemulsion formulation should be heavy enough to lower the mobility ratio, thus to promote the increment in oil. However, this recovery scheme is challenged by the composition of the microemulsion. Some authors proposed to formulate the microemulsions from a material of which solubilization (or emulsification) yields to microemulsion-gel type heavier than the native residual oil. This approach implies extensive and synergistic studies between the slug, the material to be solubilized and the residual oil. Rather, our approach considered formulating microemulsions from the actual oil to be displaced.

In theory, this scheme is thought to eliminate the incompatibility and the intermediate steps aforementioned. More oil is expected as results of a subsequent reduction of mobility ratio. One may think that oil production is primarily a physical process involving the reduction of capillary forces. This observation, if solely considered, could be misleading. In reality, as the microemulsion propagates through the formation, it interacts with the native minerals of the formation rock. Depending of the chemistry resulting from these interactions, the composition of the microemulsion, and thus its efficiency as displacing agent, could be altered (Yildiz and Morrow, 1996). This production scheme must consider therefore the use of a preflush.

Moreover, if a microemulsion-gel type is poorly formulated, its displacement may suffer from a phase separation occurring at both the leading and trailing edges. Therefore, it should be advisable to investigate on the mobilization of heavy oil concurrently with (or subsequently to) the interactions of the microemulsions with the reservoir rocks. This is to say that the efficiency of this flooding scheme is expected to also be dependent of (*i*) formation requirement (i.e. small spacing), (*ii*) the formation water salinity, and/or (*iii*) the retention of the slug on the porous medium.

5.2 Experimental Section

5.2.1 Reservoir fluids and slugs

5.2.1.1 Preparation of dead crude oils at 25ºC

The candidate crude was Oil-J2. The properties are presented in Chapter 1. However, a prior the core flood tests, Oil-J2 was centrifuged for 3 hours at 4000 rpm. This step ensured a complete dewatering and the removal of any form of emulsified oil.

5.2.1.2 Synthetic reservoir waters

Three synthetic brine formations were used at this stage. The compositions of synthetic formation brines are summarized in Table 5.1. Their syntheses were performed in-house primarily from sodium chloride (NaCl) purchased from Junsei chemicals (Japan), calcium chloride ($CaCl_2$), magnesium chloride hexahydrated ($MgCl_2 \bullet 7H_2O$), hydrogen sodium carbonate ($NaHCO_3$), potassium chloride (KCl) and magnesium sulfate ($MgSO_4$) all supplied by Wako pure chemicals (Japan). It is worth mentioning that all the chemicals were used as received and were 99.99% pure.

Table 5.1 Composition of synthetic formation waters [a]

Synthetic formation water			
Code	SFW-1	SFW-2	SFW-3
	Na^+: 3026; K^+: 79; Ca^{2+}: 541; Mg^{2+}: 39 Cl^-: 4799; HCO_3^-: 726; SO_4^{2-}: 65	Na^+: 4283; K^+: 210; Ca^{2+}: 722; Mg^{2+}: 99 Cl^-: 6594; HCO_3^-: 1452; SO_4^{2-}: 163	Na^+: 7309; K^+: 288; Ca^{2+}: 1263; Mg^{2+}: 138 Cl^-: 11393; HCO_3^-: 2178; SO_4^{2-}: 228
	TDS: 9275	TDS: 13522	TDS: 22797
	Preflush		*Chase water*
Code	P-1	P-2	P-3
	Na^+: 1574 Cl^-: 2426 TDS: 4000	Na^+: 3161 Cl^-: 609; HCO_3^-: 734 TDS: 4504	Na^+: 393; Cl^-: 607; TDS: 1000

[a] Na^+: sodium ion; K^+: potassium ion; Ca^{2+}: calcium ion; Mg^{2+}: magnesium ion; Cl^-: chloride ion; HCO_3^-: hydrogenocarbonate ion; SO_4^{2-}: sulfate ion; TDS: total dissolved solid; all concentrations are given in ppm.

5.2.1.3 Aqueous slugs

Slugs, used in this set of experiments, are those which showed promising solubilizing potential during the phase behavior tests. The preparations, the physico-chemical properties are presented in Chapter 2.

5.2.1.4 Berea sandstone cores

Four Berea sandstone cores were selected for the coreflood experiments. The properties and the mineralogy are outlined in Tables Table 5.2 and Table 5.3 respectively.

Table 5.2 Berea sandstone properties [a]

Nature	Conventional		Unconventional	
	Homogeneous		*Artificially fractured*	*Heterogeneous*
Core ID	#4-01	#4-03	#4-04	#4-05
L (cm)	7.23	7.20	7.19	7.15
D (cm)	4.50	4.46	4.45	4.56
PV (cm^3)[b]	14.2	12.0	12.5	17.5
Φ (%)[b]	13	11	11	15

[a] *L*: length; *D*: diameter; *PV*: pore volume; *Φ*:porosity;
[b] *PV* and *φ* were determined by saturation method prior conducting coreflood tests.

Table 5.3 Mineralogy of Berea sandstone

Mineral	Formula	Composition (%)
Quartz	SiO_2	80.0
Orthoclase	$KAlSi_3O_8$	5.00
Calcite	$CaCO_3$	6.00
Kaolinite	$Al_4S_{i4}O_{10}(OH)_8$	7.00
Montmorillonite	$(Na,Ca)_{0.33}(Al, Mg)_2(S_{i4}O_{10})(OH)_2, nH_2O$	1.00

An artificial fracture was created in core #4-04 by cutting it in half following the length. The aperture of the fracture was measured to be lesser than 0.1 mm. The plug was then insulated with resin. On the other hand, a high permeable zone was created in core #4-05 by drilling a hole (diameter = 10 mm) in the center of the plug following the length. The hole was, then, filled with glass beads (diameter =0.4 mm). To ensure a perfect consolidation of the glass beads pack, the sandstone was air-vacuumed for a 30 mins after what, the plug was then insulated with resin. Once the cores were prepared, below procedure was followed:

(1) Dry the clean or insulated plugs oven overnight at 105°C to remove of interstitial water.
(2) Record the weight of the dried core.
(3) Mount the core in the core holder of the flooding apparatus.
(4) Confine the core at 4.0 MPa. A backpressure regulator, set up to open automatically at 3.0 MPA, controlled the pressure across the core holder during the fluid injection.

5.2.2 Methods

5.2.2.1 Ex-situ formulation of microemulsions

The gravimetric titration method was used to formulate the microemulsion *ex-situ*. The titrant was an aqueous phase with a low concentration in salt and the analyte was a mixture of Oil-J2 and R/H^x. The titration was conducted for different analyte ratios. The gravimetric titration, conducted at room temperature, followed the sequential steps described below:

(1) Mix at different volume ratios of Oil-J2 and either R/H^x. The mixture had a dark color.

(2) Titrate the mixture with the low saline water until a specific microemulsion is formed and remains unchanged. The change (or microemulsion formation) was observed visually by the formation of a brownish phase.

(3) Allow the microemulsion formed to equilibrate for a minimum of 30 mins.

(4) By visual observation, determine the type of microemulsion and record the volume of titrant.

Four types of microemulsions were yielded including a WI, in which the brownish phase (corresponding to the solubilized water) was in equilibrium with an excess of oil. When the brownish phase (corresponding to solubilized oil) was in equilibrium with the excess of water, the microemulsion was labeled as WII. A WIII corresponded to the brownish phase in equilibrium with oil and water. The gel or WIV was assigned for a microemulsion in which there was no excess of either water or oil.

5.2.2.2 Core flood tests

The core flood tests were conducted in an apparatus illustrated in Fig. 5.2. The injection assays were performed at reservoir temperature.

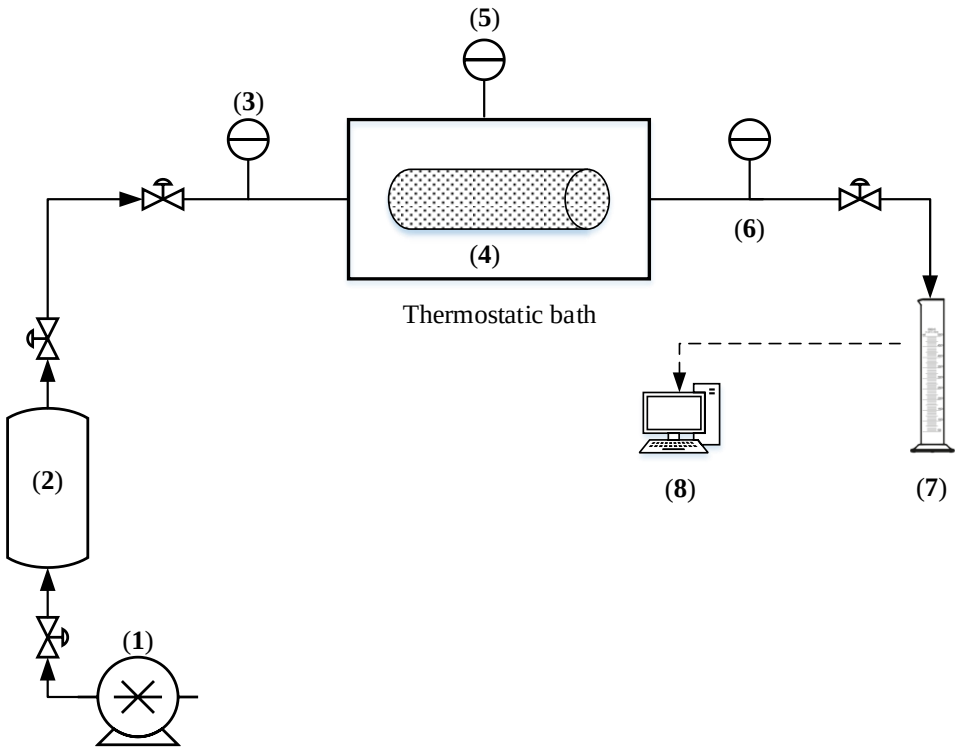

Fig. 5.2 Schematic representation of microemulsion flooding apparatus (1) Pump; (2) Cell containing the fluid to be injected; (3) Pressure controller at the injecting head; (4) Mounted core; (5) Temperature controller; (6) Backpressure regulator; (7) Fractionator; (8) UV spectrophotometer

Table 5.4 Summary of injection assays

Flooding	**Flood-01**	**Flood-03**	**Flood-04**	**Flood-05**
Core type	Conventional		Unconventional	
Berea sandstone used	# 4-01	# 4-03	# 4-04	# 4-05
PV (ml)	14.2	12.0	12.5	17.5
Relative Permeability data				
Initial water saturation (-)	0.48	0.69	0.68	0.77
Initial oil saturation (-)	0.52	0.31	0.32	0.23
Synthetic water data				
Formation brine	SFW-1	SFW-3	SFW-2	SFW-3
Salinity (wt. % NaCl)	0.70	1.65	0.95	1.65
pH, (-)	7.50	7.71	6.90	7.71
M^{2+} *concentration* (ppm)	580.7	1401.0	820	1401.0
Confined Pressure (MPa)	5.0			
T (^{o}C)	55			
Aging time (day)	10	10	19	20
Preflush stage data				
Code	P-1		P-2	
Salinity (wt. % NaCl)	0.40		0.10	
pH, (-)	6.48		9.84	
Injection rate (ml/min)	1.50		1.00	0.75
PV injected (PV)	2.92	1.33	2.21	2.38
Microemulsion flooding data				
Slug Code	NR-3	NR-2		NR-3
Injection rate (ml/min)	0.25	0.25	0.15	0.1
PV injected (PV)	0.51	0.69	0.68	0.35
Chase water flood data				
Code	P-3			
Salinity (wt. % NaCl)	0.10			
pH, (-)	7.92			
Injection rate (ml/min)	1.50		0.75	
PV injected (PV)	3.78	4.10	2.11	1.96

The summary of the core flooding tests is outlined in Table 5.4. The detailed sequence of the injection assays, as performed in this work, is presented below:

(1) *Fresh water flooding.* This step aims at determining the base permeability of the core. Fresh water (distilled water) was injected at constant flow rate of 0.5 ml/min. The rate was increased subsequently to 1.0 and 1.5 ml/min. For each flow rate, this step was conducted for 1 PV. Water permeability for each run was then computed using Darcy's law,

$$Q = \frac{K_{abs}}{\mu} \times \frac{A\Delta P}{L} \tag{5.1}$$

where Q is the flowrate (m^3/sec), K_{abs} the permeability (in D = $9.87*10^{-13}$ m^2), μ is the water viscosity (in N.sec/m^2), ΔP is the pressure drop across the plug (in Pa) and L is the length of the core (in m).

The effluent water was collected at the production outlet. We used the aqueous fractions to prepare the calibration curves for chemical analyses.

(2) *Synthetic formation water and heavy oil flooding*. SFW-1 (or SFW-2 or SFW-3) and oil flooding were conducted both following the unsteady state method. The core was first imbibed with 100% of synthetic formation water followed by a drainage using the candidate heavy oil, Oil-J2. The heavy oil was flooded down to initial water saturation (S_{wi}). This method was chosen over the conventional steady method because it resembles to the displacement occurring in a typical oil reservoir. Also, it is reported to give a better endpoint. Both candidate oil and SSW were injected at a constant rate of 1.5 ml/min.

(3) *Preflush flood*. The preflush was low-saline water (P-1 or P-2). The injection was performed at 1 ml/min. The preflush was conducted until residual oil saturation (S_{or}) was reached. The core was then allowed to age for 20 days at 55^{o}C and at confined pressure around 4 MPa.

(4) *Microemulsion and chase water flooding*. The microemulsion formulation size was about 0.10-0.25 PV and was injected rate of 0.25 ml/min. At the breakthrough, a postflush (P-3) was injected at the rate of 0.75 ml/min for approximately 2 to 3 PV. The effluent fractions were collected in a fractionator. The volumes of heavy oil and water, recovered therefrom, were recorded.

5.2.2.3 Chemistry of effluent fractions

The pH of effluent fractions was monitored using a Laqua Twin pH-meter (Model S010, Horiba Scientific, Japan). The concentrations in sodium (Na^+) and calcium (Ca^{2+}) were determined using Beer-lambert law. The calibration as well as the determination of sample concentration was done using UV-Visible spectrophotometer (Model 2450, Shimadzu, Japan).

5.2.2.4 Dynamic adsorption test

The dynamic adsorption was computed from the concentration of micellar slug in the effluent fractions. The concentration was measured using UV spectrophotometer (Model 2450,

Shimadzu, Japan) based on Beer-lambert principle. The calibration curves were prepared from the produced water during water permeability test.

5.3 Microemulsions Formulations and Their Properties

Fig. 5.3 illustrates the pseudo-ternary diagram obtained from gravimetric titration of the mixture (Oil-J2 + micellar slug) by low saline water, which encompasses four major regions.

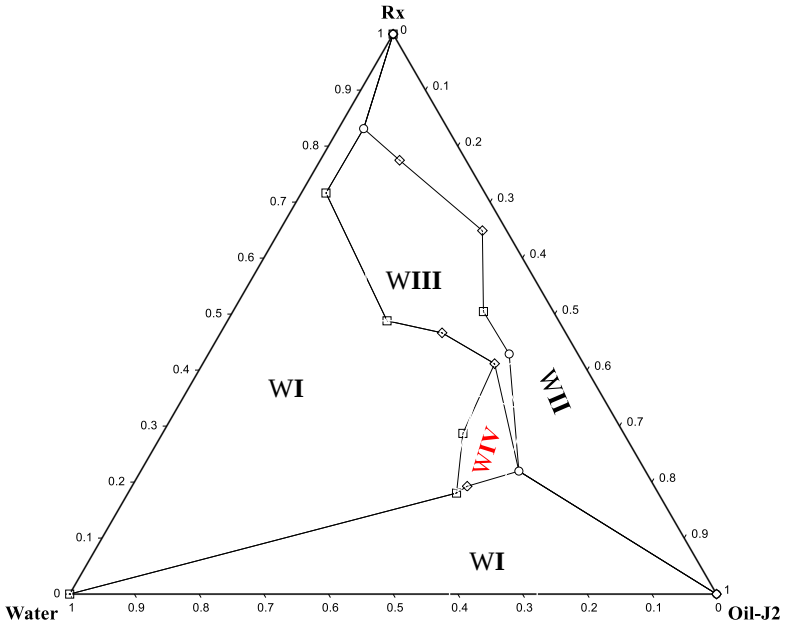

(**a**) Using R^x slugs

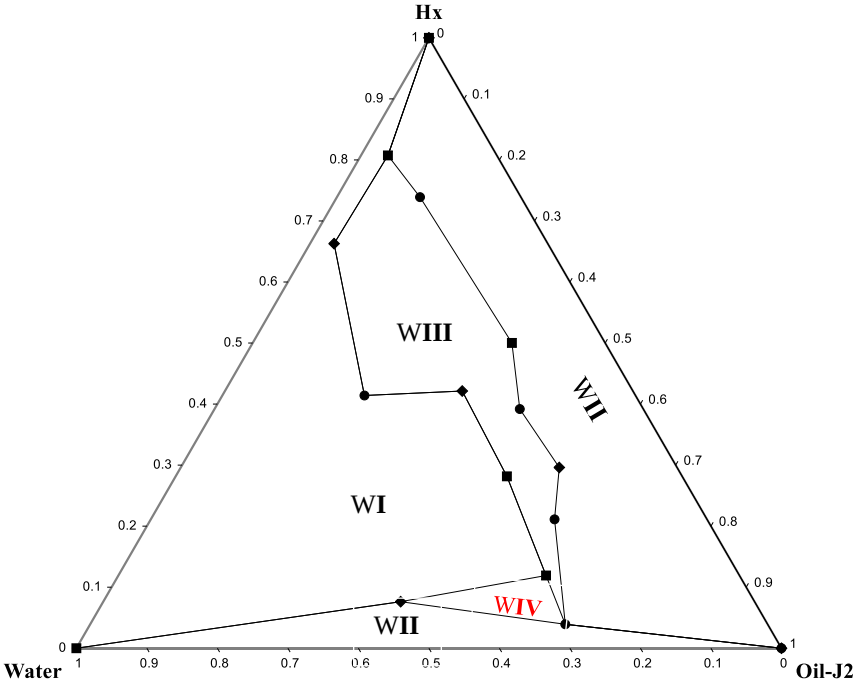

(**b**) Using H^x slugs

Fig. 5.3 Pseudo-ternary diagram of (Oil-J2-0.1 wt. % NaCl -micellar slug)

These regions included (1) a WI in which the investigated slug was in excess in the aqueous phase, (2) a WII in which the slug solubilized/emulsified preferentially the oil phase, (3) a WIII and (4) a WIV. Neither of the two formers was suitable to displace the heavy oil based on our proposed production scheme, largely because of either an eventual fingering effect (WI) or plausible loss of micellar slug (WII). For a concentration in R^x between the ranges of 40 – 85 wt. %, a WIII was yielded. Likewise, WIII was obtained when the concentration in H^x ranged from 18 – 80 wt. %.

Although this case is desirable for a classic chemical-EOR, formulating a microemulsion from this region might have led to misleading results as the microemulsion had an excess of oil and water. However, we noticed that beyond, at a defined concentration of oil and water, a fully solubilized mixture consisting of oil – water – micellar slug was obtained (WIV). The formulation, further injected, was selected therefrom. Both formulations had a brownish and gelatinous appearance, which suggested the formation of petroleum sulfonates. Table 5.5 summarizes the properties and the composition of the microemulsion formulations.

The rheological study of the formulated microemulsions revealed that NR3 was about 1.8 heavier than NR2 at the same shear rate and temperature (Fig. 5.4). NR2 and NR3 exhibited both a pseudo-plastic behavior i.e. their respective viscosities decreased with the shear rate. This observation is consistent with the results discussed in Chapter 4. On the average, the viscosity of NR2 and NR3 was 2.5 and 4.2 times higher than that of Oil-J2 respectively. The difference lied to the extent to which the primary slug solubilized (or emulsified) the residual oil.

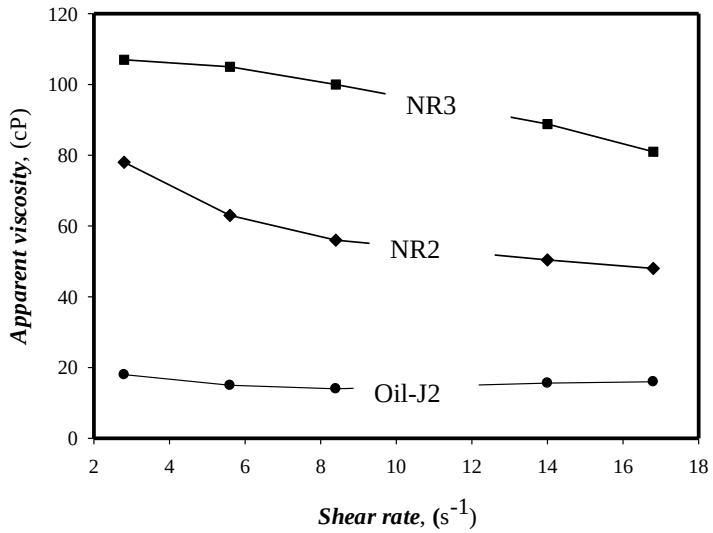

Fig. 5.4 Rheology of microemulsion-gel type at 55°C

Table 5.5 Composition and properties of microemulsion-gel type [a]

	Chemical composition, wt.%			Physical properties	
Formulation code	Heavy oil	Micellar slug	Brine	ρ, kg/m^3	MW, g/mol
NR2	46.4	28.7	24.9	0.982	134.5
NR3	67.5	3.7	28.8	0.995	235.0

[a] ρ: fluid density measured at 25°C; μ: absolute viscosity measured at experiment conditions (55°C, 14 s^{-1}); MW: molecular weight.

If the chemical structure of cationic Gemini surfactant is recalled, it appears that the micellar slugs prepared from longer molecular chains (i.e. H^x) have better solubilization/emulsification degree even at low concentration. Furthermore, not only these results corroborated with the phase behavior results discussed in the earlier chapters, but also they tend to confirm the significance of alkyl chain and that of the microemulsion clustering. In other words, the rheology of the microemulsion depended on (*i*) nature of alkyl chain of the surfactant, (*ii*) the formation of reverse micelles and (*iii*) the synergy between oil and micellar slug.

5.4 Oil Recovery

5.4.1 Heavy oil production from conventional cores

The secondary recovery using a classical water flooding (P-1) displaced about 33.6 and only 0.29 % of the initial oil-in-place in Flood-01 (Fig. 5.5a) and Flood-03 (Fig. 5.5b) respectively. In this flooding scheme, the prime purpose of the P-1 was the wettability alteration rather than recovery of the residual oil. Moreover, the preflush stage aimed at ionizing the surface charges of both residual oil and the plug with the further purpose to investigate the effect of enrichment of the preflush. This step was performed until the oil cut was less than 1% at which NR2 (or NR3) was injected. Subsequently, an increment in oil production of about 31 and 20% in Flood-01 and Flood-03 respectively was observed when the sandstones were flooded by NR3 and NR2 respectively.

The oil production was accompanied with a sharp increase in pressure drop, which reflected the occurrence of interactions between the oil bank and each flooding fluid. In other words, the response in pressure should be viewed as a decrease of viscous forces that keep the oil trapped between the interstices of the sandstone. The increase in pressure drop was gradual until it peaked to its maximal at/or few PVs after MF flooding. At the trailing edge of the microemulsion, P-3 was injected. We conducted this step until the residual oil saturation was reached. The pressure drop was fairly altered in Flood-03 (Fig. 5.5b), which was concurrent with a low increment in oil that was about 21% (Fig. 5.5a). On the other hand, in Flood-01, the

pressure drop decreases monotonically until it reaches a value close to that of P-1. This observation is concurrent with an oil production of 20% of IOIP.

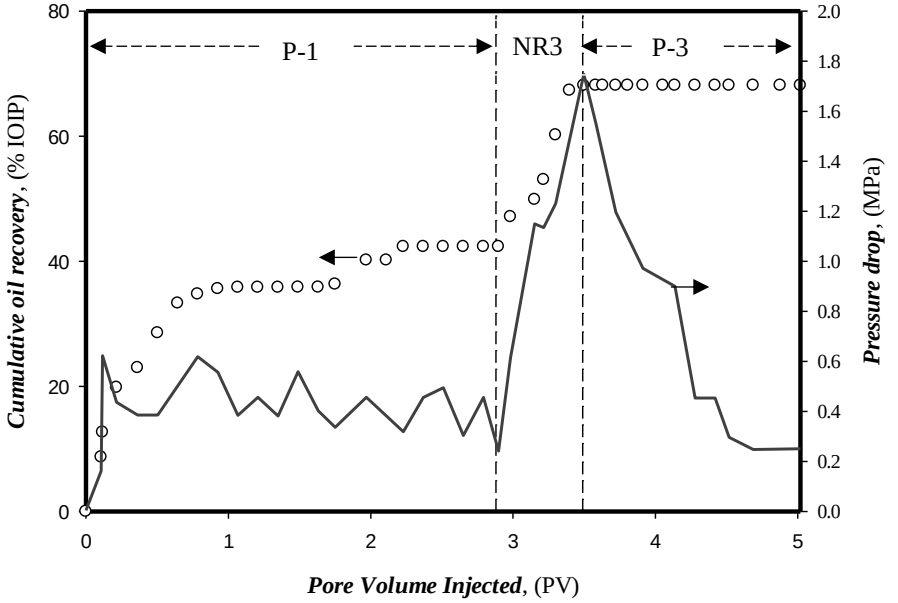

(**a**) Flood-01

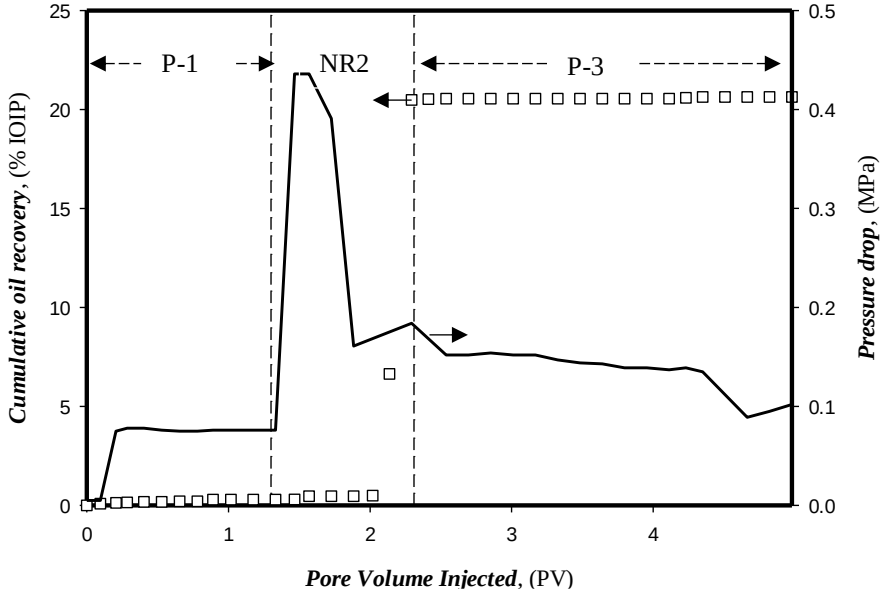

(**b**) Flood-03

Fig. 5.5 Oil recovery from conventional Berea sandstones; P-1: Preflush stage; NR2/3: microemulsion flood; P-3: Chase water flood

5.4.2 Heavy oil production from unconventional cores

The microemulsion flooding performed in unconventional sandstones i.e. an artificially fractured Berea sandstone (Flood-04) and heterogeneous sandstone (Flood-05) is presented in Fig. 5.6a and Fig. 5.6b respectively. Up to 37 and 70% of IOIP were achieved in Flood-04 and Flood-05 using P-2, an alkaline and low saline water. The fracture and the high permeability

zone provided both a matrix within which hydrocarbons are stored. This means as P-2 propagated through the core, it channeled preferentially within the network developed by the matrix. The weak capillary driving forces, existing therein, favored the oil to be displaced easily. This mechanism explained presumably the high recovery at this stage. Also, it was interesting to see the different pattern follows by the pressure drop. In fact, with the artificial fracture within the sandstone (Fig. 5.6a), P-2 seemed to propagate similarly to a homogeneous core (Fig. 5.5a). However, a porous medium promoted a sharp increase in pressure drop (Fig. 5.6b).

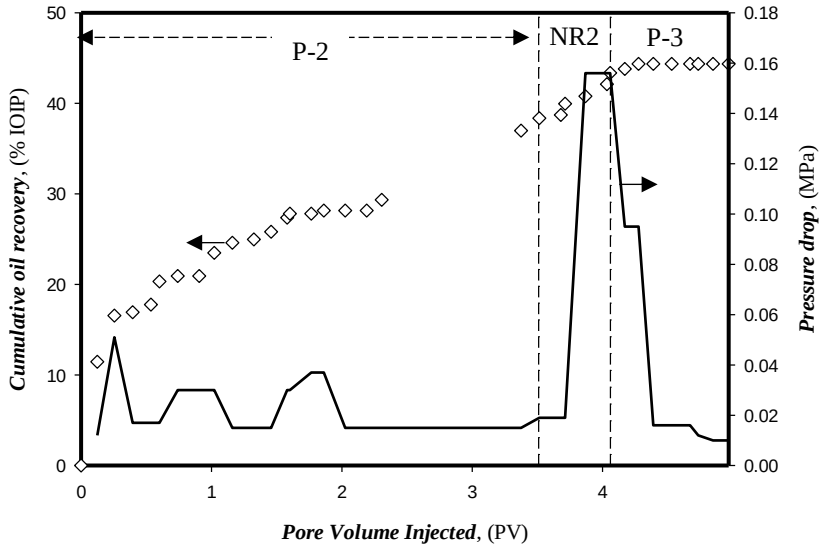

(**a**) Flood-04

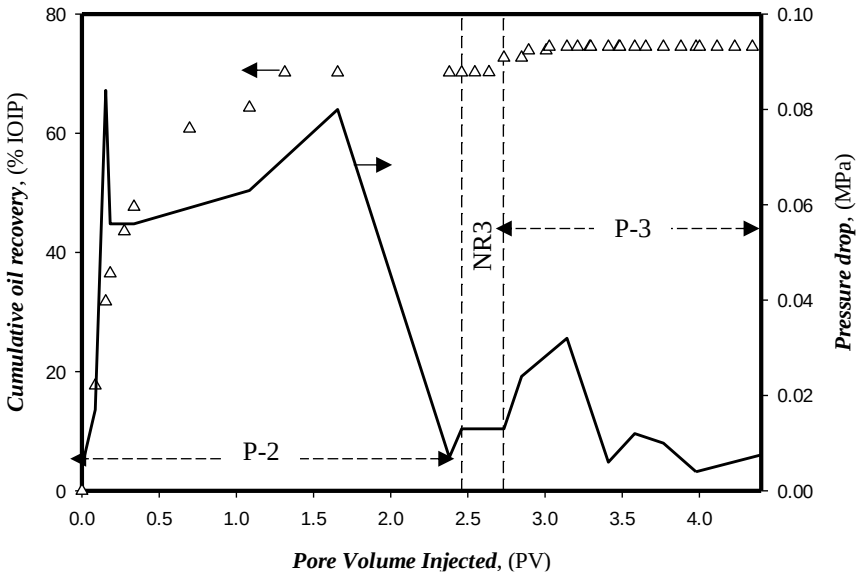

(**b**) Flood-05

Fig. 5.6 Oil recovery from unconventional sandstone cores; P-2: Alkaline preflush; NR2/3: microemulsion flood; P-3: Chase water flood

With the injection of NR2 (or NR3), the pressure drop increases steeply in both sandstones with the sharpest increase observed for the artificially fractured core (Fig. 5.6a). This was equally marked by an oil production of 6.4 and 8.4% of IOIP in Flood-04 (Fig. 5.6a) and Flood-05 (Fig. 5.6b) respectively. A little increment in oil was observed upon flooding the unconventional sandstones with P-3 (3.3 and 6.7% of IOIP in Flood-04 and Flood-05 respectively). Plausibly, both the pre-flush and the microemulsion flooding have exhausted the oil trapped within the thief zone. Another possibility is that flow of the displacing fluid is high in the thief zone to the point that the pressure drop does not play as important role in production.

Perhaps in unconventional cores, Oil-J2 was produced subsequently to the fracture/matrix interactions. The literature reports that the efficiency of an oil recovery method in fractured formation and/or highly permeable medium relies primarily on spontaneous imbibition, which itself is efficient when the formation is at its strongly water-wet state (Salehi et al., 2008; Tarek, 2001).

5.5 Wettability Alteration

5.5.1 Relative permeability ratio

In reviewing the relative permeability ratio during the oil production considering this flooding scheme, we observed that the wetting state changed gradually from oil-wet to mixed wet (Fig. 5.7a and Fig. 5.7b) and from neutral wet to strongly water-wet (Fig. 5.7c and 5.7d). A priori, aforementioned results showed that the injection, and the propagation, of the microemulsion formulations reduce the capillary forces within the core. The preflush (P-1) increased the water saturation (S_w) from 0.11 to 0.67 (Fig. 5.7a). On the other hand, P-1 altered fairly flood-03 from 0.48 to 0.49, which corresponds to a little increase of 0.31% (Fig. 5.7b). The alteration of S_w was lowered to 8% (Fig. 5.7b).

With the implementation of the tertiary recovery i.e. NR2 (or NR3) + P-3, S_w increased subsequently from S_{wi} to 65.3% in Flood-01 (Fig. 5.7a) and 58.7% in Flood-03 (Fig. 5.7b). A similar analysis for unconventional sandstones reveals that S_w increases from its initial value of about 67 and 81% during the preflush (P-2) and the tertiary recovery respectively in Flood-04 (Fig. 5.7c). These values were lowered to about 66.1 % in Flood-05 (Fig. 5.7d). The weak alteration in Flood-05 is directly attributed to the large storage capacity through which Oil-J2 flows preferentially. Therefore, one may think that the reasoning provides for the artificially fractured core could be valid for the heterogeneous sandstone.

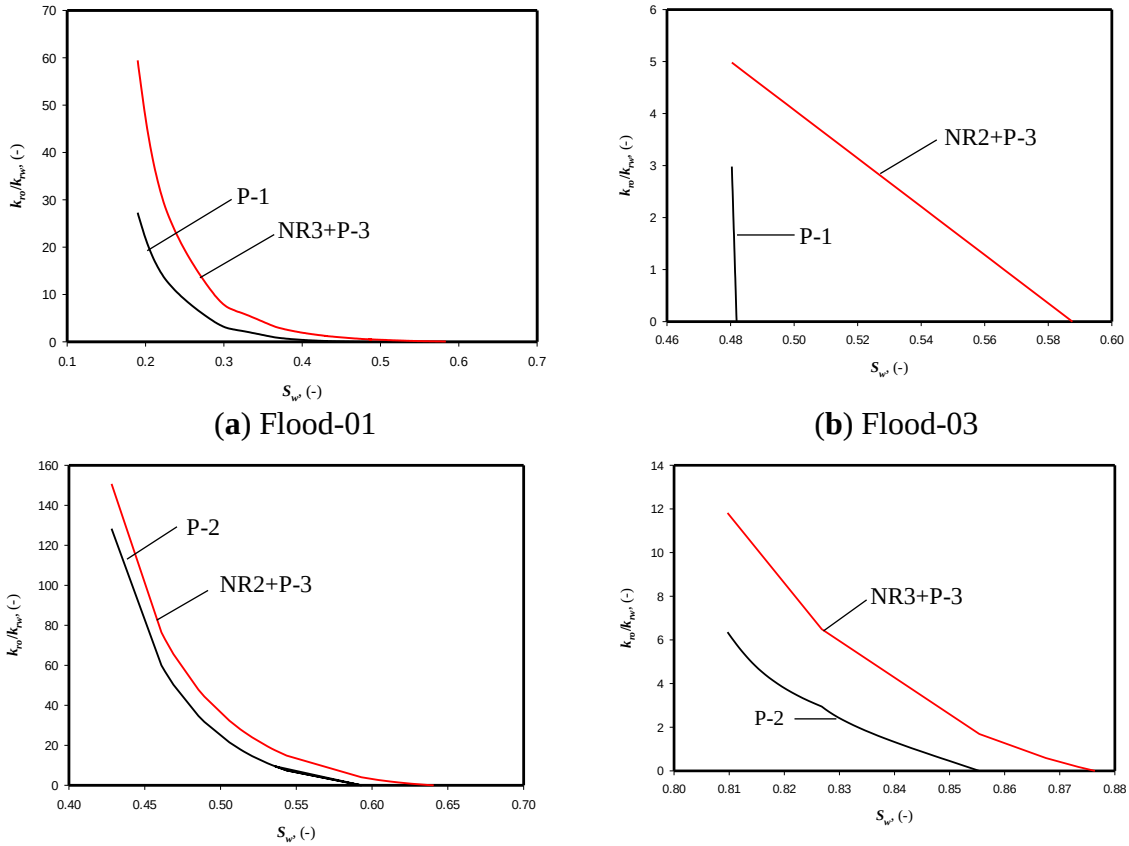

(**a**) Flood-01 (**b**) Flood-03

(**c**) Flood-04 (**d**) Flood-05

Fig. 5.7 Wettability alteration as function of water saturation, S_{or}: residual oil saturation

5.5.2 Effect of preflush composition

It is conjectured in the literature that altering the composition of the advancing fluid could produce more oil (Austad et al., 2010). This is so because, the chemical composition of displacing fluid acts upon the capillary forces through several physico-chemical mechanisms. Therefore, in the sought of verifying the extent to which the chemistry of P-1 and P-2 decreased the oil saturation, and subsequently alters the core wettability, we measured the effluent pH at each stage of the oil production with the assumptions that the pH hints at a chemistry occurring within the core. The results are shown in Fig. 5.8.

The injection of a fairly acidic preflush decreased the pH at the effluent the first few PV, which increased subsequently upon injecting the microemulsion formulation (Fig. 5.8 a, Fig. 5.8b). A reverse trend was observed for an alkaline preflush, which increases steadily the pH at the effluent (Fig. 5.8c, Fig. 5.8d). Subsequently, the oil saturation decreases (S_o). This is a clear indication that the acidity (or the chemical composition) of the preflush alters the saturation of the residual oil. While comparing, for example Flood-01 (homogeneous core) and Flood-05 (heterogeneous sandstone), we can see that the pH at the effluent increases steadily

until it reaches its maximum after 1.5 PV and 1.66 PV in the homogeneous and heterogeneous cores respectively (Fig. 5.8a, Fig. 5.8d). This observation is concurrent with a sharp decrease in S_o of an average computed rate of 17 % per PV of injected brine (Fig. 5.8a) and 39 % per PV injected (Fig. 5.8d). The increasing pH, and subsequently the decrease in S_o, highlights somewhat the potential of both low saline waters to alter the properties of the sandstone.

We believe the extent to which this alteration occurs is related to the ionic strength (and/or the acidity) of the injected water. Considering the work of Mohan et al. (1993), whom hypothesized a cationic exchange between the hydronium ions (H_3O^+) and sodium ions (Na^+), it is plausible that the weak acidity of P-1 and the alkalinity of P-2 were sufficient to ionize the native minerals of the cores leaving at their rears an ionized sandstone. With the injection of microemulsion formulations, we observed an abrupt decrease in the pH at the effluent water (Fig. 5.8a, Fig. 5.8c,, and Fig. 5.8d). While this observation was true for Flood-01, 04 and 05, a reverse trend is seen for Flood-03 (Fig. 5.8b). Presumably, the propagation of microemulsions prompted a series of chemical reactions.

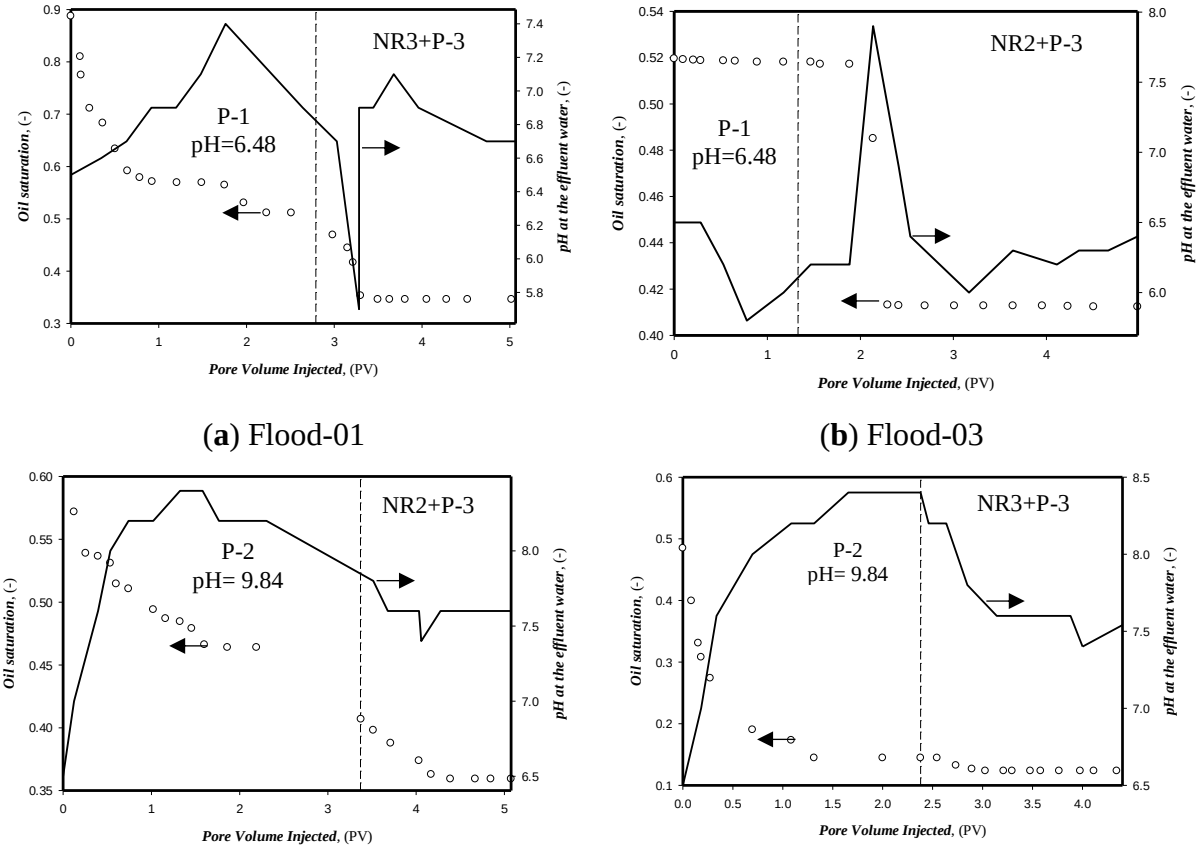

Fig. 5.8 Oil saturation alteration by change in preflush composition

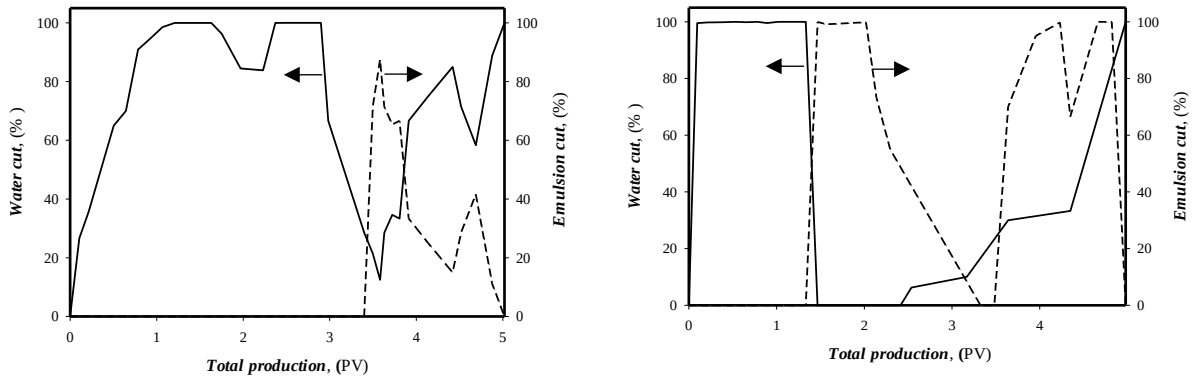

(**a**) Flood-01 (**b**) Flood-05

Fig. 5.9 Emulsion and water cuts from conventional sandstones

These chemical reactions that promoted favorable conditions for *in-situ* saponification and/or emulsification, which accounts the emulsion cut observed during the oil production (Fig. 5.9). We could correlate therefore that the recovery during the postflush depends primarily of the state of the core prior its injection. If the minerals of the core are sufficiently ionized, it results an enrichment of the propagating fluid. The propagation will further resemble to an alkaline flooding, hence the incremental oil recovery and the shift to a more water-wet of the sandstone.

5.6 Alteration of Heavy Oil Production by Microemulsion-Oil-Rock Interactions

5.6.1 Ion tracking and its influence of formulation performance

In the previous sections, it has been shown that the wettability, and thus the oil production, is dependent on crude oil/brine/rock (COBR) interactions. In order to increase and/or maximize the oil production, perhaps it is vital to understand the mechanisms of wettability alteration during this production scheme.

For this purpose, we tracked the concentration of Ca^{2+} and that of Na^{+} in the effluent water with the assumption that both ions are representative of the composition of the native core and the formation water. The results, performed only for Flood-01, are shown in Fig. 5.10a. A monotonic decrease in concentration in respect of preflush size was observed, which inverted when NR3 is injected. Both ions reached their optimal values at/around the water breakthrough beyond which, their concentration decreased. It seems clearly that each displacing fluid interacts, its own way, with the reservoir rock and the resident fluids.

In theory, if a fluid flows through a core without interacting chemically with the native minerals of the core, the concentration in any of its ionic element should be equal to that of the

diluted concentration of original fluid. Also, the curves diluted concentration vs. that of injected volume of the liquid, if plotted, should follow the same pattern. This implied that any reverse pattern between the diluted and measured concentration should be interpreted as result of chemistry between the propagating fluid and reservoir rock. In this research, we computed the diluted concentration of Na^+ (that is the concentration of Na^+ if there was no chemical interaction) and compare graphically with that of its equivalent concentration in the effluent fraction. The results are presented in Fig. 5.10b.

Preflush stage. It can be seen that both diluted and measured concentrations decrease with the size of the preflush, P-2.

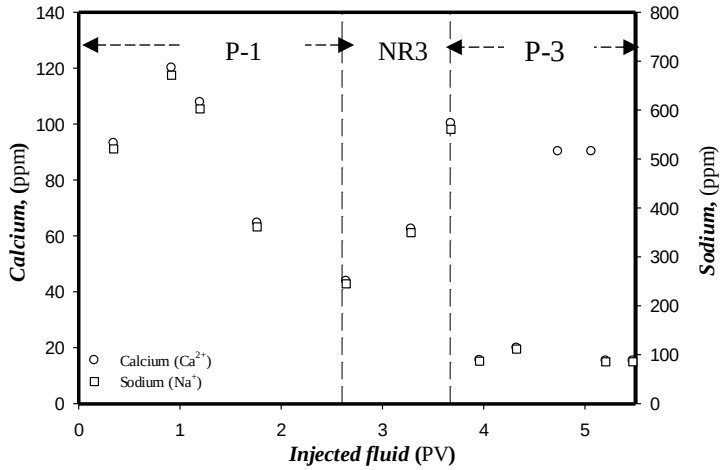

(a) Calcium and sodium tracking analysis

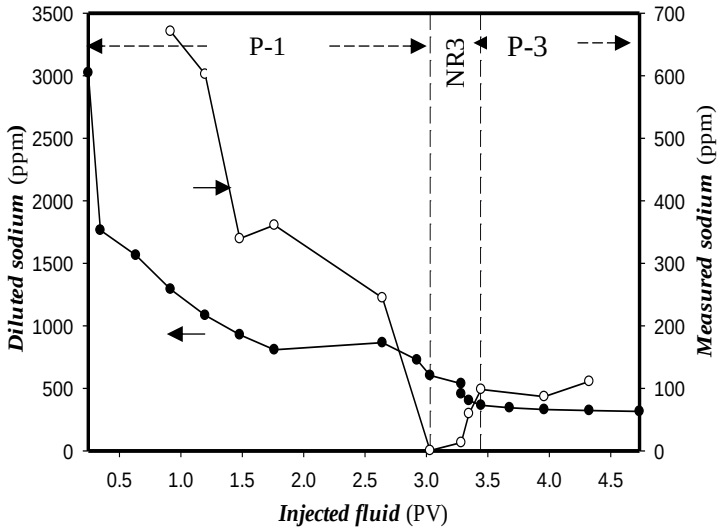

(**b**) Diluted and measured concentration of Na^+ during flood-01

Fig. 5.10 Ion tracking and effect of flooding fluid

On the average, we found that the concentration in Na^+ was on average 43.4% lower than that of the diluted one in Flood-01 (Fig. 5.10b). Considering that investigated plug is rich in orthoclase ($KAlSiO_3$), it is plausible from a geochemical point of view that the native mineral may undergo through a chemistry shown in equations (4.2 and 4.3). If the preflush is a low-saline water weakly acidic (P-1),

$$KAlSi_3O_{8(s)} + Na^+_{(aq)} \longrightarrow NaAlSi_3O_{8(s)} + K^+_{(aq)} \tag{5.2}$$

If however, the preflush is alkaline (P-2), plausibly during flood-04 or flood-05,

$$KAlSi_3O_{8(s)} + 4OH^-_{(aq)} + Ca^{2+}_{(aq)} + Al^{3+}_{(aq)} \leftrightarrow CaAl_2Si_3O_{8(s)} + K^+_{(aq)} + H_4SiO_{4(aq)} \tag{5.3}$$

With enrichment of preflush with a weak base (Flood-04 or Flood-05), the formation of anorthite ($CaAl_2Si_3O_8$) is prompted from the native orthoclase ($KAlSiO_3$), while a preflush with weakly acid low-saline water yields albite (Flood-01 or Flood-03). Following equations (4.2) – (4.3), the decrease observed in Na^+, and thus that in Ca^{2+} during preflush stage, are justified.

Microemulsion formulation injection. NR3 prompted a sharp increase in measured Na^+ concentration increased (Fig. 5.10b). More interesting, we observed that the heavy oil production was accompanied with a sludge deposition (Fig. 5.11), which is noticeable drawback for this method. This was true regardless the composition of the preflush and the microemulsion formulations. With the understanding that NR3 was prepared from divalent-free materials, there is no apparent reason that justifies the build-up in divalent ions. The only rational thought would be the assumption of a series of chemical reactions (equations 4.4 and 4.5) prompted by the formulation during its propagation inside the pore throats.

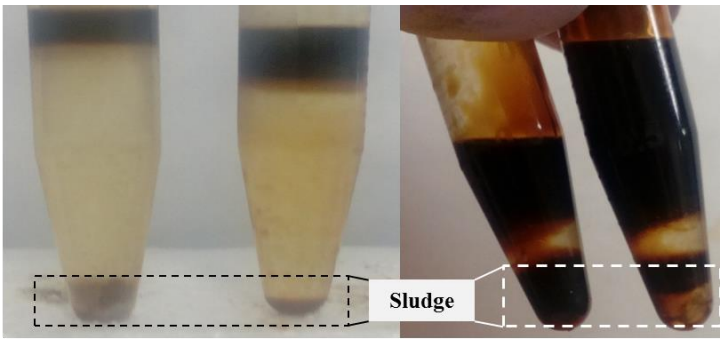

(**a**) Flood-01 (**b**) Flood-05

Fig. 5.11 Sludge deposition at the water breakthrough; from Nguele et al. (2017)

Therefore, in an acidic environment, we proposed the following reaction,

$$NaAlSi_3O_{8(s)} + 4H^+_{(aq)} + 18H_2O_{(aq)} \longleftrightarrow Al_4Si_4O_{10}(OH)_{8(s)} + 4Na^+_{(aq)} + 8H_4SiO_{4(aq)} \quad (5.4)$$

On the other hand, the microemulsion propagates in an alkaline medium, we think that the sludge is formed subsequently to reaction between anorthite and silic acid:

$$CaAl_2Si_3O_{8(s)} + 4OH^-_{(aq)} + 2Al^{3+}_{(aq)} + H_4SiO_{4(aq)} \rightleftharpoons Al_4Si_4O_{10}(OH)_{8(s)} + Ca^{2+}_{(aq)} + 2H_2O_{(aq)} \quad (5.5)$$

Equations (5.4 - 5.5) are consistent with the pH profile of the effluent fraction (Fig.5.8). We were lead to think that both microemulsion formulations promote the adsorption of free cations on ionized sites of the core. This mechanism is known as ion binding effect. Therefore, the sludge is believed to be an aggregate of kaolinite or $Al_4Si_4O_{10}(OH)_8$. The results reported in this research are consistent also with the literature, which stated that the ion binding is likely to be pronounced if the crude oil is highly acidic and the reservoir formation rich in clay i.e. kaolinite and/or montmorillonite (Anderson, 1986).

The latter effect was verified by the dynamic adsorption analysis shown in Fig. 5.12, which revealed that the slug was retained more either at the early stage of micro emulsion formulation injection (Fig. 5.12a) or during water breakthrough (Fig. 5.12b). As NR3 journeyed through the sandstone, it leached the minerals of the sandstone. If the core is rich in kaolinite and/or montmorillonite, the large surface area of the mineral (and its charged sites) would favor a high retention (Fig. 5.12a). On the other hand, if there are less interaction between the residual oil and the formulation (probably due to the existence of high permeability zone and/or fracture network), we believe that the slug retention was subsequent to an ion binding promoted by the preflush.

Chase water. The concentration in Na^+ decreases during P-3 flooding. It was equally observed that the volume of deposited sludge was reduced. Both observations suggest that the P-3 favor dissolution of aggregates. The decrease in Na^+ weakened the columbic interactions between ionic materials dissolved within the reservoir fluids. Depending on the ionic strength of the effluent, Morrow et al. (1996) proposed several interactions between resident oil, divalent (or monovalent) ion and the mineral rock. These interactions include [oil – M^{2+} – oil], [mineral – M^{2+} – mineral] and [oil – M^{2+} – mineral], where M^{2+} is the divalent ion. The latter combination is similar to what is known as Calcium Bridge. In this type of interactions, the

divalent ions (present in the formation brine) form a buffer layer between residual oil and the propagating fluid. Their presence, if proven, could provide a deeper explanation in the loss of efficiency of the microemulsion formulation. We ran several infrared spectra of effluent fractions, i.e. produced heavy oil and its corresponding effluent water at different stages of production, for Flood-01 and flood-05 to confirm the presence of calcium bridges.

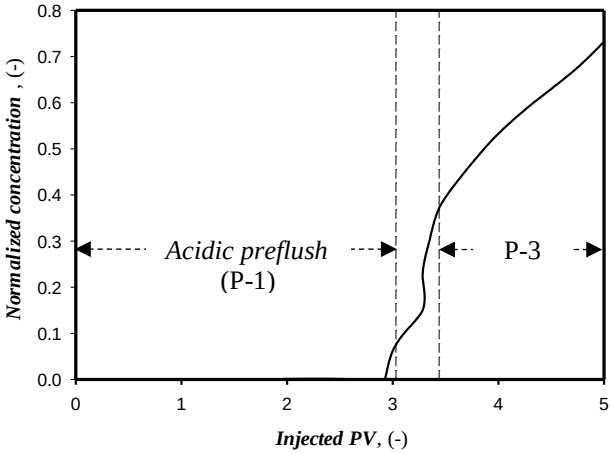

(a) Flood-01

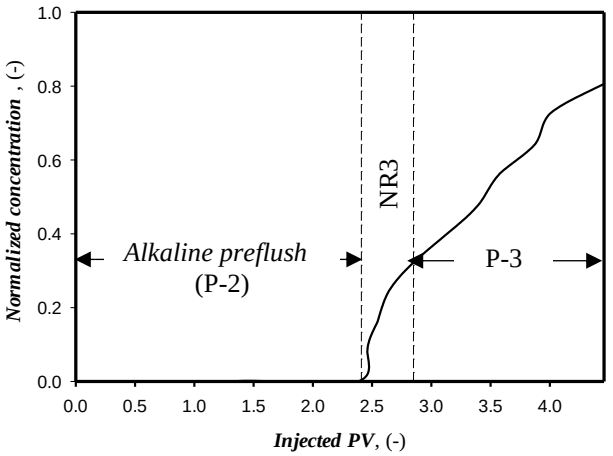

(b) Flood-05

Fig. 5.12 Dynamic adsorption during microemulsion flooding

Therefrom, we think that acid environment, within which the NR3 is propagating, promoted the complexation of petroleum acids by divalent ions, following a plausible chemistry shown in Equations 5.6 - 5.7 as proposed by Nguele et al. (Nguele et al., 2017) ,

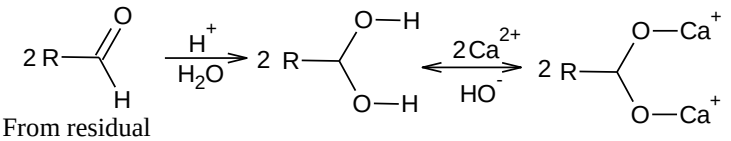

(5.6)

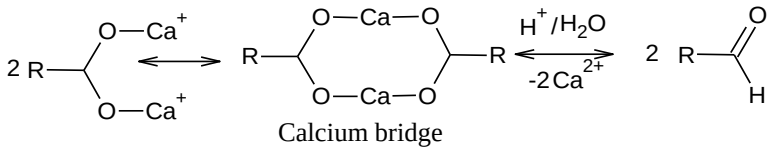

(5.7)

However, the microemulsion leaves at its trail an alkaline environment, calcium bridges can be re-dissolved following Equation 5.8,

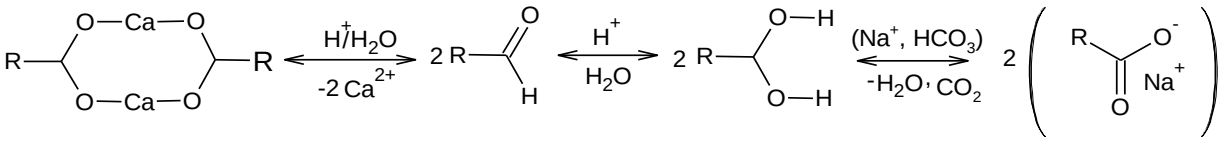

(5.8)

5.6.2 Formation of clusters

The phase behavior tests, discussed in Chapter 3, have revealed that the built-up in M^{2+} reduces the efficiency of the cationic microemulsion. Moreover, we have shown in above sections that concentration in M^{2+} could increase due to the leaching of the native minerals of the sandstone. Therefore, in sought of understanding deeply the efficiency loss of NR3, we analyzed at the microscopic level the different aqueous phase of the effluent fractions. These experiments were only performed for Flood-01 and Flood-02 (Fig. 5.12).

This was equally marked by an increase in particle size distribution, which tends to confirm the occurrence of Equations (5.4 and 5.5). The use of the chase water, P-3, prompts a disaggregation of the clusters. We should note that that the clusters were pronounced when the concentration in divalent ions increased. Therefore, it should be rational to guess the existence of threshold concentration in M^{2+} above which these ions develop an electrostatic and/or electrical field that further promotes clustering of water and oil molecules and/or presumably the formation of calcium bridges. Following this assumption, we used the model presented in Chapter 3 with consideration that the concentration in M^{2+} is considerable to promote the clustering, which is in reality, close to the actual case study.

The results are shown in Fig. 5.14. The clusters and/or the sludge formation were found dependent of the concentration in M^{2+} and the acidity/alkalinity. Each production stage is accompanied by a change in acidity depending of the propagating fluid. This is to say that the preflush (or microemulsion formulations) favors a phase transition, which is enhanced by the complexation of hydrophobic parts of the oil by M^{2+}.

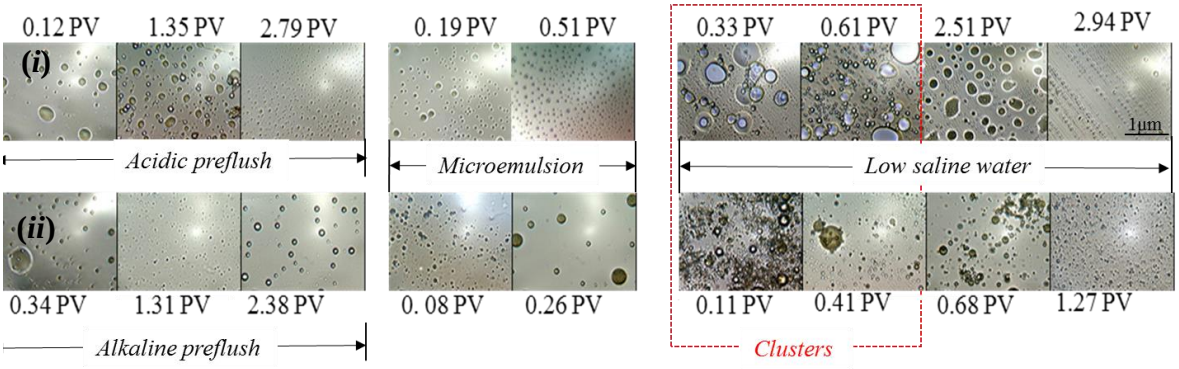

(**a**) Microphotographs of emulsion formed in the effluent fractions; (*i*) Flood-01 and (*ii*) Flood-05

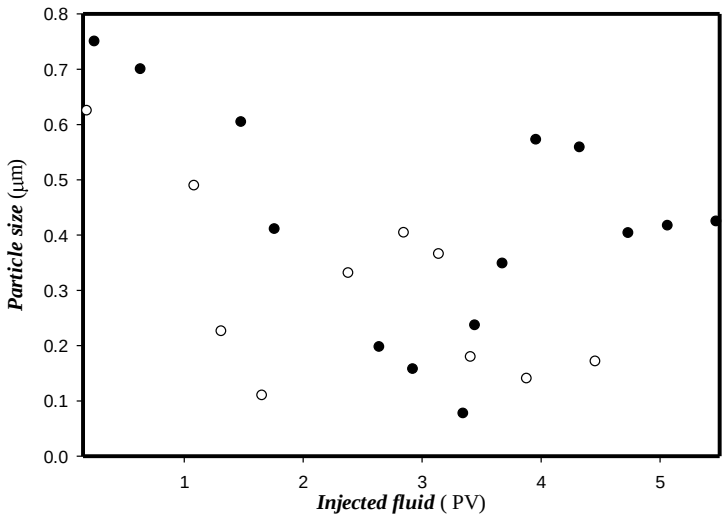

(**b**) Particle size distribution at the different stages of oil production; (●) Flood-01 and (○) Flood-05

Fig. 5.13 Particle size distribution at the different stages of oil production

The phase transition resulting from the displacement of heavy oil by a NR3 could be seen as W/O → O/ NR3 → NR3/W. While this phase transition was found valid when PF_1 was used, P-2 inverted the sequence. Also, Fig. 5.14 revealed that particle size, predicted by the electrostatic model is much higher compared to that of emulsions. The chase water flooding, the corresponding values for Flood-01 and Flood-05 were found to be 36.2 and 39.1% respectively, which implied that beyond the chemical occurrence included in the electrostatic model, there are probably more factors that promote also the emulsion clustering. Also, this model highlighted the significance of the preflush composition in clustering, and thus the microemulsion formulation efficiency. For example, it shows that with the addition of as an alkali in the preflush, the size of the clusters decreases steeply.

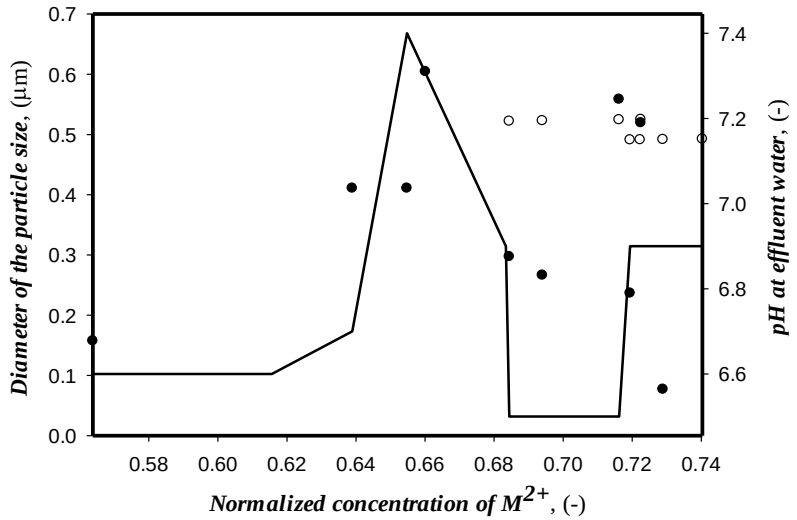

(**a**) Flood-01

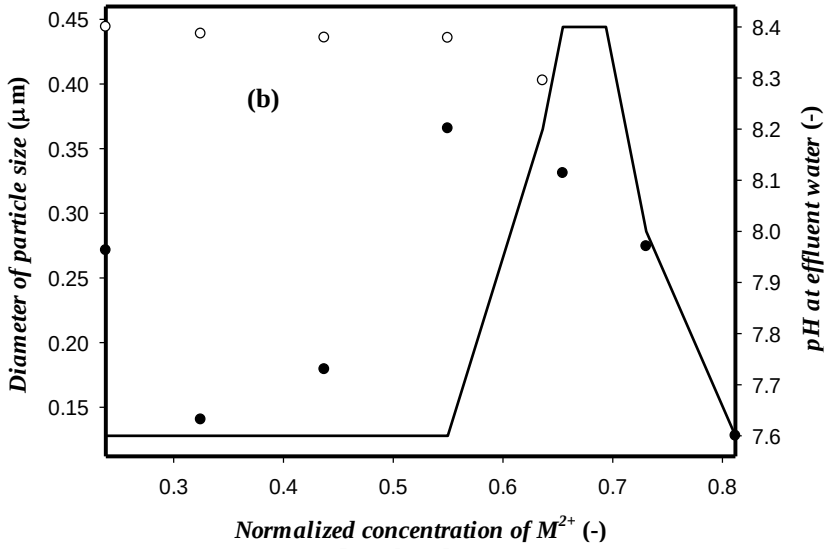

(**b**) Flood-05

Fig. 5.14 Modeling of particle clustering; (○) Predicted; (●) Experimental

5.7 Summary

In this chapter, we have investigated experimentally the potential of microemulsion flooding for heavy oils in different Berea sandstones. Herein was discussed a flooding scheme consisting of the injection of a microemulsion formulated ex-situ. Not only was presented a mechanistic study, but also we presented the impact of the interactions microemulsion-oil-reservoir rock. The major outlines of this chapter are:

(1) The salinity at which the microemulsion formulations should be prepared is sensitive to (*i*) the length of the alkyl chain of the primary Gemini surfactant, (*ii*) the nature and the molecular weight of its cosolvent and (*iii*) the acidity of the residual crude oil.

(2) The incremental oil recovery using microemulsion formulations displaced about 31, 20% of the initial oil-in-place (IOIP) in conventional water-flooded sandstones. From unconventional sandstones, the values were lowered to 6.4 and 8.4% of IOIP.

(3) The propagation of microemulsion formulations promoted favorable conditions for *in-situ* saponification and/or emulsification which yield an interfacial tension low enough to alter the wettability of the sandstone.

(4) The composition and the pH of the advancing formation brines defined the type of interactions mechanisms with the native minerals and residual oil, which further dictated the wettability.

(5) Microemulsion formulations prompted an increase in divalent/monovalent ion concentrations and the formation of sludge. Both mechanisms were influenced by the composition of the preflush.

(6) Emulsion clustering, the sludge deposition and the formation of calcium bridges were dependent of (*i*) concentration in divalent ions, (*ii*) acidity/alkalinity and (*iii*) the nature of propagating fluid.

Chapter 6.
SUMMARY and CONCLUSIONS

6.1 Summary

The current trend in oil production reveals that most of the supplied resources come from mature oilfields that have undergone through a primary and/or secondary recovery. These observations associated with the fact that few fields have been discovered over the past decades, there is an obvious for the oil industry to develop technologies that will sustain the increasing demand in energy. Heavy oils, and to a further extent extra-heavy oils, could be a providential alternative. On average, the primary and secondary oil recovery account for about one-third of the initial oil-in-place (IOIP), which leaves behind a considerable amount of oils underground. The untapped heavy oils are trapped primarily because of the high capillary forces existing within the pore of the sandstones. They prevent the oil to flow the wellbore for production.

Therefore, this research presented the screening and the laboratory evaluation of two tertiary recovery methods for heavy oil trapped within the pore throats of a sandstone formation. The motivation was to highlight their potential application in the candidate fields. Ultimately, it was sought to propose an improved recovery technique, which is (*i*) technically achievable, (*ii*) eliminates (or at least reduces) the energy requirements and (*iii*) is environment-friendly. Primarily experimental, this work has used as starting materials two candidate heavy oils (11.5^{o} and 16.6^{o} API), collected from the surface equipment in Akebono oilfield (Akita, Japan). Given the low oil saturation and permeability of the candidate formations, two non-thermal improved oil recovery (IOR) methods were pre-screened including miscible gas-EOR and chemical-EOR.

6.2 Heavy Oil Production in Respect of the Petro-physical Properties of the Candidate Formations

Gas injection is one of the oldest EOR methods. Successfully implemented for light to medium crudes oils, miscible gas-EOR (CO_2-EOR in particular) is the only EOR method, of which importance keeps growing worldwide despite the fluctuating oil price. This is so because the mechanisms of miscible gas-EOR have been mastered as a result of extensive laboratory and field experience. Additionally, CO_2 has the ability to achieve a low minimum miscibility pressure (MMP) in a wide type of crude oils compared to other gases like N_2 and CH_4. From the experiments conducted in this research the following conclusions could be drawn:

(1) Supercritical state (sCO_2), has a better solvating potential than sub-critical CO_2. If injected in the candidate formations, its ability as solvating agent will be altered by the gravity i.e. the oiliness of the residual oils. Moreover, the formation water is also expected to lower the solubility of sCO_2 as it acts as a kinetic barrier.

(2) sCO_2 perturbed better the kinetics and the stability of the equilibrium of intermolecular forces than CO_2. This means, from a technical point of view, that sCO_2 will develop a better foaminess in the candidate heavy oils.

(3) However, during the development of the miscibility front, sCO_2 will promote the desaphalting of the residual oil, which strips the light fractions of the residual to the heavier fractions. This study revealed this mechanism will increase with the saturation pressure.

(4) The challenge in implementing sCO_2 injection in the candidate field would be the asphaltene deposition, which was shown to be subsequent to the concentration in sCO_2 within the oil phase.

(5) The purity of sCO_2 would force the solubility of asphaltene to increase following an *S*-shape. However, an impure sCO_2 (that is sCO_2 diluted with a lean gas) is expected to decrease the asphaltene solubility, thus to increase its tendency to aggregate. Furthermore, the impurity of sCO_2 will enhance either the flocculation or the coagulation of asphaltene depending on the specific gravity of the residual oils.

(6) The formation temperature enhance the solvating power of sCO_2, thus decreases the solubility of asphaltene, which means that at the reservoir conditions asphaltene will be less soluble. However, if the temperature at the equilibrium is lower than that of the formation. a re-dissolution of suspended asphaltenes is expected.

(7) For sCO_2 to be applicable in the candidate oilfields, proper injecting conditions, at which the dissolved gas would keep asphaltene in suspension, should be defined.

6.3 Heavy Oil Production in Respect of the Physico-Physical Properties of the Candidate Heavy Oils

A chemical method, among the existing IOR techniques, involves the injection of a chemical (slug), which supplements the natural reservoir energy by interacting with the rock-oil-brine system. This creates favorable conditions for maximum oil recovery. These interactions EOR involve generally the lowering of the interfacial tension (IFT), the rock wettability alteration and a favorable phase behavior. In a classical chemical-EOR, the reservoir is pre-flushed with buffer solution, which neutralizes the ionic elements that reduce the efficient of the slug. The slug could be a surfactant, an alkali, a polymer or a combination of them. The success of a chemical-IOR resides on the ability of the slug to mobilize efficiently the oil droplets trapped within the pore throats. In this regard, a new class of surfactants i.e. Gemini surfactants were investigated in this research.

6.3.1 Cationic Gemini surfactants for improved heavy oil recovery

Gemini surfactants are a group of new class of surfactants with more than one hydrophilic head group and hydrophobic tail group linked by a spacer at/or near the head groups. Two cationic Gemini surfactants were investigated including a 12-3-12 (trimethylene-1,3-bis(dodecyldimethylammonium bromide) and 16-3-16 (trimethylene-1,3-bis(hexadecyldimethylammonium bromide). Their unique features in respect of oil recovery were investigated including the surface tension, the critical micelle concentration (CMC), the adsorption and the corrosion inhibiting potential of the slugs. Further analyses on the physico-chemical properties of their inherent microemulsions from the candidate residual oils were carried out. The key findings are:

(1) Both the length of the hydrophobic tail of the cationic Gemini surfactant and the formation salinity would alter the CMC. However, formulating a micellar slug with a non-ionic cosolvent would alleviate the latter effect.

(2) The hardness of the candidate formation water (i.e. its concentration in divalent ions) would alter the CMC, and thus the static surface tension, regardless the length of the alkyl chain, the cosurfactant and the concentration.

(3) The static adsorption of cationic micellar slug followed the sequence kaolinite > montmorillonite > and dolomite > Berea sandstone, where the highest adsorption was found

in kaolinite. With the knowledge that the formation is a sandstone type, a low adsorption may be expected.

(4) Using a micellar slug prepared from a cationic Gemini surfactant, it is possible to control the formation of acidic materials yielded during sCO_2 injection.

(5) The micellar slugs from cationic Gemini surfactants showed an extraordinary ability to achieve an ultra-low interfacial tension (IFT) even at a low-surfactant concentration. However, the achievable IFT is dependent on the length of the hydrophobic tail of the primary surfactant, the nature of the respective cosurfactant, the presence in divalent ions in the formation water and the concentration in acidic materials within the residual oil.

(6) The candidate formation temperature increases the achievable IFT, while its hardness altered the optimal salinity. Both observations were found valid regardless the type of candidate heavy oils.

(7) The viscosity of the microemulsions showed a pseudo-plastic behavior, with the heaviest microemulsion yielded by the slug prepared from the cationic Gemini surfactants with the longest alkyl chain. The apparent viscosity was equally altered by the salinity with the highest value recorded at/around the optimal salinity.

6.3.2 Laboratory evaluation of microemulsion flooding for heavy oils

The potential of microemulsion as displacing agent was verified by a series of core flood tests. The recovery scheme proposed the injection of a microemulsion prepared *ex-situ*. A systematic mechanistic study is presented. Additionally, the alteration of the potential of microemulsion as displacing agent due to the interactions with the system oil-reservoir rock was investigated. The key conclusions drawn are:

(1) The incremental oil recovery using microemulsion formulations displaced about 31 and 20% of the initial oil-in-place (IOIP) in conventional water-flooded sandstones. The same formulations injected in an artificially fractured and heterogeneous cores yielded a recovery of about to 6.4 and 8.4% of IOIP respectively.

(2) The composition and the acidity of the preflush would define the type of interactions mechanisms between the microemulsion formulation, the residual petroleum fluids and the native minerals. The resulting wettability alteration is inherent to these interactions.

(3) Microemulsion formulations were found not only to prompt a build-up in divalent and/or monovalent ion concentration, but also to promote the precipitation of sludgy materials.

(4) The sludge deposition is the main challenge in this production scheme. A tentative mitigation route would be the use of an alkaline preflush.

(5) Emulsion clustering and the sludge deposition were found dependent of (*i*) concentration in divalent ions, (*ii*) acidity/alkalinity and (*iii*) the nature of propagating fluid.

6.4 Future Challenges and Considerations

Heavy oils and extra-heavy oils represent a huge potential for the growing energy demand with large volumes still trapped underground. Several tertiary methods have been investigated over the past decades with mitigated results. This is because the choice, the implementation and the success of an EOR technique is severely affected by the geometry of the reservoir, the properties of the residual oil. Throughout this work, several factors and challenges, highlighted as possible drawbacks, required further investigations prior considering the method for a trial field. These key points, among many others, include:

- Candidate formation data are essential to the design process, and should be collected and used whenever possible for more realistic (compared to Berea sandstones).

- Investigation on mechanisms of asphaltene aggregation during the swelling process of the oil, which requires more experiments that will validate the thermodynamic model proposed.

- A core-flood tests using sCO_2 should be conducted in order to define the injecting parameters window for the test field.

- The clustering within the microemulsion is an interesting topic as it can help to understand the rheology of microemulsions and thus its propagation within the formation.

The model, proposed in this work, should be further investigated and validated by additional experiments.

- A deeper study on interactions [crude oil – reservoir brine – microemulsion] should be extended. This will be helpful to understand, and perhaps to predict, the mechanisms of sludge deposition.

- A numerical simulation should be carried to evaluate the potential of the proposed production scheme on a field scale. However, it should be noted that a typical simulation is based upon assumption specially when building the geological model. This means that for the results to reflect the reality, not only the experiments should be conducted from the candidate formation cores, but also the actual petro-physical properties of the formation are needed.

REFERENCES

Agency, I.E., 2013. Resources to Reserves. Paris.

Alagorni, A.H., Yaacob, Z. Bin, Nour, A.H., 2015. An Overview of Oil Production Stages: Enhanced Oil Recovery Techniques and Nitrogen Injection. Int. J. Environ. Sci. Dev. 6, 693–701.

Anderson, W., 1986. Wettability Literature Survey- Part 1: Rock/Oil/Brine Interactions and the Effects of Core Handling on Wettability. J. Pet. Technol. 38.

Austad, T., Rezaeidoust, A., Puntervold, T., 2010. Chemical Mechanism of Low Salinity Water Flooding in Sandstone Reservoirs, in: SPE Improved Oil Recovery Symposium. Society of Petroleum Engineers, pp. 1–18.

Begemann, M.H., Gudeman, C.S., Pfaff, J., Saykally, R.J., 1983. Detection of the Hydronium Ion (H_3O^+) by High-Resolution Infrared Spectroscopy. Phys. Rev. Lett. 51, 554–557.

Bennett, K.E., Davis, H.T., Macosko, C.W., Scriven, L.E., 1981. Microemulsion Rheology: Newtonian and Non-Newtonian Regimes, in: SPE Annual Technical Conference and Exhibition. Society of Petroleum Engineers.

Bera, A., Mandal, A., 2015. Microemulsions: A Novel Approach to Enhanced Oil Recovery: A Review. J. Pet. Explor. Prod. Technol. 5, 255–268.

Bera, A., Ojha, K., Kumar, T., Mandal, A., 2012. Phase Behavior and Physicochemical Properties of (Sodium Dodecyl Sulfate + Brine + Propan-1-ol + Heptane) Microemulsions. J. Chem. Eng. Data 57, 1000–1006.

Brons, G., Yu, J.M., 1995. Solvent Deasphalting Effects on Whole Cold Lake Bitumen. Energy Fuels 9, 641–647.

Buckley, J.S., Liu, Y., 1998. Some Mechanisms of Crude Oil/Brine/Solid Interactions. J. Pet. Sci. Eng. 20, 155–160.

Bunton, C.A., Robinson, L., Schaak, J., Stam, M.F., 1971. Catalysis of Nucleophilic Substitutions by Micelles of Dicationic Detergents. J. Org. Chem. 36, 2346–2350.

Cannan, R.K., Kibrick, A., 1938. Complex Formation Between Carboxylic Acids and Divalent Metal Cations. J. Am. Chem. Soc. 60, 2314–2320.

Cao, M., Gu, Y., 2013. Oil Recovery Mechanisms and Asphaltene Precipitation Phenomenon in Immiscible and Miscible CO_2 Flooding Processes. Fuel 109, 157–166.

Castro, M.J.L., Kovensky, J., Fernandez Cirelli, A., Mariano J. L. Castro, José Kovensky, and, Cirelli, A.F., Castro, M.J.L., Kovensky, J., Fernández Cirelli, A., 2002. New Family of Nonionic Gemini Surfactants. Determination and Analysis of Interfacial Properties. Langmuir

18, 2477–2482.

Cayias, J.L., Schechter, R.S., 1976. Modeling Crude Oils for Low Interfacial Tension. Soc. Pet. Eng. J. 16.

Chukwudeme, E. A., Hamouda, A. A., 2009. Enhanced Oil Recovery (EOR) by Miscible CO_2 and Water Flooding of Asphaltenic and Non-Asphaltenic Oils. Energies 2, 714–737.

Chung, F., Sarathi, P., Jones, R., 1991. Modeling of Asphaltene and Wax Precipitation. Bartlesville.

Cuthiell, D., Kissel, G., Jackson, C., Frauenfeld, T., Fisher, D., Rispler, K., 2006. Viscous Fingering Effects in Solvent Displacement of Heavy Oil. J. Can. Pet. Technol. 45, 29–38.

Dam, T., Engberts, J.B.F.N., Karthauser, J., Karaborni, S., Van Os, N.M., 1996. Synthesis, Surface Properties and Oil Solubilisation Capacity of Cationic Gemini Surfactants. Colloids Surfaces A Physicochemical Eng. Asp. 118, 41–49.

Danesh, A., 1998. PVT And Phase Behaviour of Petroleum Reservoir Fluids. Elsevier, Amsterdam.

Danielsson, I., Lindman, B., 1981. The Definition of Microemulsion. Colloids and Surfaces 3, 391–392.

Dashti, G., 2014. A Study of Microemulsion Viscosity with Consideration of Polymer and Co-solvent Additives. The University of Texas at Austin.

David Ting, P., Hirasaki, G.J., Chapman, W.G., 2003. Modeling of Asphaltene Phase Behavior with the SAFT Equation of State. Pet. Sci. Technol. 21, 647–661.

Davies, J.T., Rideal, E.K., 1961. Interfacial Phenomena. Academic Press, New York.

Devendiran, D.K., Amirtham, V.A., 2016. A Review on Preparation, Characterization, Properties and Applications of Nanofluids. Renew. Sustain. Energy Rev. 60, 21–40.

Devinsky, F., Masarova, L., Lacko, I., 1985. Surface Activity and Micelle Formation of Some New Bisquaternary Ammonium Salts. J. Colloid Interface Sci. 105, 235–239.

Diamant, H., Andelman, D., 2003. Models of Gemini Surfactants, in: (eds), R.Z. and J.X. (Ed.), Gemini Surfactants: Interfacial & Solution Phase Behavior. Marcel Dekker, New York, p. 16.

Donaldson, E.C., Chilingar, G. V., Fu Yen, T., 1989. Enhanced Oil Recovery, II processes and operations. Elsevier, New York.

Eicke, H.F., Christen, H., 1974. On the stability of micelles in apolar media. J. Colloid Interface Sci. 46, 417–427.

El Achouri, M., Infante, M., Izquierdo, F., Kertit, S., Gouttaya, H., Nciri, B., 2001. Synthesis of Some Cationic Gemini Surfactants And Their Inhibitive Effect on Iron Corrosion in Hydrochloric Acid Medium. Corros. Sci. 43, 19–35.

Enge, I.B., 2014. The Effect of Brine Composition and Rock Type on Oil Recovery by the Use of Combined Low-Salinity Waterflooding and Surfactant Flooding: A Literature Review and Experimental Study Ida Baltzersen Enge. Norwegian University of Science and Technology.

Favre, H.A., Powell, W.H., 2013. Nomenclature of Organic Chemistry. Royal Society of Chemistry, Cambridge.

Gao, B., 2012. Development of Novel EOR Surfactatant and Design of an Alkaline/Surfactant/Polymer Field Pilot. The University of Texas at Austin.

Gao, B., Sharma, M.M., 2013. A Family of Alkyl Sulfate Gemini Surfactants. 2. Water-Oil Interfacial Tension Reduction. J. Colloid Interface Sci. 407, 375–381.

Garcia-Rio, L., Leis, J.R., Mejuto, J.C., Pena, M.E., Iglesias, E., 1994. Effects of Additives on the Internal Dynamics and Properties of Water/AOT/Isooctane Microemulsions. Langmuir 10, 1676–1683.

Goddard, W. A., Tang, Y., Shuler, P., Blanco, M., 2004. Lower Cost Methods for Improved Oil Recovery (IOR) Via Surfactant Flooding. doi:DE-FC26-01BC15362

Gray, M., Yeung, A., Foght, J., Yarranton, H.W., 2008. Potential Microbial Enhanced Oil Recovery Processes: A Critical Analysis, in: SPE Annual Technical Conference and Exhibition. Society of Petroleum Engineers.

Green, D.W., Willhite, G.P., 1998. Enhanced Oil Recovery. Society of Petroleum Engineers, Richardson.

Healy, R.N., Reed, R.L., Stenmark, D.G., 1976. Multiphase Microemulsion Systems. Soc. Pet. Eng. J. 16, 147–160.

Hitchen, S.M., Dean, J.R., 1993. Properties of Supercritical Fluids, In: Applications of Supercritical Fluids In Industrial Analysis. Springer Netherlands, Dordrecht, pp. 1–11.

Holm, L.W., 1971. Use of Soluble Oils for Oil Recovery. J. Pet. Technol. 23, 1475–1483.

Holmberg, K., Shah, D., Schwuger, M., 2002. Handbook of Applied Surface and Colloid Chemistry.

Hu, Y.F., Li, S., Liu, N., Chu, Y.P., Park, S.J., Mansoori, G.A., Guo, T.M., 2004. Measurement and Corresponding States Modeling of Asphaltene Precipitation in Jilin Reservoir Oils. J. Pet. Sci. Eng. 41, 169–182.

Hua, X.Y., Rosen, M.J., 1991. Dynamic Surface Tension of Aqueous Surfactant Solutions. J. Colloid Interface Sci. 141, 180–190.

Huh, C., 1979. Interfacial Tensions and Solubilizing Ability of A Microemulsion Phase That Coexists With Oil And Brine. J. Colloid Interface Sci. 71, 408–426.

Jafari Behbahani, T., Ghotbi, C., Taghikhani, V., Shahrabadi, A., 2012. Investigation on

Asphaltene Deposition Mechanisms During CO_2 Flooding Processes in Porous Media: A Novel Experimental Study And A Modified Model Based On Multilayer Theory For Asphaltene Adsorption. Energy and Fuels 26, 5080–5091.

Jayasekera, A.J., Goodyear, S.G., 2000. The Development of Heavy Oil Fields in the United Kingdom Continental Shelf: Past, Present, and Future. SPE Reserv. Eval. Eng. 3, 317–379.

Jones, S.C., Dreher, K.D., 1976. Cosurfactants in Micellar Systems Used for Tertiary Oil Recovery. Soc. Pet. Eng. J. 16, 10–11.

Kim, T.-S., Hirao, T., Ikeda, I., 1996. Preparation ofbis-quaternary ammonium salts from epichlorohydrin. J. Am. Oil Chem. Soc. 73, 67–71.

Kohse, B.F., Nghiem, L.X., Maeda, H., Ohno, K., 2000. Modelling Phase Behaviour Including the Effect of Pressure and Temperature on Asphaltene Precipitation, in: SPE Asia Pacific Oil and Gas Conference and Exhibition. Society of Petroleum Engineers, pp. 1–13.

Kokal, S., Al-Kaabi, A, 2010. Enhanced Oil Recovery: Challenges and Opportunities. Glob. Energy Solut. 64–69.

Liu, Q., Dong, M., Asghari, K., Tu, Y., 2007. Wettability alteration by magnesium ion binding in heavy oil/brine/chemical/sand systems — Analysis of electrostatic forces. J. Pet. Sci. Eng. 59, 147–156.

Magdassi, S., Ben Moshe, M., Talmon, Y., Danino, D., 2003. Microemulsions based on anionic gemini surfactant. Colloids Surfaces A Physicochem. Eng. Asp. 212, 1–7.

Mai, a., Bryan, J., Goodarzi, N., Kantzas, A., 2009. Insights Into Non-Thermal Recovery of Heavy Oil. J. Can. Pet. Technol. 48, 27–35.

Mannistu, K.D., Yarranton, H.W., Masliyah, J.H., 1997. Solubility Modeling of Asphaltenes in Organic Solvents. Energy Fuels 11, 615–622.

Menger, F.M., Keiper, J.S., 2000. Gemini Surfactants. Angew. Chemie Int. Ed. 39, 1906–1920.

Mohan, K.K., Vaidya, R.N., Reed, M.G., Fogler, H.S., 1993. Water sensitivity of sandstones containing swelling and non-swelling clays. Colloids Surfaces A Physicochem. Eng. Asp. 73, 237–254.

Moradi, S., Dabiri, M., Dabir, B., Rashtchian, D., Emadi, M. A., 2012. Investigation Of Asphaltene Precipitation in Miscible Gas Injection Processes: Experimental Study and Modeling. Brazilian J. Chem. Eng. 29, 665–676.

Morrow, N.R., Valat, M., Yidliz, H., 1996. Effect of Brine Composition on Recovery of an Alaskan Crude Oil By Waterflooding, in: Annual Technical Meeting. Petroleum Society of Canada, Calgary. doi:10.2118/96-94

Nelson, R.C., Pope, G. A., 1978. Phase Relationships in Chemical Flooding. Soc. Pet. Eng. J.

18.

Nghiem, L.X., Hassam, M.S., Nutakki, R., George, A.E.D., 1993. Efficient Modelling of Asphaltene Precipitation, in: SPE Annual Technical Conference and Exhibition. Society of Petroleum Engineers, pp. 375–384.

Nguele, R., Ghulami, M.R., Sasaki, K., Said-Al Salim, H., Widiatmojo, A., Sugai, Y., Nakano, M., 2016a. Asphaltene Aggregation in Crude Oils During Supercritical Gas Injection. Energy Fuels 30, 1266-1278.

Nguele, R., Sasaki, K., Ghulami, M.R., Sugai, Y., Nakano, M., 2016b. Pseudo-Phase Equilibrium of Light and Heavy Crude Oils For Enhanced Oil Recovery. J. Pet. Explor. Prod. Technol. 6, 419–432.

Nguele, R., Sasaki, K., Salim, H.S.-A., Sugai, Y., Widiatmojo, A., Nakano, M., 2016c. Microemulsion and Phase Behavior Properties of (Dimeric ammonium surfactant salt – heavy crude oil – connate water) System. J. Unconv. Oil Gas Resour. 14, 62–71.

Nguele, R., Sasaki, K., Salim, H.S., Sugai, Y., 2015a. Physicochemical And Microemulsion Properties of Dimeric Quaternary Ammonium Salts With Trimethylene Spacer For Enhanced Oil Recovery. Colloid Polym. Sci. 293, 3487–3497.

Nguele, R., Sasaki, K., Sugai, Y., Omondi, B., Said Al-Salim, H., Ueda, R., 2017. Interactions between Formation Rock and Petroleum Fluids during Microemulsion Flooding and Alteration of Heavy Oil Recovery Performance. Energy Fuels 31, 255–270.

Nguele, R., Sasaki, K., Sugai, Y., Said-Al Salim, H., Ghulami, M.R., Nakano, M., 2015b. Experimental Investigation of Brine Hardness and Its Induced Chemistry During Heavy Crude Recovery Through CO_2 Injection. Int. J. Eng. Pract. Res. 4, 60–66.

Nguele, R., Sasaki, K., Sugai, Y., Said Al-Salim, H., Ueda, R., 2016d. Supercritical CO_2 Injection in Heavy Oils – Solubility and Influence of Temperature in Asphaltene Deposition, in: World Heavy Oil Congress. Calgary, p. WHOC16.

Novosad, J., 1982. Surfactant Retention in Berea Sandstone- Effects of Phase Behavior and Temperature. Soc. Pet. Eng. J. 22.

Okumura, M., Yeh, L.I., Myers, J.D., Lee, Y.T., 1990. Infrared Spectra of The Solvated Hydronium Ion: Vibrational Predissociation Spectroscopy of Mass-Selected $H_3O^+ \cdot (H_2O)n \cdot (H_2)m$. J. Phys. Chem. 94, 3416–3427.

Pillai, V., Kanicky, J.R., Shah, D.O., 1999. Applications of Microemulsions in Enhanced Oil Recovery, in: Handbook of Microemulsion Science and Technology. Marcel Dekker, New York.

Pine, S.H., 2011. The Base-Promoted Rearrangements of Quaternary Ammonium Salts. Org. React. 18, 403–464.

Pintér, J., Wolfram, E., 1981. Surface Phenomena in Enhanced Oil Recovery, in: Shah, D.O. (Ed.), Surface Phenomena in Enhanced Oil Recovery. Springer, New York, pp. 479–493.

Puerto, M.C., Reed, R.L., 1983. A Three-Parameter Representation of Surfactant / Oil / Brine Interaction. Soc. Automob. Eng. 23.

Ramakrishnan, T.S., Wasan, D.T., 1983. A Model for Interfacial Activity of Acidic Crude Oil/Caustic Systems for Alkaline Flooding. Soc. Pet. Eng. J. 23, 602–612.

Raveendran, P., Ikushima, Y., Wallen, S.L., 2005. Polar Attributes of Supercritical Carbon Dioxide. Acc. Chem. Res. 38, 478–485.

Reed, R.L., Healy, R.N., 1977. Some Physicochemical Aspects of Microemulsion Flooding: a Review, in: Improved Oil Recovery by Surfactant and Polymer Flooding. Elsevier, pp. 383–437.

Rogner, H.-H., 1997. An Assessment of World Hydrocarbon Resources. Annu. Rev. Energy Environ. 22, 217–262.

Salehi, M., Johnson, S.J., Liang, J.-T., 2008. Mechanistic Study of Wettability Alteration Using Surfactants with Applications in Naturally Fractured Reservoirs. Langmuir 24, 14099–14107.

Santanna, V.C., Curbelo, F.D.S., Castro Dantas, T.N., Dantas Neto, A.A., Albuquerque, H.S., Garnica, A.I.C., 2009. Microemulsion Flooding For Enhanced Oil Recovery. J. Pet. Sci. Eng. 66, 117–120.

Sasaki, K., Akibayashi, S., Yazawa, N., Doan, Q., Ali, S.M.F., 1999. Experimental Modelling of the SAGD Process 3/4 Enhancing SAGD Performance with Periodic Stimulation of the Horizontal Producer, in: SPE Annual Technical Conference and Exhibition. Society of Petroleum Engineers. doi:10.2118/56544-MS

Schick, M.J., 1963. Effect of Temperature on the Critical Micelle Concentration of Nonionic Detergents. Thermodynamics of Micelle Formation. J. Phys. Chem. 67, 1796–1799.

Schulman, J.H., Stoeckenius, W., Prince, L.M., 1959. Mechanism of Formation and Structure of Micro Emulsions by Electron Microscopy. J. Phys. Chem. 63, 1677–1680.

Sebastian, H.M., Wenger, R.S., Renner, T. A., 1985. Correlation of Minimum Miscibility Pressure for Impure CO_2 Streams. J. Pet. Technol. 37, 2076–2082.

Sekhon, B.S., 2004. Gemini (dimeric) Surfactants. Resonance 9, 42–49.

Selby, R., Alikhan, A.A., Ali, S.M.F., 1989. Potential of Non-Thermal Methods for Heavy Oil Recovery. J. Can. Pet. Technol. 28. doi:10.2118/89-04-02

Shah, A., Fishwick, R., Wood, J., Leeke, G., Rigby, S., Greaves, M., 2010. A Review of Novel

Techniques for Heavy Oil and Bitumen Extraction And Upgrading. Energy Environ. Sci. 3, 700.

Shah, D.O., Schechter, R.S., 1977. Improved Oil Recovery by Surfactant and Polymer Flooding. Academic Press, New York.

Sheng, J.J., 2011. Modern Chemical Enhanced Oil Recovery: Theory and Practice. Elsevier, Burlington.

Sheng, J.J., 2010. Optimum Phase Type and Optimum Salinity Profile in Surfactant Flooding. J. Pet. Sci. Eng. 75, 143–153.

Simanzhenkov, V., Idem, R., 2003. Crude Oil Chemistry. Marcel Dekker, New York.

Sjoblom, J., Lindberg, R., Friberg, S.E., 1996. Microemulsions- Phase Equilibria Characterization, Structures, Applications And Chemical Reactions. Adv. Colloid Interface Sci. 65, 125–287.

Speight, J.G., 2004. Petroleum asphaltenes - Part 1: Asphaltenes, Resins and the Structure of Petroleum. Oil Gas Sci. Technol. 59, 467–477.

Speight, J.G., Loyalka, S.K., 2007. Handbook of Alternative Fuel Technologies, CRC Press. ed. Taylor & Francis, Boca Raton.

Taber, J.J., Martin, F.D., Seright, R.S., 1997a. EOR Screening Criteria Revisited - Part 2: Applications and Impact of Oil Prices. SPE Reserv. Eval. Eng. 12, 21–24.

Taber, J.J., Martin, F.D., Seright, R.S., 1997b. EOR Screening Criteria Revisited - Part 1: Introduction to Screening Criteria and Enhanced Recovery Field Projects. SPE Reserv. Eng. 12, 189–198.

Tarek, A., 2007. Equations of State and PVT Analysis: Application for Improved Reservoir Modeling. Gulf Publishing Company, Houston.

Tarek, A., 2001. Reservoir Engineering Handbook. Gulf Publishing Company, Houston, Texas.

Thomas, S., 2008. Enhanced oil recovery-an overview. Oil Gas Sci. Technol. 63, 9–19.

Wilt, B.K., Welch, W.T., Rankin, J.G., 1998. Determination of Asphaltenes in Petroleum Crude Oils by Fourier Transform Infrared Spectroscopy. Energy Fuels 12, 1008–1012.

Yildiz, H.O., Morrow, N.R., 1996. Effect of Brine Composition on Recovery of Moutray Crude Oil By Waterflooding. J. Pet. Sci. Eng. 14, 159–168.

Yoshimura, T., Ohno, A., Esumi, K., 2004. Mixed Micellar Properties of Cationic Trimeric-Type Quaternary Ammonium Salts and Anionic Sodium N-Octyl Sulfate Surfactants. J. Colloid Interface Sci. 272, 191–196. doi:10.1016/j.jcis.2003.12.021

Yoshimura, T., Sakato, A., Esumi, K., 2013. Solution Properties and Emulsification Properties of Amino Acid-Based Gemini Surfactants Derived from Cysteine. J. Oleo Sci. J. Oleo Sci 62,

579–586.

Yuan, H., Johns, R.T., 2005. Simplified Method for Calculation of Minimum Miscibility Pressure or Enrichment. SPE J. 10, 416–425.

Zana, R., 2002. Dimeric and oligomeric surfactants. Behavior at Interfaces and in Aqueous Solution: A Review. Adv. Colloid Interface Sci. 97, 205–253.

Zana, R., Benrraou, M., Rueff, R., 1991. Alkanediyl-.Alpha.,.Omega.-Bis(Dimethylalkylammonium Bromide) Surfactants. 1. Effect of The Spacer Chain Length on the Critical Micelle Concentration and Micelle Ionization Degree. Langmuir 7, 1072–1075.

Zhang, D., Creek, J., Jamaluddin, A J., Marshall, A.G., Rodgers, R.P., Mullins, O.C., 2007. Asphaltenes - Problematic but Rich in Potential. Oilf. Rev. 22–43.

Zielilqski, R., Ikeda, S., Nomura, H., Kato, S., 1989. Effect of Temperature on Micelle Formation in Aqueous Solutions of Alkyltrimethylammonium Bromides. J. Colloid Interface Sci. 129, 16–20.